# MORPHOLOGIC ANALYSIS OF MERAPI EDIFICE IN STUDYING MERAPI – TYPE ERUPTION, TO IMPROVE VOLCANIC HAZARD MAP

**By:**

**Komang Sri Hartini**

# MORPHOLOGIC ANALYSIS OF MERAPI EDIFICE IN STUDYING MERAPI – TYPE ERUPTION, TO IMPROVE VOLCANIC HAZARD MAP

Thesis submitted to the Graduate School, Faculty of Geography, Gadjah Mada University in partial fulfillment of the requirement for the degree of Master of Science in Geo-Information for Spatial Planning and Risk Management


**By:**

**Komang Sri Hartini**

**08/276583/PMU/05631**

**hartini20739@itc.nl**


**SUPERVISOR:**

**Dr.rer.nat. Junun Sartohadi., M. Sc (UGM)**

**Dr. Tsehaie Woldai (ITC)**

**Drs. R.P.G.A. Voskuil (ITC)**


**GADJAH MADA UNIVERSITY**

**FACULTY OF GEO-INFORMATION SCIENCE AND EARTH OBSERVATION, UNIVERSITY OF TWENTE**

**2010**

# THESIS

# MORPHOLOGIC ANALYSIS OF MERAPI EDIFICE IN STUDYING MERAPI – TYPE ERUPTION, TO IMPROVE VOLCANIC HAZARD MAP

**By:**

**Komang Sri Hartini**
**08/276583/PMU/05631**
**AES 20739**

Has been approved in Yogyakarta
On February 2010

By Team of Supervisors:
Chairman

**Dr. H.A. Sudibyakto., M.S.**

External Examiner

**Prof. Dr. Freek van der Meer**

Supervisor 1 | Supervisor 2 | Supervisor 3

**Dr. Junun Sartohadi M. Sc** | **Dr. Tsehaie Woldai** | **Drs. R.P.G.A. Voskuil**

Certified by:
Program Director of Geo-Information for Spatial Planning and Risk Management,
Graduate School Faculty of Geography, Gadjah Mada University

**Dr. H.A. Sudibyakto., M.S.**

**DISCLAIMER**

**This document describes work undertaken as part of a programme of study at the Faculty of Geo-information Science and Earth Observation, University of Twente. All views and opinions expressed therein remain the sole responsibility of the author, and do not necessarily represent those of the institute.**

**Hartini, K.S**

## Abstract

Merapi – type is categorized as regular eruption of Merapi with 8 – 15 year interval (Thouret *et al.*, 2000). The increasing number of population on forbidden zone has exposed the inhabitants to major threat of pyroclastic flows produced from this type of eruption.

Morphologic analysis of summit and vicinity area was conducted on series of digital elevation models (DEMs), to observe dynamic changes over 70 years and to define factors ascertain the direction and major distribution of Merapi – type eruption in the past, to be used as factors to determine direction and to predict affected area in the near future. Slope angle (°), plan curvature, shaded DEM and travel distances of Merapi – type eruptions were combined to produce proposed pyroclastic flows hazard zone that used to assess the fitness of forbidden zone of existing hazard map toward dynamic changes in Merapi eruptive behavior. As the quality of morphologic analysis was determined by quality of DEM, the assessment of efficacy and accuracy of input data was essential to conduct. Initial and visual observations and three statistical parameters: mean error, range error and root mean square error of elevation (RMSEz) were utilized to assess the usefulness of IFSAR DEM to that of reference DEM.

Based on reconstruction of past time eruptions, from six features observed in Merapi edifice: crater rim form, crater breaching, crater floor, adjacent ridges, breaches and remnant of domes, crater breaching and its adjacent ridges are the main factors ascertain direction of Merapi – type eruption and shifting trends of Merapi – type eruption of west - southwest – southeast are able to observe. Prediction in direction and area affected by pyroclastic flows reveals almost 18.000 inhabitants in four villages Hargobinangun, Umbulharjo, Kepuharjo and Glagaharjo in southern flank of Merapi to be likely affected by the hazard in the near future.

Proposed pyroclastic flow hazard zone discovers the extent distance and area to those of forbidden zone of existing hazard map as far as 1.42 km with 2.2 hectare covered area in northern part and as far as 0.43 km with 0.9 hectare of covered area in southern part. Detail of area and river channel probably channelized by pyroclastic flow hazard was carried out to improve existing hazard map, to finally provide appropriate and effective mitigation plans during the activity considering 132.000 inhabitants in forbidden zone, and to provide guidelines for long term landuse planning well as.

The initial observation of shaded DEMs showed that scale 1: 25.000 was appropriate to study morphology of vicinity area and scale 1: 5.000 (pixel size 5 m) or even larger is needed to study morphology of summit area. DEM produced from topographic maps (ground survey and photogrammetry techniques), give better topographic representation rather than that of produced from IFSAR DEM but those methods have been started to lose their ability to deliver most up to date topographic representation. However, assessment of IFSAR DEM through three statistical parameters, mean error (3.879 m), range error (15.269 m) and RMSEz (5.711 m) showed that absolute vertical accuracy of this data less than its product specification although it delivers similar height distribution to that of reference DEM.

**Keywords: Merapi – type eruption, morphologic analysis, proposed pyroclastic flow hazard zone, digital elevation models**

## Acknowledgment

My sincere thanks to Ir. Waskito Pandu, M.Sc, Chairman of Central Data Processing, Department of Public Works, Dra. Sri Yumadiati, SP1, Dra. Marcellina Rinny, M.Sc and Ir. Anum Kurniawan, M.Sc for opportunity to pursue higher education and their supports during my study.

My deep gratefully thanks for my supervisors, Dr. Junun Sartohadi for his patience to orientate my thesis in right direction, his advices and encourages overcoming difficulties along the way to complete this work. I'm also very thankful to Dr. Tsehaie Woldai for his information regarding data used in my research. My gratefully thanks also go to Drs. Robert P.G.A Voskuil for his patience to make me understand more about Volcanology and his critical review of my writing.

My gratefully thanks to faculty members of UGM, for their kindly help and support. My special thanks goes to Dr. Sudibyakto for his supporting during my study, Dr. Danang Sri Hadmoko for kindly conveying the contour map data from SNVT Sabo Project and link of Merapi article from Prof. Frank Lavigne. Dr. Aris Marfai for geomorphology articles and discussions. Taufik Hery Purwanto. M. Si, Muhamad Kamal. M. GIS and Nur M. Farda. M.Cs for discussions about remote sensing and GIS techniques for deriving digital elevation Model.

My deep gratefully thanks to faculty members of ITC, for their kind and warm discussion, especially for Dr. David G. Rossiter for his critical comments during field work and midterm evaluation, Drs. Michiel Damen for his valuable data of Merapi, long discussions about geomorphology and tracing back of old data from www.kit.nl, M.Sc. Gerrit C. Huurneman for discussion about data accuracy.

My truthful thanks to Prof. Frank Lavigne for kindly giving valuable article related to Merapi, warm discussions about how to study morphology of Merapi and lightening some parts of my research during his visit in Indonesia.

My sincere thanks to all classmates, especially for Bonaventura Firman for his kindly help and discussion regarding GIS software, Emba Tampang Allo for helping miscellaneous things of Endnote and MS. Word, Fetty Febrianti and Sri Eka Wati for sharing thought and friendship, Tandang Yuliadi for his companion in collecting and sharing data, Sigit Kurniawan for giving two valuable publications of Merapi and Ratna Sari Dewi for valuable discussions, critical comments and enlighten my work from different perspective.

My gratefully thanks for Stephen Griffiths and Daniel Adi Nugroho from Intermap Technologies for providing IFSAR DEM, especially Daniel for his critical review of my abstract and helping to gain the data without second thought. My truthful thanks also go to Bambang Cosmas Sukatja for allowing utilization of contour map from SNVT Sabo Project.

My sincere thanks to my colleagues: Ruli Andaru for sharing data and discussion about digital elevation model, Yollian Dwiyanti for kindly providing statistic data of Yogyakarta and Central Java Province, Gede Sastrawangsa for helping in modeling software and Bagiyo for providing topographic map of 1944.

My deep gratefully thank to Tri Wahyu Widagdo for his companion collecting EDM data from Merapi Observatory Posts for almost two months and information, book and discussion of Merapi, Greg Horrall for valuable discussion in photogrammetry and his encouraging messages, Tata and her family for being my second family during my study in Yogyakarta, my sincere thanks to Ibu Windarti for her love, kindly support and encourage.

I'm also fully appreciating the guardians of Merapi Volcano, who risk their lives to warn the community during the peak of Merapi activity: Yulianto, Triyono (MOP Babadan), Singat and Ismail (MOP Selo), Trimujiyanto (MOP Jrakah) and Suramto (MOP Kaliurang) for providing EDM data, discussion and sharing story about Merapi.

No words could express how deep thankfully and sincere to my beloved parents, to whom I dedicate most of achievement and accomplishment. ”Thanks for bringing me here”. Brother and sister for their loves and encourages during my hardest time.

Finally, my heart deep submission to My Almighty and My Master, Ida Hyang Widhi Waca, for his blessing, miracles and courage always.

## Table of Contents

## List of Figures

## List of Tables

## Abbreviations

| | |
|---|---|
| ALOS PRISM | Advanced Land Observing Satellite, Panchromatic Remote-sensing Instrument Stereo Mapping |
| AMS | U.S. Army Map Service |
| ANUDEM | Australian National University Digital Elevation Model |
| ASTER GDEM | Advanced Spaceborne Thermal Emission and Reflection Radiometer, Global Digital Elevation Map |
| BAKOSURTANAL | Badan Koordinasi Survei dan Pemetaan Nasional; National Coordinating Agency for Survey and Mapping |
| BPN | Badan Pertanahan Nasional; National Land Administration Agency |
| BAPPEDA | Badan Perencanaan Pembangunan Daerah; Regional Development Planning Agency |
| BPPD | Badan Pengelolaan Pertanahan Daerah; Regional Land Management Agency |
| CVGHM | Central of Volcanology and Geology Hazard Mitigation, Department of Energy and Mineral Resources, previously VSI |
| D | Growing lava dome |
| DEM | Digital Elevation Model |
| DGN 95 | Datum Geodesi Nasional 1995; Indonesian Geodetic Datum 1995 |
| Dinas P3BA | Dinas Perairan, Pertambangan dan Penangulangan Bencana Alam; Local Agency for Irrigation, Mining and Disaster Management |
| DPW | Department of Public Works |
| DSM | Digital Surface Model |
| DTM | Digital Terrain Model |
| EDM | Electronic Distance Meter |
| EGM 96 | Earth Gravitational Model 96 |
| GCP | Ground Control Point |
| GMU | Gadjah Mada University |
| Gn | Gunung; Mount or Volcano |
| ITRF 2000 | International Terrestrial Reference Frame 2000 |
| JAXA | Japan Aerospace Exploration Agency |
| K | Kali; River |
| Km | Kilometer |
| L | Remnant of domes and coulees |
| LAPAN | Lembaga Penerbangan dan Antariksa Nasional; National Institute of Aeronautics and Space |
| MOP | Merapi Observation Post |
| MVO | Merapi Volcano Observatory |
| PIC | Person In Charge |
| PSBA | Pusat Study Bencana Alam; Center of Natural Hazard Study, Gadjah Mada University |
| PUSPICS | Program Penginderaan Jauh untuk Sumberdaya dengan Pendekatan Interpretasi Citra dan Survei Terpadu; Center for Remote Sensing and Geographic Information System |
| SRTM DEM | Shuttle Radar Topography Mission, Digital Elevation Model |
| SNVT SABO | Satuan Non Vertikal Tertentu SABO |
| TAGANA | Taruna Siaga Bencana; Cadet for Disaster Mitigation and Response |
| TIN | Triangulated Irregular Network |
| TM | Transverse Mercator |
| TNGM | Taman Nasional Gunung Merapi; Merapi National Park |
| UTM | Universal Transverse Mercator |
| VEI | Volcanic Explosivity Index |
| VSI | Volcanological Survey of Indonesia |
| WGS | World Geodetic System |

## Glossaries

| | | |
|---|---|---|
| **Ash fall or Tephra** | : | fine-grained rock and mineral fragments and glass shards ejected by volcanic eruption, dangerous for aviation |
| **Lava dome** | : | thick, bulbous, usually volatile poor masses of highly viscous lava |
| **Lava tongue or Coulee** | : | stubby flows transitional between conventional flows and domes |
| **Remnant of domes** | : | lava dome or coulee which not tore down during eruption and changes morphology of Merapi edifice |
| **Merapi – type eruption** | : | pyroclastic flow generated by dome collapse, nuees ardentes d' avalanche (French) |
| **Pyroclastic density current** | : | A particulate gaseous volcanic flow moving along the ground. This term includes both pyroclastic flows and pyroclastic surges but has no connotation of particle concentration or flow steadiness. |
| **Pyroclastic flow** | : | a flow of volcanic material ranging from vesiculated, low-density pumice to unvesiculated, dense lava and clasts which tend to follow topographic lows, mostly restricted to valley floor |
| **Pyroclastic surge** | : | a turbulent, low-density, high-velocity part of a pyroclastic density current. It is not so constrained by topography and can effect areas high on valley walls and even overtop ridges to enter adjacent valleys |
| **St. Vincent – type eruption** | : | Pyroclastic flow generated by fountain collapse, nuees ardentes d' explosion (French) |

# Chapter 1. Introduction

*This chapter describes the background of the research, problem statement, research objectives, research questions, benefit of the research, scope and limitations and thesis structure.*

## 1.1. Background

The Merapi volcano (2968m) is one of the most active volcanoes in Indonesia. It is situated on the administrative boundary between Central Java and Yogyakarta provinces. Merapi is famous for *Merapi – types* or dome collapse pyroclastic flows that are characterized by continuous growth of lava domes, interrupted by collapses and phases of quiescence (Camus *et al.*, 2000; Voight *et al.*, 2000).

Ever since Merapi activities have been recorded, it has erupted for 53 times, which can be differentiated into brief and violent explosion (Voight *et al.*, 2000). Merapi brief explosions at 8 – 15 year intervals generate dome collapse pyroclastic flows and destroy whole or part of the existing domes. Violent explosive episodes occurred on an average recurrence of 26 - 54 years have generated pyroclastic flows, surges, tephra-falls, and subsequent lahars (Lavigne *et al.*, 2000; Thouret *et al.*, 2000).

The morphology of the summit region has a significant effect in directing volcanogenic flows, particularly if there are distinct crater breaches (Davidson and Silva, 1999), which then produce the hazards on the slopes. Thus, changes in summit morphology whether caused by eruption activities or by hydrothermal altered processes would change the direction of those flows including dome collapse pyroclastic flows (Bacharudin, 1990). Based on historical data, Merapi has changed its eruption direction several times following summit morphology. For instance, from 1931 to 1945, Merapi eruptions were directed toward the west – southwest direction whilst from 1961 to 1998, Merapi eruption shifted into the west – southwest - south direction.

The southern flank of Merapi was previously protected by Geger Boyo, part of West dome formed by the 1930 eruption, impeded lava flow toward south direction. After it finally collapsed in 2006, the southern flank was opened to unstable and growing lava dome (Wilson *et al.*, 2007). This condition shifted hazard direction from west and southwest direction to the southern flank of Merapi volcano in which Yogyakarta, the capital city of Yogyakarta province, is located.

Although Merapi – type eruptions are considered as regular activities of Merapi volcano and usually distributed in relatively narrow sectors, dense populated area in southern flank of this active volcano, over 123 thousand above elevation 500 m in 2008, has leading the community to threaten hazards. The economic activity of sand mining has invited people to live nearby the volcanic cone, the most dangerous area affected by Merapi – type eruptions. Thus, in order to give preliminary view of hazard potential, the study of morphologic changes of Merapi edifice and possible directions of Merapi – type eruption are needed to reduce the effect of those hazards.

## 1.2. Problem Statement

Two largest Merapi – type eruptions in the last two decades were in 1994 and 2006. In 1994, Merapi eruption produced roughly 2.5–3 million cubic meters of deposition (Abdurachman *et al.*, 2000), killed 64 people and made more than 6.000 refugees. In the 2006's eruption, 2 people were buried inside an escape bunker where they tried to hide from pyroclastic flows (CVGHM, 2006).

Insufficient forecasting on direction of dome collapse, following dynamic morphologic changes of summit area resulted in inappropriate mitigation programs which should reduce the number of victims and losses. For instance, 2006 eruption neglected development of structural counter measures i.e. SABO dams, built to reduce effects of lava flow and lahar, which mainly located in west and southwest flank of Merapi and leaved south flank unprotected (Wilson *et al.*, 2007). On the other hands, development of SABO dams to close to volcanic cone has directed overland pyroclastic flow and buried Kaliadem tourism object (Frank Lavigne, personal communication).

Merapi flanks areas are densely populated because fertile soil invites people to stay and grow corps and to mine sand from volcanic deposition. Local communities in those areas are vulnerable element at risks when Merapi erupts. In order to prevent casualties and losses, predictions in direction of Merapi – type eruptions are needed as consideration for local authority's mitigation and preparedness plans. Therefore, the study of summit morphology related to Merapi – type eruptions are necessary to give preliminary information of hazards and extent of affected areas.

The study of volcanic geomorphology for risk assessment by geomorphic hazard zonation and composite risk zonation could be achieved through improvement of quantitative classification of volcanic landforms, which blends morphometry and ground observation, remote sensing data, and laboratory experiments and diversity used of airborne images and digital data acquired through radar and satellites (Thouret, 1999; Huggett, 2007). Combination of those techniques provides useful sources to develop digital elevation models (DEMs) dataset. By means of geographic information system, the useful tools to integrate, to input, to analyze and to manage all data from different scales and sources, those dataset can provide numerous sources for developing digital representation of surface topography.

Topographic elements of volcanic landforms can be computed directly from a DEM (Huggett, 2007) including primary and secondary attribute e.g. slope, aspect, plan and profile curvature which useful to study landform (Hutchinson and Gallant, 2000). Thus, digital elevation model derived from ground survey, photogrammetry and remote sensing techniques by means of GIS tools provide powerful sources to study morphologic changes of Merapi edifice regarding Merapi – type of eruption.

## 1.3. Research Objectives

The objectives of this research are to study morphologic changes of Merapi edifice in the last 70 years related to Merapi – type eruptions. Morphologic analyses of past time eruptions on a series of DEM were carried out to determine morphologic factors ascertain direction of dome collapse. Utilization of those factors to determine direction of dome collapse and identification of areas prone to pyroclastic flows in the near future are carried out by means of remote sensing and geographic information systems. This main objective is carried out through four specific research objectives:

1. To study morphologic changes of summit area related to Merapi – type eruption using existing data of remote sensing imageries and detail contour maps.
2. To forecast the direction dome collapse in the near future based on morphologic analyses of past time eruptions.
3. To identify areas prone to pyroclastic flow hazard in the near based on recent morphology of the slopes, especially on the river valleys and to develop proposed hazard zone for Merapi – type eruption in order to improve forbidden zone of Merapi hazard map.
4. To compare the accuracy and efficacy of different types of input data for studying morphology of summit and vicinity area.

## 1.4. Research Questions

In order to answer research objectives above, these following questions are to be addressed:

Table 1-1. Research objectives and research questions

| No | Research Objectives | Research Questions |
|---|---|---|
| 1 | To study changes in summit morphology using existing data of remote sensing imageries and detail contour maps. | a. What kind of data needed to study morphology of summit and vicinity area?<br>b. How to reconstruct changes in summit morphology from 1930 to 2006 eruptions?<br>c. How to reconstruct the lava dome growth from past 70 years?<br>d. How to represent the result of morphologic changes in the summit area?<br>e. How to assess morphologic changes in recent year after 2006 eruption? |
| 2 | To forecast the direction dome collapse in the near future based on morphologic analyses of past time eruptions. | a. Which morphologic features need to be observed in summit area to be utilized as factors ascertain direction of Merapi – type eruption?<br>b. Which morphologic features need to be observed in vicinity area regarding direction of Merapi – type eruption?<br>c. Which morphologic factors ascertain the direction of dome collapse from 1930 to 2006 eruptions?<br>d. Which morphologic factors play the most important roles to determine the direction of dome collapse in the past?<br>e. How accurate do the trend we have in comparison to Merapi historical data?<br>f. How to predict the direction of dome collapse in the near future by using those factors? |
| 3 | To identify areas prone to Merapi – type eruptions in the near future based on recent morphology of the slope, especially on the river valleys and to improve forbidden zone of Merapi hazard map | a. What type of data needed to determine the extent of pyroclastic flows in the near future?<br>b. How to determine the affected area by considering morphology of river channel and DEMs?<br>c. How to determine the pyroclastic flow hazard zone of Merapi – type eruption?<br>d. How the result of proposed pyroclastic flow hazard zone to improve forbidden zone of Merapi hazard map? |
| 4 | To compare the accuracy and efficacy of different types of input data for studying morphology of summit and vicinity area. | a. How the surface representation of input data establishes DEMs quality for studying morphology of summit and vicinity area and how to compare them?<br>b. How is the usefulness of each type of the data?<br>c. How to compare between DEM of topographic map derived from photogrammetry and active remote sensing?<br>d. What is minimum accuracy of input data to provide appropriate morphologic quality for this research? |

## 1.5. Benefit of the Research

This research provided information about the morphologic changes of Merapi edifice from the last 70 years regarding Merapi – type eruptions, dimension of dome remnants, prediction in direction and extended area affected by Merapi – type eruption in the near future, proposed hazard zone for Merapi – type eruption and efficacy of input data for studying volcanic morphology. Thus, the result of this study will be useful for government, local community and other stakeholders for several purposes as follows:

1. It is useful to observe morphologic changes of summit area using spatial geo-reference data and revealing the relation between the changes and Merapi – type eruptions.
2. It can be useful to expose dimension of dome remnants and their relative positions on Merapi edifice.

3. It will be useful to predict direction of Merapi – type eruptions by observing morphologic factors ascertain the direction and to provide more reliable forbidden hazard zone for Merapi – type eruption.
4. It will be useful to figure out appropriate input data to study morphology of summit and vicinity area.
5. It can be useful for developing effective mitigation and preparedness plans prior to Merapi eruptions as well as local government consideration for purposed landuse planning to reduce the negative effects of Merapi's eruptions.
6. It can be useful for further study about Merapi.

## 1.6. Scope and Limitation of the Research

### 1.6.1. Scope

This research focuses on morphologic analyses of Merapi edifice on a series of DEMs in the past, to determine factors ascertain direction of Merapi – type eruptions. Those factors will be used to determine the direction of Merapi – type eruption and predicted area affected by pyroclastic flows it produced in the near future and proposed hazard zone for Merapi – type eruption. Comparison of DEM derived from various types of input data e.g. topographic map and IFSAR DEM was carried out to reveal efficacy of input data type.

### 1.6.2. Limitation

Some limitations in this research were underlined including focus of this research, various scale and source of input data and modeling of the pyroclastic flows.

1. This research focus on Merapi – type eruption or dome collapse pyroclastic flow although Merapi produces other types of hazards affected broader area i.e. pyroclastic surges.
2. Various scales and sources of input data, low data quality and insufficient series of digital elevation models before and after each eruption in the past prevent better result in determining precise direction of dome collapse in the past.
3. Modeling of pyroclastic flow could not be conducted due to data availability and time constraint so prediction of affected area was carried out based on morphologic analysis of slope and plan curvature combined with historical data on predicted direction. Unavailability of digital elevation model after eruption 2006 made the utilization of DEM 2006 as terrain surface model to carry out morphologic analysis for predicted affected area and proposed hazard zone for Merapi – type eruption.

## 1.7. Research Structure

This research is composed of eight chapters, which are described briefly in this following section:

*Chapter 1 - Introduction*
This chapter describes introduction of the research including background, research problems, research objectives, research questions, benefit of the research, scope and limitation of the research and research structure.

*Chapter 2 – Literature Review*
The literature review provides theoretical background related to this research including volcanoes, strato volcano, lava dome, digital elevation model (DEM), DEM interpolation methods, DEM quality assessment, application of DEM for studying volcanic landform, electronic distance meter (EDM) for trilateration network and GIS for morphologic analysis.

*Chapter 3 – Merapi Strato Volcano*
This chapter gives the overview of the study area including general overview of Merapi, selection of study area, summary of Merapi history, characteristic of Merapi eruptions and morpho – chronology of lava domes.

*Chapter 4 – Research Methodology*
This chapter provides the methodology including data, software and equipment and method used to derive purposed objectives of this research, separated based on the activity during pre – field work, field work and post – field work.

*Chapter 5 – DEM Generation and Quality Comparison*
This chapter provides result of DEMs preprocessing, DEM generation from dataset, DEMs quality comparison by initial observation, height distribution and statistical parameter and concluding remarks.

*Chapter 6 – Morphologic Analysis*
This chapter provides utilization of EDM data for morphologic changes, morphologic features recognition and quantification, morphologic analysis for verifying factor ascertain Merapi – type direction, reconstruction of Merapi – type eruption in the past using those factors, comparison of reconstruction results to historical data and concluding remarks

*Chapter 7 – Predicted Affected Area and Improvement of Forbidden Hazard Zone*
This chapter provides predicted affected area in the near future by morphologic analysis of recent summit topography and vicinity area, proposed hazard zone for Merapi – type eruption through travel distance from historical data and morphologic analysis, improvement of existing Merapi hazard map, social and economic activities on forbidden zone and concluding remarks.

*Chapter 8 – Recommendation*
This chapter defines achievements of this research n as well as contribution of this research for present circumstances related to Merapi – type hazard. The recommendation is also presented for future research regarding Merapi hazards.

# Chapter 2. Literature Review

*The literature review provides theoretical background related to this research including volcanoes, strato volcano, lava dome, digital elevation model (DEM), DEM interpolation methods, DEM quality assessment, application of DEM for studying volcanic landform, electronic distance meter (EDM) for trilateration network and GIS for morphologic analysis.*

## 2.1. Volcanoes

A volcano is usually a cone – shaped hill or mountain composed of materials erupted through an opening in the Earth's crust which extends from the hotter zones below (Scarth, 1994). Volcanoes seem to occur in many places around the World but actually, they are restricted to narrow and specific places. Volcanoes are clearly associated with plate boundaries and their activities depend on the type of plate boundary (Hamblin, 1989).

Volcanic activity commonly occurs in divergent and convergent boundaries with different type of magma produced (Scarth, 1994). Divergent boundaries usually take form of basaltic fissure magma, which commonly occur under the ocean so called mid ocean ridges. Convergent or collusion boundaries mostly produce more viscous magma due to higher silica content. This leads to more explosive eruption because the captured gasses cannot escape easily. However, there are areas where volcanic activity can occur far away from a plate boundary, known as hotspot areas.

## 2.2. Strato volcanoes

Volcanoes can be differentiated based on several categories i.e. shape, size, type of magma and style of activity. Thompson and Turk, 1997 had differentiated volcanoes into five categories: basalt plateau, calderas, cinder cones, shield volcanoes and strato or composite volcanoes, see table 2-1.

Table 2-1. Characteristic of different type of volcanoes (Source: Thompson and Turk, 1997)

| Type | Form | Size | Type of Magma | Style |
|---|---|---|---|---|
| Basalt plateau | Flat to Gentle slope | 100.000 to 1.000.000 $km^2$ in area; 1 to 3 km thick | Basalt | Gentle eruption from long fissures |
| Calderas | Cataclysmic eruption leaving a circular depression called a caldera | Less than 40 km in diameter | Granite | Very violent |
| Cinder | Moderate slope | 100 to 400 m high | Basalt or andesite | Ejection of pyroclastic materials |
| Shield volcanoes | Slightly slope 6° to 12° | Up to 9000 m high | Basalt | Gentle, some fire fountains |
| Strato or composite volcanoes | Alternate layers of flows and pyroclastic | 100 to 3500 m high | Variety types of magma and ash | Often violent |

Strato or composite volcanoes commonly occur in convergent boundaries and they are differentiated from volcanoes occurring in divergent zone because of their silicic magma. Thus, this type of volcano has more viscous lava forming thicker flow that extent less far from the vent (MacDonald, 1972). Viscosity of lava sometimes hampers gas to escape resulting in explosive and violent eruption accompanied by large quantities of tephra.

As a part of collision boundaries of Eurasian Plate and Indo-Australian Plate, Indonesia is littered with a major strato - volcanoes line ranging from Sumatera, Java, Bali, Nusa Tenggara, Sulawesi to Papua, figure 2-1. One of the most active and dangerous volcanoes in Indonesia is Merapi, due to its frequent activities which often produce pyroclastic flows and surges.


Figure 2-1. Major Strato - volcano's lines in Indonesia (Source: Google image)

## 2.3. Lava Dome

A lava dome is a rounded, convex – sided, dome shaped mass of volcanic rock, which is usually silicic and too viscous to flow far from the vent (Scarth, 1994). A dome of silicic lava tends to pile up over the vent to form large, bulbous domes (Hamblin, 1989), which can grow quickly and destroy even faster than its growth, especially when lava dome seals the vent of strato – volcanoes.

The degree to which the edges of a growing dome spread out from the margin of the vent depends on the viscosity of the liquid (MacDonald, 1972). Some of domes form by the enlargement of a lava dome as successive, discrete lobes of lava pile on one another, known as *exogenic dome growth* and the others form by the enlargement of its interior, which expands to accommodate an influx of new lava, known as *endogenic dome growth* (Fink and Anderson, 1999).

Merapi's historical eruptions have been characterized by repeated growth and collapse of the summit lava dome, with the form of horseshoe - shaped and open ended summit crater, figure 2-2 (Voight *et al.*, 2000). Those processes will produce pyroclastic flows and surges, one of the most dangerous hazards of Merapi, because of its high speed and hot gases.

Figure 2-2. Merapi lava dome was captured in spring of 2006 (Source: Syamsul L)

Growth and collapse of Merapi's' lava domes make a necessity to monitor them. Observation of lava dome morphology, structure and texture comes from remote sensing, terrestrial surveying and other field techniques. Repeated aerial photograph or other remotely sensed data record changes in diameter, height, volume and structure of active domes (Fink and Anderson, 1999).

## 2.4. Digital Elevation Model

Digital elevation model (DEM) is a general term used to specify elevation model of a given surface for both topography of land surface or sub marine, known as bathymetry. DEM is commonly used interchangeably with digital terrain model (DTM) and digital surface model (DSM) with slightly different of surface representation. Digital terrain model is regarded as a 2.5D representation of terrain information in 3D geographical space (Li *et al.*, 2005) for better representation of bare earth surface whilst digital surface model is similar to DTM that includes the elevation of vegetation and man – made structure (Rahman, 2006). Thus, in specific bare land area e.g. cone of active volcano, DSM can be categorized as DTM. In this study, DEM, more widely accepted term, will be used to deliver surface representation.

DEM can be obtained through some methods such as: point elevation data through field surveys, contour data of topographic maps, photogrammetric techniques and radargrammetry and SAR interferometry (Hutchinson and Gallant, 2000 and Li *et al.*, 2005). However, contour lines, delivered from topographic maps and aerial photogrammetry, are the most widely sources of DEM all over the world. In general, different types of data acquisition will deliver different accuracy of DEM as shown in table 2-2.

Table 2-2. Comparison of the accuracy of DTM data obtained by different techniques (Source: Li et al., 2005)

| Methods of data acquisition | Accuracy of data |
|---|---|
| Ground measurement (including GPS) | 1 – 10 m |
| Digitized contour data | About 1/3 of contour interval |
| Laser altimetry | 0.5 – 2 m |
| Radargrammetry | 10 – 100 m |
| Aerial photogrammetry | 0.1 – 1 m |
| SAR interferometry | 5 – 20 m |

Digital elevation models representation usually organized into one of three data structure: regular or square grids; triangulated irregular networks (TIN) and contours, figure 2-3 (Wilson and Gallant, 2008). In actual applications, the triangle-based and grid-based modeling are more widely used and are considered as the two basic approaches (Li *et al.*, 2005).

Square grids have been widely used because of its simplicity and easy computation. However, this type of data structure has disadvantages: size of grid often affect the storage requirement, computational efficiency and results quality. Square grids cannot easily handle abrupt elevation and often skips details in flat surface (Wilson and Gallant, 2008).

TINs are based on triangular facets at vertices at the sample points and usually construct based on Delauney triangulations. TINs can incorporate discontinuities along the lines of particular triangle and the equations for slope and curvature between the triangles that have a discontinuity are simply omitted. Moreover, TIN can cancel out the additional storage (Wilson and Gallant, 2008; Konecny, 2003).

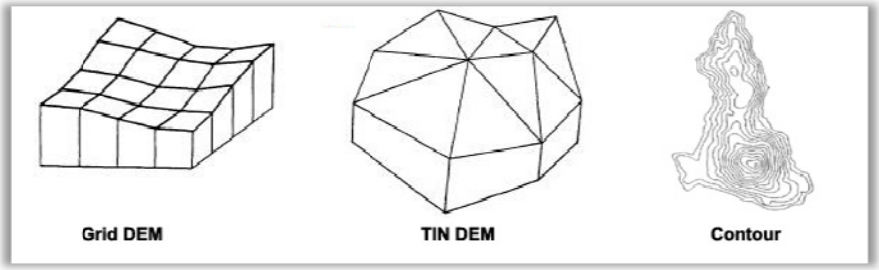


Figure 2-3. Type of digital elevation model structures (Source: Li *et al*., 2000)

## 2.5. DEM Interpolation methods

Interpolation in digital elevation modeling is used to determine the height value of a point by using the known heights of neighboring points. There are two implicit assumptions behind interpolation techniques: the terrain surface is continuous and smooth and there is a high correlation between the neighboring data points (Li *et al.*, 2005). Broad interpolation methods exist, with advantages and disadvantages for particular study, namely triangulation, local surface patches, local adaptive gridding, moving averages, inverse distance weighting, splines, kriging and ANUDEM.

Terrain interpolation methods for areas with different geomorphologic classes e.g. a coastal plain area might required different interpolation method compared with mountainous area (Chaplot *et al.*, 2006; Rahman, 2006). Moreover, besides interpolation methods, the quality of DEM might be different based on the purpose, quality of data sources and operator experiences (Podobnikar, 2008).

Li *et al.*, 2005 and Podobnikar, 2008 reveal the source of noises in elevation dataset could be originated from measurement error, errors in processing methods, huge gap in overlapping elevation, etc. Four interpolation methods would be discussed here: inverse distance weighting, splines, kriging and ANUDEM which are commonly used in GIS software and geomorphological researches.

### 2.5.1. Inverse distance weighting (IDW)

Inverse distance weighting interpolation method uses the basic principle of inverse distance in which the points that are located closer to a predicted point will have greater influence rather than that of located further. Thus, IDW assumes that each measured point has a local influence that diminishes with distance and the weight value will control how the weighting factors drop off when distance to a grid node is increase, see figure 2-4. However, this assumption is not valid for terrain interpolation (Maune, 2001 in Rahman, 2006).

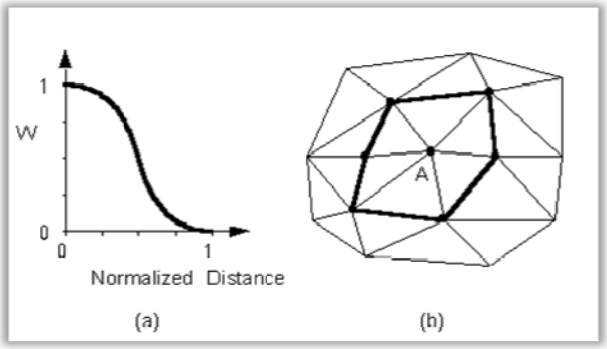


Figure 2-4. Inverse distance weighted interpolation; a) weighting function with normalized distance in X axis and weight value in Y axis, b) predicted point marked as “A” (Source: www.ems-i.com)

Inverse distance weighted interpolation used the equation 1 and the effective distance using equation 2 (Rifai, 2008).

### 2.5.2. Splines

The Spline method is an interpolation method that estimates values using a mathematical function that minimizes overall surface curvature, resulting in a smooth surface that passes exactly through the input points. There are two types of spline interpolation methods: regularized method which creates a smooth, gradually changing surface with values that may lie outside the sample data range and tension method which controls the stiffness of the surface according to the character of the modeled phenomenon and

creates a less smooth surface with values more closely constrained by the sample data range (Arc GIS 9.3 help).

The spline method yields the best estimation for landscape with low coefficient of variation (Chaplot *et al.*, 2006). This method is very sensitive to abrupt elevation changes in a short distance. Thus, the terrain interpolation should avoid man – made terrain features to be incorporated in natural terrain interpolation. In general, the neighboring cells should have less variance than the farther cell (Rahman, 2006).

$$\widehat{Z_j} = \frac{\sum_{i=1}^{n} \frac{Z_i}{h_y^{\beta}}}{\sum_{i=1}^{n} \frac{1}{h_y^{\beta}}} \quad \text{(Eq. 1)}$$

$$h_{ij} = \sqrt{d_{ij}^2 + \delta^2} \quad \text{(Eq. 2)}$$

Where:

$h_{ij}$ is the effective separation distance between grid node j and the neighboring point i
$\hat{Z}_j$ is the interpolated value for grid node j
$Z_i$ are the neighboring points
$d_{ij}$ is the distance between grid node j and the neighboring point i
$\beta$ is the weighting power
$\delta$ is the smoothing parameter

### 2.5.3. Kriging

Kriging interpolation method is somewhat similar to IDW interpolation method with more sophisticated weighting than that of IDW method. Kriging method is weighting neighboring cells not only based on distance but also the strength of autocorrelation among measured points. Kriging is a multistep process including exploratory statistical analysis of the data, variogram modeling, creating the surface, and optionally exploring a variance surface (Arc GIS Help).

The spatial structure of values in short and larger distances could be analyzed through an experimental semi variance model that defines the degree of spatial dependence among pairs at a specific distance, equation 3.

$$\gamma(h) = \frac{1}{2n}\sum_{i=1}^{n}\{Z(xi) - Z(xi+h)\}^2 \quad \text{(Eq. 3)}$$

Where:

$\gamma(h)$ is semi variance at distance h
$n$ is the number of observation separated by a distance $h$
$Z(x)$ is elevation value at position i

After building the experimental variogram, an appropriate theoretical function e.g. Linear, Gaussian, Exponential, Spherical is needed to build the model of spatial variation, see figure 2-5.

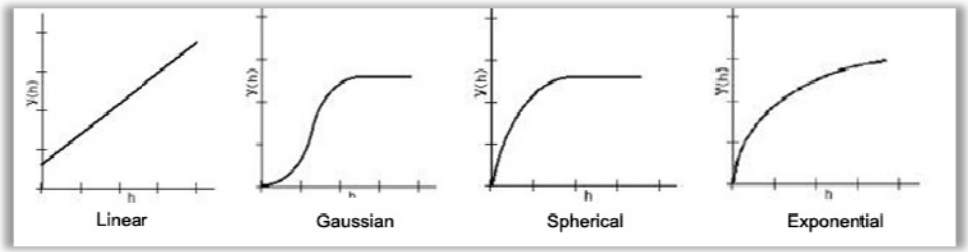


Figure 2-5. Types of empirical semi variogram

Spatial variation model developed from equation three were described through three parameters: nugget, sill and range as shown in figure 2-6. Nugget is a semivariance as

the separation between elevation data approaches zero. Sill is a maximum semivariance values that represent variability in the absence of spatial dependence. Range represents the separation between points pairs at which the sill is reached (distance at which there is no evidence of spatial dependence) (Rahman, 2006).

There are two types of kriging methods: ordinary which is the most widely used and assumes that the constant mean of dataset is unknown and universal which assumes there is an overriding trend in the data, the best used when we know the trend in our dataset to be able to give scientific justification to describe it. Dowman (2002) in Rahman (2006) stated that kriging is sensitive to inhomogeneous elevation data instead of those dataset can also be derived for a complex geomorphological features, as revealed by Chaplot *et al.*, 2006 in his research.

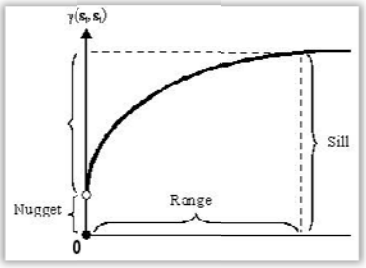


Figure 2-6. Relationship between nugget, sill and range

## 2.5.4. Australian National University Digital Elevation Model

Australia National University Digital Elevation Model (ANUDEM) interpolation methods were developed by Michael Hutchinson. This model was designed and optimized to have the computational efficiency of local interpolation methods, such as IDW interpolation, without losing the surface continuity of global interpolation methods, such as Kriging and Spline (Arc GIS Help).

ANUDEM method is designed to create a hydrological correct terrain models by hydrographic enforcement that will create a network of valleys and ridges and remove spurious sink and pits, figure 2-7. Moreover, locally adaptive ANUDEM gridding procedure is shown to be able to produce such representations for contour, stream – line and point data from less input data (Hutchinson and Gallant, 2000). Thus, this interpolation method is very useful to produce accurate representations of terrain shape and drainage pattern were primary need in various applications e.g. hydrology, geomorphology, geology, etc.

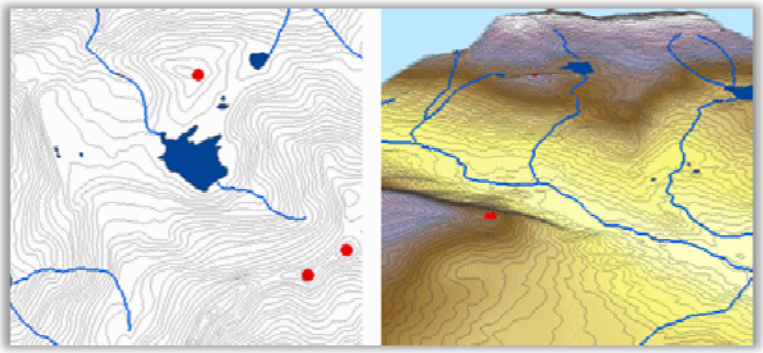

Figure 2-7. Terrain representation from ANUDEM interpolation (Source: resources.esri.com)

Some advantageous of ANUDEM – based interpolation method were underlined by Sinha, 2000 in Rahman, 2006 as follow:

1. Efficient interpolation processing time e.g. DEMs with over a million points can be easily interpolated using computer workstation.
2. The roughness penalty can be modified to preserve sharp changes in terrain associated with ridges, stream and other features.
3. A drainage enforcement algorithm that attempts to remove all sinks in the fitted DEM.
4. Drainage enforcement is further enhanced to incorporate streamline data supplied by user in interpolation process.
5. ANUDEM can recognize and preserve sinks in the landscape.
6. User can specify the output resolution of the DTM.

## 2.6. Application of DEM in Studying Volcanic Landform

Representation of terrain surface in form of DEM plays a fundamental role in modeling the Earth surface which can directly confer understanding of the nature of the process acting in the Earth surface (Hutchinson and Gallant, 2000) which made widely usage of DEM for different types of applications in geosciences including geomorphology.

Geomorphology is the area of study leading to an understanding of and appreciation for landforms and landscapes including continents and islands, those beneath water bodies, as well as those on the terrestrial planets and moons of our Solar System (Goudie, 2004). Geomorphology delivers the study of landform using four main aspects: morpho-genesis, morpho-chronology, morpho-arrangement and morphology (Zuidam, 1983).

Morphology delivers the general relief of landform through morphography, the descriptive aspects of geomorphology of an area and morphometry, the quantitative aspects of an area (Zuidam, 1983). Those aspects could be achieved by analyzing digital representation of surface known as digital elevation model (DEM). Terrain morphometry or commonly term as geomorphometry is an important component of terrain analysis and surface modeling (Huggett, 2007; Evans *et al.* 2003 in Miliaresis, 2008) to improve mapping and modeling in some field e.g. geomorphological and geological features of volcanic landform.

According to Huggett (2007), the resurgence of geomorphometry for various geosciences applications were measured due to two developments, first, development and use of GIS which allow input, storage, and manipulation of digital data representing spatial and non spatial features of the Earth's surface and second, the development of electronic distance meter (EDM) and global positioning system (GPS). Those developments made the process of making large-scale maps much quicker and more fun as well as made the modeling of surface topography in more various and broader ways.

Application of DEM is very useful in deciphering geomorphic and structural features in volcanic landform, especially those of large-scale edifices and deposits which be readily studied or identified in the field cannot (Székely and Karátson, 2004). Moreover, volcanic morphometric modeling provides reliable measurements of eruption edifice morphology and its derivatives, important for constraining both aggradation and degradation models of volcanic landforms (Rodriguez-Gonzalez *et al.*, 2009).

## 2.7. EDM for Monitoring Volcanic Deformation

For several decades, ground deformation studies in volcanic area have provided useful information to enable eruption forecasts and to constrain the shape and the evolution of volcano plumbing systems with time (Peltier *et al.*, 2009). By advances in remote sensing technologies, some methods for studying volcanic are provided e.g. utilization of LIDAR or SAR interferometry for monitoring volcanic movement. However, in most volcanic area, older surveying techniques i.e. leveling or distance measurement are still used to monitoring the movement of part of an active volcano.

Electronic distance meter is one of measurement techniques used to measure distance from fix base stations to reflectors. This measurement technique is based on the invariant speed of light or electronic waves in a vacuum (Davis *et al.*, 1981). EDM equipment consists of electro-optical (light waves) and electromagnetic (microwaves). The basic principle of electro-optical is the indirect information of the time required to travel between two stations and the velocity of light is the basis for computation of the distances, as shown in equation 4 and figure 2-8.

$$D = \frac{1}{2}(n\lambda + d) \quad \text{(Eq. 4)}$$

Where:

*D* is distance between *A* and *C*
*N* is integral number of wavelengths in the double path of light
*D* is increment

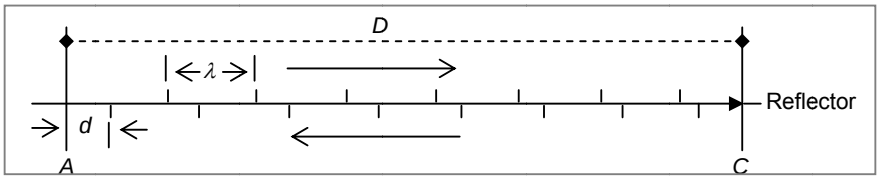


Figure 2-8. Measurement principle of EDM (Source: Davis *et al.*, 1981)

Monitoring of volcanic deformation is commonly conducted in form of trilateration or triangulation network depending on the area. For instance, for monitoring deformation of Mount St. Helen, scientists from USGS perform combination of triangulation and trilateration methods by measuring the position of the prisms from base station to reflectors or fixed prisms and horizontal angle between them (Klimasauskas, 2001) whilst for monitoring deformation of Merapi volcano, trilateration network conducted by VSI through MVO, USGS and US AID since 1988 for monitoring movement in the edifice and flank area, see figure 2-9 (Young *et al.*, 2000).

Since distance resulted from EDM is transmitted through atmosphere, temperature, atmospheric pressure and humidity will strongly affect the distances. These three parameters are computed in very detail distance measurement but they often eliminated when using electro – optic equipment (Brinker and Wolf, 1984).

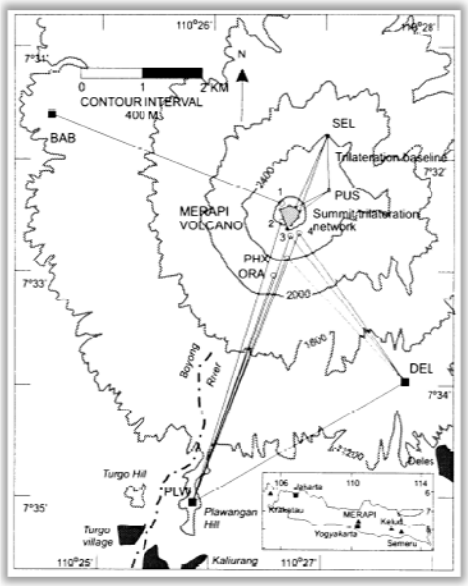


Figure 2-9. Geometry of the observatory network of fixed prisms in Merapi Volcano (Source: Young *et al.*, 2000)

## 2.8. GIS for Morphologic Analysis of Volcanic Landform

Advances in GIS technology, the rising availability of high accuracy DEM and remote sensing imagery have led to the growing application of GIS tools in many areas of geomorphology. In geomorphology, spatial and temporal relationships between features and processes are essential. Thus, GIS techniques are extremely useful for the representation, visualization, analysis and comprehension of landforms (Remondo and Oguchi, 2009) through morphologic analysis.

GIS also allows various computations using numbers of pixel size, interpolation methods to produce appropriate DEMs for different types of applications which considerable as no single interpolation method would fit all of them. Moreover, much of valuable information of surface attribute can be developed from interpretation of DEM by means of GIS such as general geomorphometric parameters (slope, aspects and curvature both profile and plan) and specific geomorphometric parameters (hydrologic modeling, view shade analysis) (Klimanek, 2007).

# Chapter 3. Merapi Strato – Volcano

*This chapter gives the overview of the study area including general overview of Merapi, selection of the scope of study area, summary of Merapi history, characteristic of Merapi eruptions and morpho chronology of lava domes.*

## 3.1. General Overview

Merapi strato – volcano, Indonesia is located approximately 25 kilometer of the north part of Yogyakarta city, on the administrative boundary of Central Java and Yogyakarta Provinces (Figure 3-1). Merapi strato – volcano is composed of layers of hardened lava, ash and rock from previous eruptions with a high, steep – sided slope and flank profile that concave downward around the vent on crater (Marti and Ernst, 2005). Crater area is the most dynamic section of Merapi due to almost unrest activities.

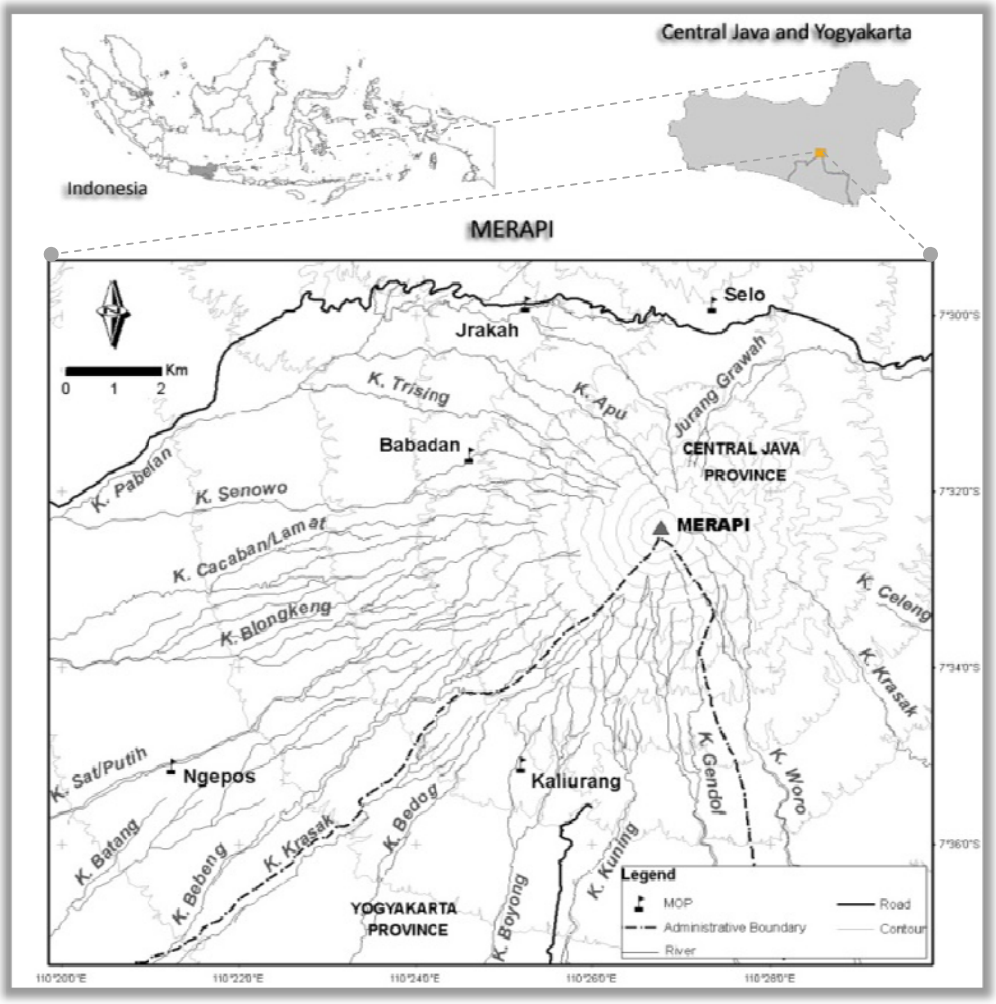


Figure 3-1. Sketches map of Merapi volcano, Indonesia (Source: own illustration)

Merapi strato – volcano belongs to a cross – island chain of four volcanoes comprising from north to south: Ungaran – Telemoyo – Merbabu – Merapi (Figure 3-2) (Ratdomopurbo and Andreastuti, 2000; Camus *et al.*, 2000; Verstappen, 2000). This

volcanic area is resulted from the south–north subduction of the Indian oceanic plate beneath an arc system that in Java is transitional from continental to oceanic (Hamilton, 1979 in Camus *et al*., 2000).

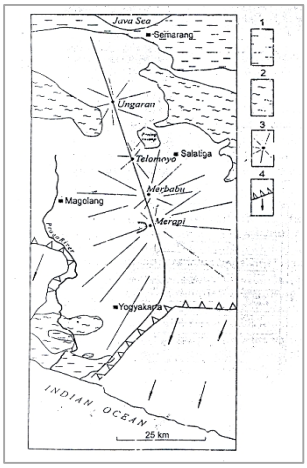


Figure 3-2. Sketch map of the alignment Ungaran, Telomoyo, Merbabu and Merapi (Source: Verstappen, 2000)

The gradual steepening of subduction plane in the course of time results in a gradual outward displacement of the rising magma and thus the central of activity. The oldest volcanism in the north and the active Merapi marks the south end (Verstappen, 2000). This gradual steepening seems to affect the evolution of Merapi, in which the rate of flow may have decreased and thick and long lava flows were progressively replaced by smaller ones, then by slow dome extrusions (Camus *et al.*, 2000). This may also employ decreasing in explosivity of Merapi, from explosive eruption (VEI 4) in ninetieth century into more effusive eruption (VEI < 3) in twentieth century.

## 3.2. Selection of Research Area

According to Ratdomopurbo and Andreastuti (2000), Merapi strato – volcano can be divided to four morphologic units: volcanic cone composed of lava and pyroclastic materials, upper volcanic slope consisting of lava and pyroclastic deposition and lahar, middle volcanic slope and volcanic foot slope which consist of pyroclastic deposition, lahar and alluvium.

This research was focused on morphologic analysis of Merapi edifice and volcanic cone, later on called summit area, with some extend of upper volcanic slope, called vicinity area (Figure 3-3). Merapi edifice and its volcanic cone are dynamic areas due to volcanic activities that change the morphology and direction of dome collapse. Some extent of upper volcanic slope was utilized to observe morphologic factors e.g. drainage pattern, lineaments and major rivers affected by pyroclastic flow for a comparison of past time eruption and for prediction of near future eruption.

## 3.3. Summary of Merapi History

According to Camus *et al*., 2000, the history of Merapi can be divided into four main periods: Ancient Merapi, Middle Merapi, Recent Merapi and Modern Merapi whilst Ratdomopurbo and Andreastuti, 2000 divided Merapi into Pre – Merapi, Ancient Merapi, Middle Merapi and Modern Merapi periods. However, they seem to refer to same development processes and evidences. Thus, the summary of Merapi history described below was a combination among their publications. Some arguments were also raised by Newhall *et al*., 2000 questioning the volcanic structures and processes related to their interpretations.

### 3.3.1. Pre – Merapi

Gn. Bibi is evidence from pre – Merapi history (Ratdomopurbo and Andreastuti, 2000), located on Merapi northeastern flank, in which Ancient Merapi lie. Gn. Bibi interpreted as a residual hill of a volcanic structure older than Ancient Merapi based on petrography (basalt and basaltic andesite) and the provisional age of sample collected close to the top of the hill (Camus *et al*., 2000). This interpretation was questioned by Newhall *et al*., (2000) which argue Gn. Bibi to be a vent that erupted through and built itself on the upper flank of Old Merapi.

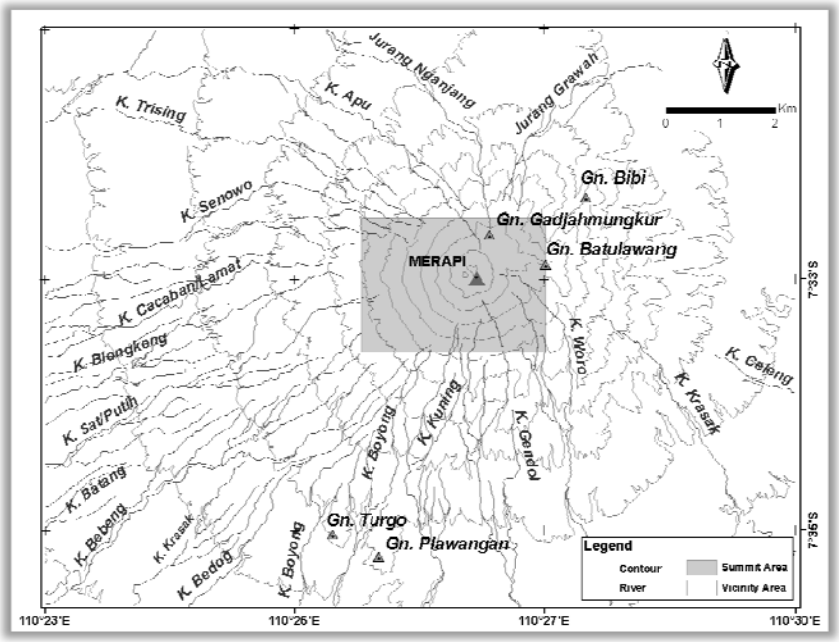


Figure 3-3. Study area of this research with some volcanic structures (Source: own illustration)

### 3.3.2. Ancient Merapi period

The ancient cone of Merapi was composed mainly by auto – brecciated lava flows, St. Vincent – type nuees ardentes and lahar deposition. Gn. Plawangan and Gn. Turgo are two hills in the southern slope of Merapi which composed of basalt flow and were interpreted as the remnant of excentric vents belonging to Ancient Merapi (Van Bemmelen, 1949 in Camus *et al*., 2000). Absence of dikes, plugs, near source spatter or cinder or other evidence of a vent raised a doubtful that these two hills were flank vents instead these hills might be blocks that rotated slightly during gravitational failure of Proto Merapi (Newhall *et al*., 2000). This doubtful was then compromised by Camus *et al*., (2000) that those hills could be also interpreted as two mega blocks shifted only several km from their origin which has important consequences for the shape of avalanche caldera in the middle Merapi period.

### 3.3.3. Middle Merapi

Two depositions of middle Merapi, Gn. Batulawang and Gn. Gadjah Mungkur comprise two thick series of andesitic lava flows and St. Vincent-type nuees ardentes deposits, separated by the north–south "Kukusan fault", figure 3-4a. This fault is now interpreted as the southern branch of an avalanche caldera (Berthommier, 1990 in Camus *et al*., 2000). Gn. Batulawang series is cut by the avalanche caldera; occurs only at the east of the caldera wall. The younger Gadjah Mungkur series constitute a post collapse cone within the caldera, but some lava flows spill over the north–east rim of the avalanche

crater, figure 3-4 b (Camus *et al*., 2000). Pasar Bubar crater, located in west part of Gn. Gadjah Mungkur, is also formed during this period (Ratdomopurbo and Andreastuti, 2000).

### 3.3.4. Recent Merapi

Deposits of the Recent Merapi Period cap Middle Merapi deposits and are composed of thinner lava flows, and St. Vincent-type nuees ardentes deposits. Episodes of violent phreatomagmatic activity occurred twice during this period. The first episode (approximately 2220–1470 y BP) emplaced widespread subplinian and phreatoplinian deposits ("Gumuk" ashes); the second episode emplaced surge deposits, the Sambisari ashes (Camus *et al*., 2000).

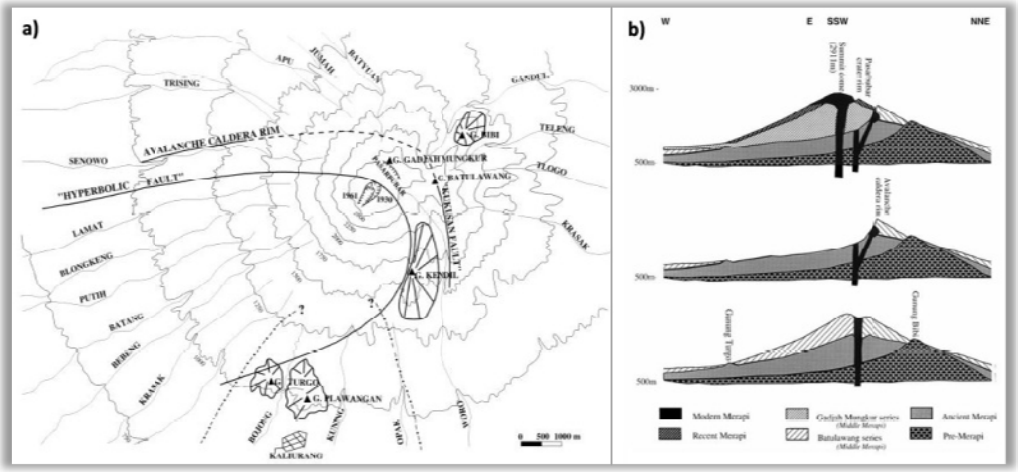


Figure 3-4. Structural features and evolution of Merapi: a) Main structural features, b) Structural evolution of before and after sector collapse (Source: Camus *et al*., 2000)

### 3.3.5. Modern Merapi

Modern Merapi is characterized by its "Merapi type activity", i.e. a more or less continuous growth of summit domes interrupted by collapses and phases of quiescence. According to Berthommier, 1990 in Camus *et al* (2000), this type of activity could have occurred at Merapi only 2–3 centuries ago. However, evidence of buried Morangan temple, destroyed soon after its edification in 9$^{th}$ century, is constituted by a series of thin (0.40–0.50 m) block and ash flow deposits, with gas pipes and charcoals and it is clear that "Merapi-type activity" was effective at this time. Newhall *et al*., 2000 dated block and ash flows deposits of buried Morangan temple at 2460 y BP. So, Camus *et al*., 2000 assume that the present or Modern type of activity progressively took the place of the former during the Middle Merapi period.

## 3.4. Characteristic of Merapi Eruptions

Characteristic of Merapi volcano has been specified by three major factors: characteristic of magma: magma composition, its viscosity, water and gas contains; internal structure and magma supply. Those factors determine type of Merapi eruption that categories as low level Vulcanian, characterized by development of dome with low to medium explosion and almost always accompanied by pyroclastic flows or nuees ardentes in France term (Ratdomopurbo and Andreastuti, 2000).

Two types of Merapi eruption that generates pyroclastic flow: fountain collapse nuees ardentes or St. Vincent – type and dome collapse nuees ardentes or Merapi – type, figure 3-5. St. Vincent – types are much larger and farther affecting area, whilst Merapi –types

comprise mainly the effusive growth of viscous lava domes and lava tongues or coulee, with occasional gravitational collapses of parts of over steepened domes to produce the nuees ardentes (Voight *et al*., 2000).

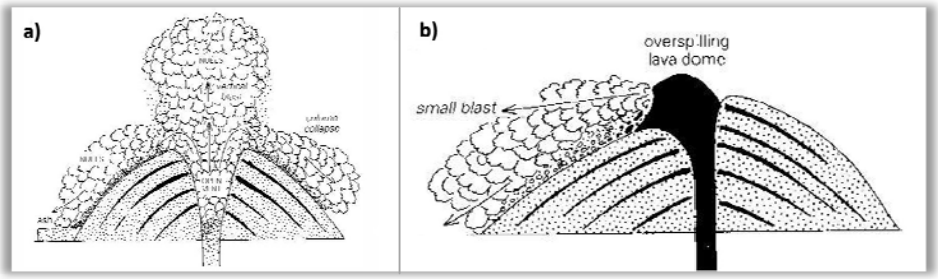


Figure 3-5. Types of Merapi eruptions that generate pyroclastic flow, (a): fountain collapse nuees ardentes or St. Vincent – type; (b). Dome collapse nuees ardentes or Merapi – type (Source: ThinkQuest, 2001)

Merapi – type eruptions usually associated with development of domes determined by magmatic type that produced. Magmatism in Merapi is a transitional from andesitic to basaltic, which performs mainly two types of magmatic extraction: lava dome and coulee. Lava dome is thick, bulbous, usually volatile poor masses of highly viscous lava whereas coulee is defined as stubby flows transitional between conventional flows which, in Merapi case, will be formed when dome growth in such steep slope e.g. sides of crater rim (Voight *et al*., 2000).

Development of domes in Merapi activities comprises of such a complex processes of growth and destruction. Growth phases of domes are process of morphologic changes because of the enlargement of its anterior, known as endogenic dome growth. These phases can be divided into four comprehensive processes, first, diameter enlargement, second, diameter and height enlargement, third, height development with constant diameter, and critical phase.

Critical phase of dome growth related to dome collapse occurs when the growth slower with constant height. In this phase, domes will be collapse accompanied explosion because of instability of lithostatic pressure of dome ($P$) and internal pressure ($P_{ex}$). The explosion will occur when $P_{ex} \leq P_2$, see figure 3-6. Soon afterward, dome becomes solid and magma will extrude through other weak zone, which could be through region adjacent to the dome or remnant of old domes, in case crater rim is already fulfill by volcanic materials (Ratdomopurbo and Andreastuti, 2000).

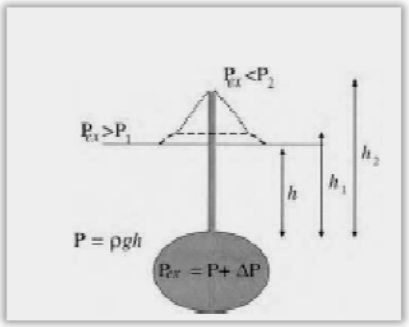


Figure 3-6. Schematic diagram showing the relation between lithostatic pressure *P* and eruption driving overpressure *P*ex in the magmatic system of an active volcano (Source: Davidson and Silva, 1999)

Remnant of old domes are a critical point to observe because weathering and hydrothermal processes make them more vulnerable to magma extrusion which then perform sliding or collapse i.e. southern flank of 1961 crater rim, lava 1911 - 1913, collapsed during the eruption phases in 2006. Increasing in magma extrusion that moment was triggered by earthquake struck in the middle of 2006 eruption. Thus, morpho

chronology of remnant of old domes, later on stated as remnant of domes for lava domes and coulees, in Merapi edifice becomes important.

## 3.5. Morpho – chronology of Domes

Ever since Merapi activities have been recorded, it has erupted for 53 times underlining significant differences in characteristic of eruption between ninetieth and twentieth century. In the 1800s, explosive eruptions of relatively large size occurred (to VEI 4); some associated with St – Vincent types while Merapi activity has comprised mainly Merapi – types during the twentieth century (Voight *et al*., 2000). This significant difference has made recent Merapi eruptions less destructive than that of ninetieth century and morphologic changes of summit area accomplishes of process development and destruction of domes or coulee.

Morpho – chronological of domes in twentieth and twentieth first centuries become one focus on this research since their growths and collapses perform morphology of summit area. On the other hands, remnant of dome which accomplishes Merapi edifice become important when the crater rim has already filled by volcanic material leading magma to find weak zone along crater rim. Strong fumarolic activity, weathering and erosion made remnant of domes become one of the weakest zone, indicated by some fractures at south flank in which remnant of dome located (Subandriyo *et al.*, 2009; Camus *et al.*, 2000). Thus, remnant of domes could become point of magma extrusion and sliding or collapse as well which could give preliminary assessment of collapse direction in the future.

Historical data of Merapi eruption and morpho – chronology of remnants of domes in Merapi edifice was summarized from Voight *et al*. (2000), MVO (2000) and CVGHM (2006). Terms used are dome collapse nuees ardentes, refer to Merapi – type eruption and fountain collapse nuess ardentes, refer to St. Vincent – type eruption. History of Merapi eruption in during twenty and twenty first centuries is described below:

1902 - 1904

Merapi activities in the beginning of twentieth century were begun on Mesjidanlama crater rim that already filled in by lava 1883. A dome began to growth in east of Mesjidanlama, a precursor of East dome or Gn. Anjar, in which the activities of Merapi centered until present day. On January 1904, several explosions destroy eastern part of East dome and "partially created" Woro breach, caused nuees ardentes that travelled 6 km, to the east–northeast and producing heavy ash fallout in Boyolali.

1905 - 1906

A less violent explosion occurred in southeast – east part of East dome, in which undifferentiated Merapi type explosion extruded to Woro valley through reopen Woro breach. After explosion, the dome resumed growth and enlarged beyond north of Mesjidanlama crater causing gravitational collapses.

1909 – 1913

Locus of active volcanism shifted towards the northwest, and the advancing dome lava overrode the crater rim. A few nuees ardentes were reported during 1909 and 1910, probably due to minor dome collapses, considered as Merapi – type.

East dome or Gn. Anjar continued to growth through 1911, especially at the northwest side, with the summit taking on a more symmetric shape. On the west side of G. Anjar, a second summit dome rose in 1911–1912 and ultimately it became higher than G. Anjar by July 1912, refer to figure 3-7. This West dome had an unstable front on the southwest that collapsed periodically, generating nuees ardentes toward the Batang.

1920 – 1923

Explosion destroyed west part of the summit, below dome of 1911 – 1913. A dome rose in this crater and the activity ended in February 1921. A year after, series of explosions were accompanied the passage of lava and block avalanches from the west dome. In April 1922, rock avalanche directed to Blongkeng without any precursor. Vapor emissions and minor rockfalls were reported after 1923 and a plateau-like depression was described on top of G. Anjar which probably as a result of the sinking-back of lava inside the dome.

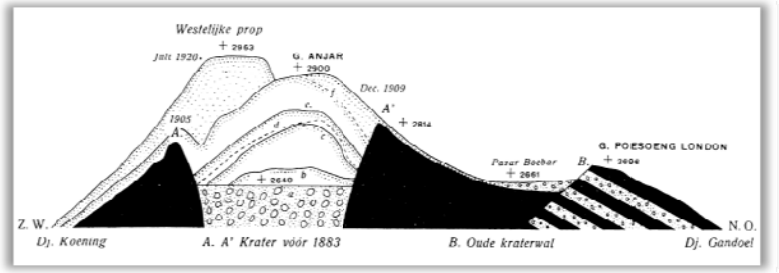


Figure 3-7. Original cross section through Merapi summit showing lava dome growth from 1902 to 1920 in 1872 crater (Source: Voight *et al*., 2000)

1930 – 1931

Series of spectacular nuees ardentes travel down as far as 12 km to Senowo, Batang and mainly Blongkeng valleys followed lava flows which broke out under pre – existing domes until 18 December 1930. A vast summit depression, 850-m long and open to the west to an elevation of 2150 m, resulted from the paroxysmal activity and indicated the gravity collapse of the old dome complex as well as the new lava. Figure 3-8a showed the opening crater of December 1930 eruption and the lava tongue emerging from a vent near the foot of the crater.

Eruption during this period destroyed West dome, western part of East dome and L, abbreviation of lava dome, 1922 and a small dome, called lava central, grew inside the crater formed by the eruptions. Gegerboyo hill is a remnant of southern part of west dome, sometimes referred as L 1911 – 1931, according to time development of West dome (K. Barat). Depression under remnant of East dome (K. Timur) by eruption is then referred as *Kawah Mati*. Morphologic changes of summit area during this period is displayed in figure 3-8b (MVO, 2000).

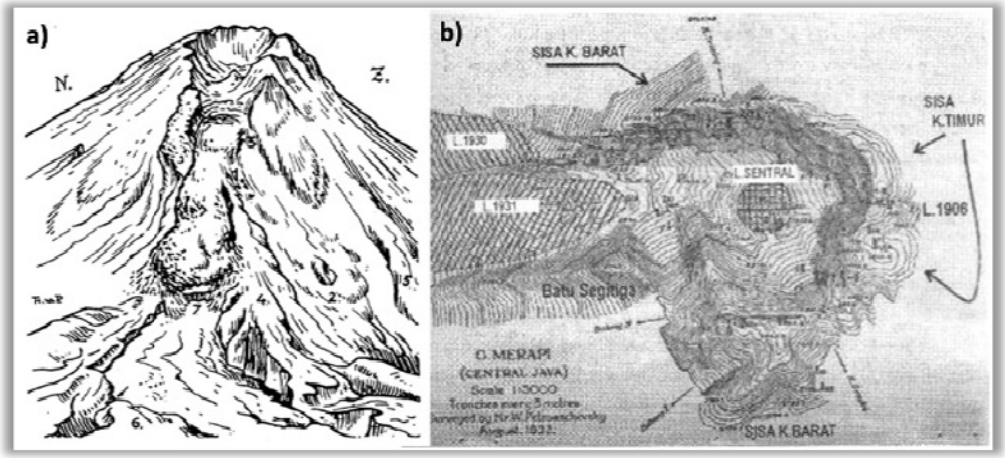


Figure 3-8. Sketches showed morphologic changes during 1930 – 1931 eruption, a) Original sketch on 28 May 1931, by Th. W. van der Plas (Source Voight et al. 2000), b) Summit topography 1932 by Petroedchecsky which shows topographic condition formed by eruption 1930 (Source: MVO, 2000)

1933 – 1934

The activity was begun in October 1933 when an explosion in lava central generating pyroclastic flow. In May 1934, a new dome grow into a complex lava tongue or coulee, that flowed around, and then over, L 1931 and part of L 1930. Simultaneously, in September, the hotter western part of the dome began to separate from the cooler eastern part, and ultimately formed a horse-shoe shaped cavity inside, of which further flows developed. Lava flux decreased in October, and then accelerated again, leading to collapses on 17 November that resulted in destructive nuees ardentes running 7 km down the Senowo. These activities had renewed summit morphology which destroyed by eruption 1930 - 1931.

1939 - 1941

An explosion, which occurs in the higher part of crater 1930, started this period of activities and produced small nuees ardentes to western, southern, and southeast slopes. An explosion pit with a diameter of about 100 m and depth of 50 m was formed in the 1934 lava. A second explosion was seen 23 December, and on 24 January 1940 an eruption plume reached a height of 3–3.5 km, generating hot avalanches in Gendol and Woro valleys. In February 1940, a lava dome then grew quietly until the lava reached the west rim of the depression in August whereupon rockfalls and small pyroclastic flow rolled down the western slope. The dome was then subsided in January 1941 which then marked as the end of period activity.

1942 - 1945

Series of explosion started this period of activities. First, in May 1942, an explosion occurred between southern part of 1940 domes and crater rim 1930 and opened *Pintu Woro* or Woro breaches. Second, on June 1942, explosion in north – northeast formed breaches toward Trising valley, called Pintu Trising or Trising breaches. Those two explosions which open Woro and Trising breaches were presumable occur because of lithostatic pressure of the active dome 1940 (MVO, 2000). On July 1942, a new lava rose in western part of lava dome 1940 which then alternated by new dome growth in southern part of dome 1942, lava dome 1943, see figure 3-9.

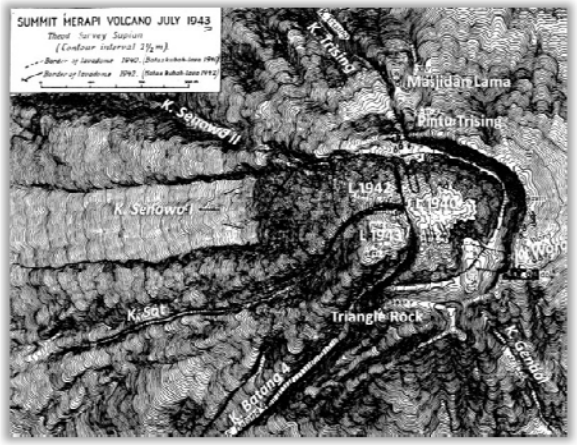


Figure 3-9. Topographic survey of Merapi summit during July 1943 (modified from Voight *et al*., 2000)

1948

On 29 September 1948, an explosion began a new effusive episode. The new lava completely covered the L 1942 and L 1943, and expanded to north – northeast direction which then closes Trising breach and upper part of L 1888.

1953 – 1956

The ensuing activity including dome growth, which spreads lava a few hundred meters toward the north comprised nuees ardentes and rockfalls was started on March 1953. On

January 1954, Merapi erupted with a series of pyroclastic flow that advanced 5 km in the Apu valley but type of pyroclastic flow could not be distinguished since summit area was covered by cloud. However, dome collapse involving the axis of the 1953 lava flow seems probable due to 150 m open breaches toward north. In mid – June of 1954, the large lava flow developed toward north and dome growth continued into 1955 and filled the breach.

On January 1956, an explosion occurred in between L 1948 and L 1955 and new dome grew to fill the breaches formed by the explosion. This lava domes, referred as L 1956, remains until present day.

Activities in 1953 – 1956 had changed morphology of northern part of crater rim 1930. L 1953 – 1955 and L 1956 covered northern part of L 1940 changing form of *Kawah Mati*, or dead crater, which is presumable it is not real crater. *Kawah Mati* is bordered by East dome in the eastern and southern part, L 1940 in the western part and L 1956 in the northern part.

1957 - 1958

New lava extruded in between L 1934 and L 1948 in which L 1931 and L 1942 was formed. Fresh lava erupted in the upper Batang breach and covered lava of 1931 and 1934 producing dome collapse nuees ardentes reached 4 km from crater rim. In 1957 and 1958, rockfalls occurred toward the Sat and Senowo drainages, with the number of rockfalls decreasing between July and December 1958, figure 3-10.

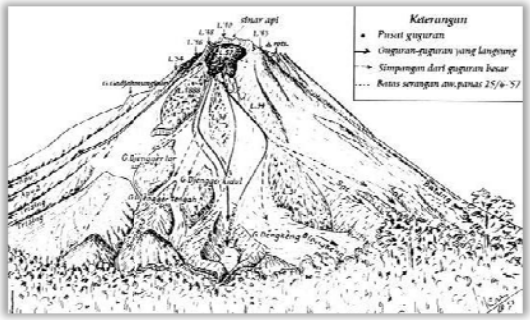


Figure 3-10. Merapi viewed from the west on 5 July 1957, unpublished sketch by Merto (Source: Voight et al., 2000)

In 1958, a topographical theodolite survey of the summit area was completed, the first since 1943, (figure 3-11) showing the distribution of lava flow until 1954. In this map, crater rim in 1943 drew as a horse-shoe shape open to west. By 1958, only the south and east rim remained, the north rim was covered by lavas extruded in 1948 and 1953 – 1956 while south rim was separated about 50 m from the lava dome.

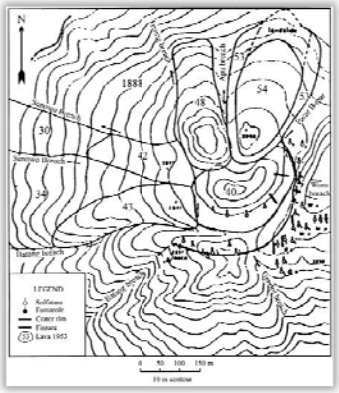


.

Figure 3-11.Maps of the Merapi summit showed distribution of lava flows to 1954 (Source: Voight *et al*., 2000)

1961

Activities during 1961 consisted of several complex processes, including fresh lava flow, dome collapses, fountain collapse. Fresh lava flowed through L 1957 vent toward Batang

on 11 April 1961. On 13 and 18 April, dome collapse nuees ardentes rolled down the Batang to extended distance of 6.5 km to Batang and destroyed Gendeng village. A second point of active avalanching also developed through the 1957 lava dome, where avalanches and nuees descended in the Senowo on 17 April.

On 7 May 1961, fountain collapse nuees ardentes with 150 m incandescent lava rose and 3 km rising plumes above the crater near Batang breaches, producing nuees ardentes to Batang and simultaneously in the Senowo, Woro and Gendol. The paroxysm occurred on 8 May when eruption generated an extended nuees ardentes up to 12 km to Batang which created a depression on the southwest part of summit. During this phase triangle rock, southern part of crater rim 1930, was collapsed widening Batang breach. On 27–28 November 1961, 90% of the dome was destroyed by a succession of 119 dome-collapse nuees reaching as far as 8 km in the Batang. No new effusion of lava was noted after the dome collapse, and only minor activity followed in the next 5 years.

Merapi activities during this period had changed morphology of summit area. Active crater rim 1930 was replaced by new crater rim, known as crater rim 1961, which remains until (at least) last of twentieth century, see figure 3-12.

Figure 3-12. Topographic map of Merapi summit 1962, sketch by S. Harto (Source: CVGHM, 2006)

1967 – 1969

After explosion which generated nuees ardentes toward Batang, a new dome growth began on 11 April. The paroxysm occurred on 7–9 October 1967, which produced 39 nuees toward Batang, the largest one reached 7 km. A large portion of L 1967 collapsed, and northwest side of Gegerboyo ridge, south part of crater rim, was eroded. Fresh lava effused in October to form a coulee.

On 7 – 8 January 1969, new phase of eruption was accompanied by a series of nuees ardentes, advancing 3 km to 13.5 km down the Bebeng and also as much as 8 or 9 km along the Batang, Krasak, and Blongkeng, burning several villages. Most nuees were considered as dome-collapse type, but as the eruption clouds rose several km above the crater, some of the largest nuees were described as “explosion - type”. According to Newhall *et al*., 2000, depositions of nuees ardentes of 1969 contained numerous breadcrust bombs, and thus represent explosion events or fountain collapse. By 9 January 1969, a new dome began to emerge, flowing 400 m to west.

1972 – 1974

This period of activity began on 6 October 1972 with an explosion centered between L 1961 and L 1969 in upper Batang sector of summit creating a black ash-plume with lightning. Fountain-collapse nuees ardentes invaded the Batang for 3 km, and a few mm of ash fell at Babadan. The explosion produced a small circular crater on the 1969 dome. Another explosion continued to produce an ash plume 700 m high, with fallout extending

to 7.5 km from summit on December 1972. Similar explosions occurred in January and February of 1973.

In April 1973, glowing lava rose in the October 1972 crater and slow effusion continued to May until almost all of lava 1969 was covered. This glowing dome then produced a dome-collapse nuee descended the Batang valley for 6 km, and lava effusion resumed. On 19 December, a new explosive phase generated nuees ardentes that extended to 7 km down the Bebeng and 5.5 km down the Batang and Blongkeng.

1976 – 1979

On the beginning of March 1976, nuees ardentes descended the Batang, Blongkeng, and Bebeng valleys as far as 6 km. Dome growth continued, accompanied by sporadic rockfalls and multiphase earthquakes. In January 1978, a collapse of a section of the 1976 crater and partial destruction of the dome took place as a result of a series of explosions. A new dome began to form over the remains of the 1967 and 1973 domes, and descended as a lava tongue to the southwest. In August, a dome collapse nuee reached 6 km and rockfalls continued until December 1979, when activity stopped.

1980 – 1983

The activity of Merapi during this period was continuing previous episode of eruption. Dome growth was continued before finally collapse on 2 December 1981 with slow effusion until June 1982. On 22 and 23 November 1982, collapse of lava dome, possibly followed by a gas explosion, led to nuees ardentes that travelled as far as 8.4 km, figure 3-13. A new dome emerged and continued to growth until March 1983. By August, this new lava had completely covered the old dome with combined volume of 1.2 million m3. Nuees ardentes extended 5–7 km down the Batang, Bebeng, Putih and Krasak valleys. By nightfall of 15 June, it was confirmed that crater had been emptied of post-1979 lava dome.

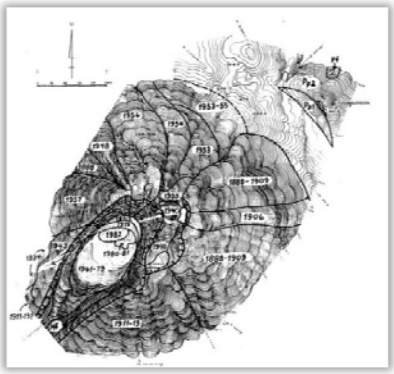

Figure 3-13.Topography and interpreted ages of lava flows and dome lobes on Merapi summit based on topographic survey of 1979 (Source: Voight et al., 2000).

1984 – 1991

The activity during this period was begun on 15 June 1984 where explosions followed by some nuees ardentes invaded Batang, Bebeng, Putih and Krasak with 9 km extended area (Ratdomopurbo and Andreastuti, 2000). Series of explosion emptied all domes formed in 1977 – 1983. These explosions were followed by rapid, then waning, dome growth. Dome volume reached about 2.8 million m3 by December 1984, and growth continued through March 1985.

On 10 October, 1986, and for the next 5 days, the dome was partially destroyed by a series of nuees ardentes, flowed to Putih that may have been prompted by strong summit rains. No seismic precursors were recognized. Dome growth resumed at an average rate of 15,000 m3 per day to February 1987, after which only the upper part of the dome grew. Dome volume was six million $m^3$ by September 1988 and 6.8 million $m^3$ by November 1991. Remnant of dome from this period was referred as L 1984 – 1986.

1992 – 1993

On 20 January 1992, lava broke out on the northeast flank of the L 1984 – 1986, or referred by Ratdomopurbo and Andreastuti as L 1986, accompanied by incandescent rockfalls and by dome-collapse nuees ardentes travelled as far as 4.5 km down the Sat valley after 31 January. Nuee activity then declined but dome growth continued and overlapped the northwest crater rim, in between L 1957 and L 1986 (Ratdomopurbo and Andreastuti, 2000) and caused incandescent rockfalls toward the Senowo.

1994 – 1998

In 1994, a resurgence of dome growth began, adding a new lobe directed to the southwest on the top of L 1992. Rockfalls had produced a talus and rockfalls deposit build up against the south runout-channel wall. As a result, some incandescent rockfalls were able to jump out of the channel and move down the south flank, towards the Boyong valley which was insufficiently appreciated, because the south sector of Merapi had not been affected by hazardous events for a long time.

On the morning of 22 November, with volume about 2.6 million $m^3$, the dome collapsed in a series of nuees ardentes that travelled south–southwest and also south, as far as 6.5 km without short term precursors. In the Boyong valley, near Turgo and Kaliurang, 64 were killed and dozens more seriously burned (Shelley and Voight, 1995 in Voight *et al*., 2000). Over 6000 people were evacuated after the disaster and authorities decided to permanently resettle about 2700 persons from higher elevation villages.

In 1995, new lava dome growth resumed from the vent of collapsed lobe, figure 3-14. The growing dome then produced a dome-collapse nuee moved 3.5 km to the upper reaches of the Boyong and Krasak drainages on 9 August 1996.

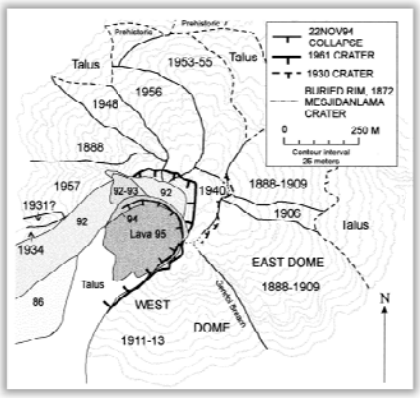


Figure 3-14. Topography and interpreted ages of lava flows and dome lobes, with emphasis on activity in the late 1980s and 1990s (Source: Voight *et al*., 2000)

The 1997 eruption included dome-collapse nuees ardentes on 14 January and a vulcanian explosion on 17 January that produced a 4-km high plume and generated a fountain-collapse nuee ardente. The 11 July eruption involved 36 nuees ardentes advancing southwest as far as 7 km, and another series of 25 nuees occurred on 19 July with runouts to 5.5 km.

In 1998, the activity was started by creeping of L 1957, which form crater rim 1961 in west – northwest direction. Explosion destroyed most part of L 1957 while L 1997 remained. Important nuees ardentes, some with 6 km runout, also occurred July 1998 toward Boyong and Krasak. Morphologic changes of summit area were observed as new depression orientation of west – northwest and new lava dome emerged through vent of collapse lobe.

2001

After two year of quiescence, Merapi showed increasing in activity on 9 January 2001 by intensive rockfalls from upper part of L 1998 toward Bebeng (6 km), Sat/Putih, Lamat and

Senowo valleys as far as 4.5 km. New lava emerged soon after, with slow effusion. By 29 January, volume of new dome was reported as much as 0.65 million $m^3$, which then producing dome collapse nuees ardentes on 10 February 2001 toward Bebeng, Sat/Putih, Lamat and Senowo. At the end of eruption, only small part of L 2001 remained, covering upper part of L 1997 – 1998. L 2001 can be clearly observed from MOP Babadan.

2006

Merapi activities in this period were started by emerging of new dome in between Gegerboyo and L 1997. New dome grew toward south and filled area toward Gendol valley with average of 0.2 million $m^3$ per day. The average of dome growth decreased to 0.07 – 0.15 million $m^3$ per day after 88 dome collapse nuees ardentes invaded 4.5 km to Krasak and Boyong (mainly) and small nuees to Gendol on 15 May 2006.

After an earthquake on 27 May 2006, the dome growth was renewed to 0.17 million $m^3$ per day. Important nuees occurred on 5 June 2006 because some part of Gegerboyo collapsed, widening Gendol breaches and changed the direction of nuees ardentes toward Gendol as far as 4.5 km (mainly). New dome then emerged inside the cavity. This dome, L 2006, can be observed from MOP Babadan (last viewed in September 2009) and can be clearly distinguished from others because of its' color.

Based on Merapi historical eruptions in twentieth and twentieth first centuries above, historical eruptions and remnants of domes on summit area in present time were comprehensively summarized in table 3-1 and 3-2 respectively.

Table 3-1. Summary of Merapi eruption during twenty and twenty first centuries

| Year | Type of eruption | Direction | River Flowed and extent distance |
|---|---|---|---|
| **1902 - 1904** | Dome collapse | E | Woro (6 km) |
| **1905 - 1906** | Undifferentiated | E | Woro |
| **1909 - 1913** | Dome collapse | SW | Batang |
| **1920 – 1923** | Undifferentiated | W – SW | Blongkeng |
| **1930** | Undifferentiated | NW, W – SW, SW | Senowo, Blongkeng (12 km), Batang |
| **1933 – 1934** | Fountain collapse | NW | Senowo |
| **1939 – 1941** | No collapse | | - |
| **1942 – 1945** | Dome collapse | NW, SW | Senowo, Blongkeng, Batang |
| **1948** | No collapse | | - |
| **1953 – 1956** | Dome collapse | N | Apu (5km) |
| **1957 – 1958** | Dome collapse | SW | Batang (4km) |
| **1961** | | | |
| 17 – 18 April | Dome collapse | NW, SW | Batang ( 6.5 km), Senowo |
| 7 – 8 May | Fountain collapse | NW, SW, SE, E | Senowo, Batang (12 km), Gendol, Woro |
| 27 – 28 Nov | Dome collapse | SW | Batang (8 km) |
| **1967 – 1969** | | | |
| 1967 - 1968 | Dome collapse | SW | Batang (7 km) |
| 1969 | Fountain collapse | SW, W – SW – S | Bebeng (13.5 km), 9 km to Blongkeng, Batang , Krasak |
| **1972 – 1974** | | | |
| 1972 | Fountain collapse | SW | Batang (3 km) |
| 1973 | Dome collapse | W – SW | Blongkeng (5.5 km), Bebeng (7 km), Batang (6 km) |
| 1976 – 1979 | Dome collapse | SW | Batang (6km) |
| 1980 – 1983 | Dome collapse | SW, SW – S | 5 – 7 km to Batang, Bebeng, Putih, Krasak |
| 1984 – 1991 | Dome collapse | SW | Sat/Putih |
| 1992 – 1993 | Dome collapse | W | Sat/Putih (4 – 5 km) |
| **1994 - 1998** | | | |
| 1994 | Dome collapse | SW, SW– S, S | Bebeng, Krasak, Bedog, Boyong (6.5 km) |
| 1995 | Dome collapse | SW, S | 3.5 km to Krasak, Boyong |
| 1997 (14 Jan) | Dome collapse | SW, SW– S | Bebeng, Krasak, Bedog |
| (17 Jan) | Fountain collapse | SW– S, S | Krasak, Bedog, Boyong (6.5 km) |
| 1998 | No collapse | | - |
| 2001 | Dome collapse | NW,W – SW, SW | Senowo, Lamat, Bebeng (4.5 km) and Sat/Putih (6 km) |
| 2006 (15 May) | Dome collapse | SW – S , S, SE | 4.5 km to Krasak, Boyong, Gendol |
| (14 June) | Dome collapse | SE | Gendol (7 km) |

*Note: E: east, SE: southeast, S: south, SW: southwest, W: west, NW: northwest, N: north*

Table 3-2. Table of dome remnants, L: remnant of domes

| Eruptions | Dome/Coulee Produced | Remarks |
|---|---|---|
| 1888 | L 1888 | Remain in northwest direction, from activity before twentieth century |
| 1902 – 1904 | - | Continue to grow until destroyed by eruption 1909 |
| 1902 – 1909 | L 1988 – 1909 | Part of East dome, remain in northeast and southeast |
| 1905 – 1906 | L 1906 | Remain in east |
| 1909 – 1913 | L 1911 – 1913 | Some destroyed by eruption 1922, some remain in south (Gegerboyo) |
| 1920 – 1923 | L 1922 | Completely destroyed during the eruption |
| 1930 – 1931 | L 1930 | Small part remains, in northwest |
| | L 1931 | Covered by L 1934 |
| 1933 – 1934 | L 1934 | Covered by L 1957 |
| 1939 – 1941 | L 1940 | Covered by L 1992 – 1993 |
| 1942 – 1945 | L 1942 | Covered by L 1948 |
| | L 1943 | Covered by L 1948 |
| 1948 | L 1948 | Small part remains in northwest – north, others covered by L 1957 |
| 1953 – 1956 | L 1953 – 1955 | Some remain in north |
| | L 1956 | Some remain in north |
| 1957 – 1959 | L 1957 | Completely destroyed by during eruption 1997 - 1998 |
| 1961 | L 1961 | Completely destroyed by eruption 1967 – 1969 |
| 1967 – 1969 | L 1969 | Completely destroyed by eruption 1972 – 1974 |
| 1972 – 1974 | L 1973 | Completely destroyed |
| 1976 – 1979 | L 1977 | Completely destroyed by eruption 1984 – 1991 |
| 1980 – 1983 | L 1983 | Completely destroyed by eruption 1984 – 1991 |
| 1984 – 1991 | L 1984 - 1986 | Some remain in southwest, some covered by L 1992 |
| 1992 – 1993 | L 1992 | Some part remain in west |
| 1994 – 1998 | L 1994 | Completely destroyed during the eruption |
| | L 1997 | Some remain in southwest |
| | L 1998 | Some remain in west, part of it covered by L 2001 |
| 2001 | L 2001 | Small part in west |
| 2006 | L 2006 | Some remains in northwest |

Changing in direction of dome collapse over time was caused by changes in active sectors and (or) aggradation and degradation processes result in changes in low land areas along the crater rims (Voight *et al*., 2000). From historical data along last century, some highlight should take into account related to prediction in direction of dome collapse nuees ardentes or Merapi – type eruption in the future:

1. Central of Merapi activities was usually centered inside horseshoe shape crater rim which opens to certain direction, which remains unchanged for 30 – 40 years e.g. crater rim 1930 finally changed after 31 years, shifting the open direction toward southwest direction and crater rim 1961 changed after 45 years toward southeast direction.
2. Shifting in active sectors could be caused by remnant of lava dome blocking the active vent which causing the eruption driving overpressure ($P_{ex}$) less than lithostatic pressure $P_2$, figure 3-6. For instance, remnant of lava dome L 1940 caused shifting of central eruption during 1942 – 1945. Some experts of MVO stated that these events were caused by lithostatic pressure of symmetrical dome L 1940, blocking magma extraction through the vent so magma extruded through other weak zone, usually adjacent to remnant of dome and indicated by explosions.
3. Shifting in direction of lava dome collapse also caused by changing in low area along crater rims, in this case crater rim was were filled by remnant of domes i.e. L 1953 – 1956 moved toward north presumably because crater rim was filled by L 1940, western part of crater rim had already filled in by L 1942, L 1943, and L 1948 while south to northeast were protected by crater wall 1930, figure 3-11 as reference.
4. Eruption during 1994 – 1998 gave an indication that south ridges of crater rim 1961 or Gegerboyo (L 1911 – 1913), a remnant of West dome, and L 1888 – L 1909, a remnant of East dome, were a critical point to slide or collapse during the eruption because they already altered by hydrothermal and erosion process.

# Chapter 4. Research Methodology

*This chapter provides the methodology including data, software and equipment and method used to derive purposed objectives of this research, separated based on the activity during pre – field work, field work and post – field work.*

This research was focused on the morphologic changes of Merapi edifice to determine morphologic factors ascertain direction of Merapi – type eruption in the past and utilization of those factors to predict the direction of Merapi – type eruption and the affected area in the future. The accuracy and efficacy of input data to study morphologic changes were also assessed through initial interpretation, visual and statistical methods.

The research processes were divided based on three stages: pre field work, field work and post field work (Figure 4-1).

## 4.1. Pre – field Work

Pre field work activities were started by intensive literature review throughout books, journals, reports, and previous studies relevant to this research. Valuable information concerning data needed, methods used, softwares and tools used to achieve research objectives was delivered from those resources. Moreover, those resources provided lots of information useable during field work and post field work stage.

### 4.1.1. Data availability, software and equipment needed

In this research, sets of DEMs were required in order to monitor morphologic changes over 70 years. Those data were collected from several institutions related to Merapi hazard and disaster management during pre field work and field work, as shown in table 4-1. However, some data cannot be used in this research due to either low quality of surface representation e.g. ASTER GDEM and SRTM DEM or not fulfill requirement for delivering DEM e.g. aerial photographs of 1969 without calibration camera report.

Some software and equipment utilized to acquire data as well as to process, analysis and visualize the input data were listed in table 4-2.

Table 4-1. List of data used in this research, year represented here were production year

| Types | Scale/Res | Format | Sheet Nr/Area | Sources | Year |
|---|---|---|---|---|---|
| AMS Topo Map | 1: 50.000 | Hardcopy | 5020 II series T725 (Muntilan) | US ARMY Service | 1964 |
| Contour map | 1: 100.000 | Scanned | Merapi - Merbabu | VSI | 2001 |
| Topographic map | 1: 25.000 | Digital | 1408 – 244 (Kaliurang) | BAKOSURTANAL | 2000 |
| Contour map | 1: 5.000 | Digital | Merapi | SNVT SABO Project | 2006 |
| IFSAR DEM | 5 m | Digital | Merapi | Intermap Tech. Inc. | 2006 |
| ALOS Prism Image | 2.5 m (Pan) | Digital | Merapi - Merbabu | JAXA, Japan via LAPAN | 2006 |
| Hazard Map | 1: 100.000 | Digital | Merapi | VSI, BAKOSURTANAL | 1978 |
| EDM data (2006 – 2009) | - | Hardcopy | Merapi | MOPs | - |
| Statistics data | - | Digital | DIY and Central Java Province | Statistical Board | 2008 |

### 4.1.2. Overview of the Data

Surface representations were crucial for studying morphologic changes of Merapi edifice over time. Hence, overview of history, acquisition date and field checking date of data available was necessary as described below.

AMS topographic map

AMS topographic map of 1964 was compiled from AMS topographic map of 1944, sheet 47/XLI – C, 47/XLI – D, 48/XLI – C, planimetric detail revised by photo planimetric method, horizontal datum: Batavia coordinate system Transverse Mercator and vertical datum: mean sea level.

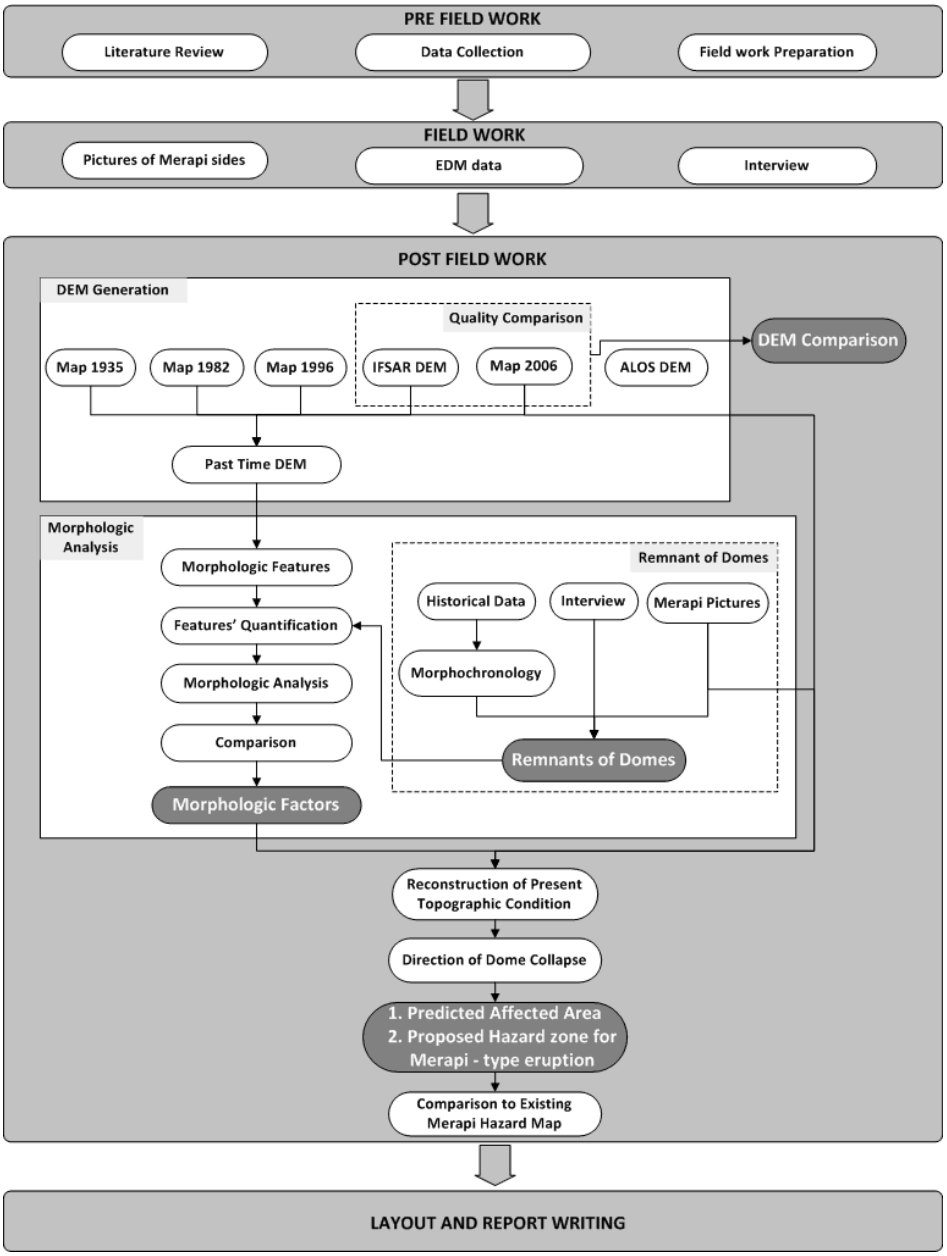


Figure 4-1. General Research Methodology (Source: own illustration)

From Dutch Colonial Institute website (www.kit.nl), the author figured out this map was copied from Dutch map of 1939 scale 1:25.000 sheets 47/XLI l partly revised in 1936, 47/XLI p revised in 1935 – 1936, 47/XLI q revised in 1934, 47/XLI D scale 1:50.000 surveyed in 1924 – 1925. Revision of topographic condition was carried out by topographic map of G. Merapi scale 1:10.000 from Volcanic Research Bureau, Bandung surveyed in 1935 – 1937. By studying the index, the author concluded that topographic representation of Merapi summit is representation of year 1935.

VSI contour map

VSI contour map was produced from mosaic orthophoto of aerial photographs scale 1:60.000 taken in 1981 – 1982 with end lap 60% and side lap 25%. Those images were processed by digital photogrammetric technique using Z/I imaging and Bentley Leica

softwares. Ground control points were taken in 1998 – 2000 using GPS static methods with approximate accuracy 1 meter. Hence, topographic representation of this map is situation of 1982.

The contour lines were produced from stereo model with coordinate system UTM zone 49 south and reference datum WGS 1984. Contour lines were overlying the orthophoto in scanned format so the visibility of contour lines was less.

Table 4-2. List of software and equipment

| No | Software and Equipment | Functions |
|---|---|---|
| Software | | |
| 1 | Adobe Photoshop | Visualization of graphs and pictures |
| 2 | Arc GIS 9.3 | Processing, analyzing and visualization of DEM data |
| 3 | Arc View 3.3 | Defining lineament and dome remnant orientations, ellipse parameters and azimuth and distance |
| 4 | ENVI 4.5 | Defining elevation of check points |
| 5 | Global Mapper | Converting IFSAR DEM to Arc GIS format |
| 6 | PCI 9.1 | DEM extraction from ALOS PRISM imageries |
| 7 | Microsoft Excel 2007 | Calculating EDM data and DEM quality comparison |
| 8 | Microsoft Word 2007 | Typing thesis report |
| 9 | Rozeta 2.0 | Drawing rose diagram |
| Equipment | | |
| 1 | Flatbed scanner | Scanning topographic map |
| 2 | GPS Garmin CS 76 | Plotting position of Merapi pictures taken, bench mark of EDM measurement |
| 3 | Panasonic LUMIX camera | Taking pictures of Merapi edifice and field work activities |
| 4 | Personal computer | Data processing, data analysis and result visualization |
| 5 | Printed Merapi sides pictures | Plotting remnant of domes in Merapi summit |
| 6 | Interview form | Filling the information related to distance measurement and precursor of Merapi eruption, information regarding the activities of Merapi |

BAKOSURTANAL topographic map

Topographic map from BAKOSURTANAL, known as RBI map, was produced from mosaic orthophoto from aerial photographs scale 1: 30.000 taken in 1993 – 1994 and field checked in 1996. The map was collected in digital format, using coordinate system UTM zone 49 south, horizontal datum: GDN 1995 which utilized WGS 1984 parameters, vertical datum: mean sea level. The topographic situation represented in this map was based on field survey in 1996.

SNVT SABO Project topographic map

This map employed photogrammetric technique to derive contour lines of Merapi edifice and surrounding area before 2006 eruption. Coordinate system used in this map is UTM zone 49 south, horizontal datum WGS 1984 and vertical reference: mean sea level. West - northwest part of Merapi edifice was covered by solfatara.

IFSAR DEM

IFSAR DEM was obtained from Intermap Technologies Inc. Denver, USA in form of digital surface model (DSM) with pixel size 5 m, geographic coordinate system, horizontal datum: ITRF 2000 and vertical datum: EGM 96. The acquisition date was in between earthquake at 27 May 2006 and Merapi eruption at 16 June 2006.

Some striped lines and voids were observed in vicinity area but the summit area is clear enough to observe. These errors occur due to the nature of data capturing process (technician of ExsaMap Asia, written communication).

JAXA ALOS PRISM imagery

Pairs of ALOS PRISM imagery 1B2 nadir and forward taken at 12 September 2006, after 2006 eruption, could be utilized to develop DSM. These images are radiometry and geometry corrected with coordinate system UTM zone 49 south, horizontal datum: WGS 1984 and vertical reference: WGS 1984. Most parts of study area were covered by cloud which may affect the DEM resulted.

Merapi Hazard Map

Merapi hazard map scale 1: 100.000 was produced by VSI in 1978 which divided Merapi hazard in three zone forbidden zone, first danger zone and second danger zone. The digital copy of this map was provided by BAKOSURTANAL.

## 4.2. Field Work

Field work activity was carried out to collect spatial data from relevant institutions, electronic distance meter (EDM) data, pictures of Merapi sides, sketches from Merapi Observation Post (MOP) and interview person in charge (PIC) at every MOP, as listed in Appendix A and showed in figure 4-2.

Figure 4-2. Activities during field work. Pictures from left to right, clockwise direction: recognition of remnant of domes from MOP Babadan, field work at MOP Jrakah, checking topographic map by David G. Rossiter from Tower at MOP Kaliurang, interview at MOP Ngepos and in the middle, distance measurement using Total Station at MOP Selo (Source: Field work 2009)

### 4.2.1. Electronic Distance Meter Data

Electronic distance meter (EDM) of fixed prism at Merapi summit is a part of *deformation study of observatory and summit trilateration networks* conducted by VSI through MVO, USGS and US AID since 1988 for monitoring morphologic changes due to magma extrusion (Young *et al.*, 2000).

Since complete EDM data could not be obtained through MVO, the author compiled EDM observatory network data from MPOs. Four of five MOPs: Kaliurang, Babadan, Jrakah and Selo conducted every day measurement depending on visibility of the prisms.

### 4.2.2. Pictures of Merapi Sides and Sketches from MPOs

Visual observation of Merapi edifice is one of the methods to determine morphologic changes as precursor of Merapi activity (Subandriyo *et al.*, 2006). In the past, sketches were drawn from every MPO to observe changing in summit morphology. However, nowadays, digital photograph replaces those sketches making difficulties to find and utilized them.

Pictures of Merapi sides were taken as additional information for recognizing remnant of domes on generated DEM since sketches were hard to find. With assistance from PIC in every MOP, all of remnant of domes could be delineated and named before finally cross checked to historical data, refer to section 3.5.

Cloud was the main obstacle to take pictures when along the day Merapi edifice was completely covered. Due to time constraint, pictures taken mainly focused from south, southwest, west, northwest and north in which Merapi activities in twentieth century

mostly directed. In case Merapi summit was covered by cloud, some pictures from other sources were used e.g. Jrakah picture was collected from Head of TAGANA Central Java Province, Ngepos picture from Sutikno *et al.*, 2007 and Deles picture from Google image, see figure 4-3.

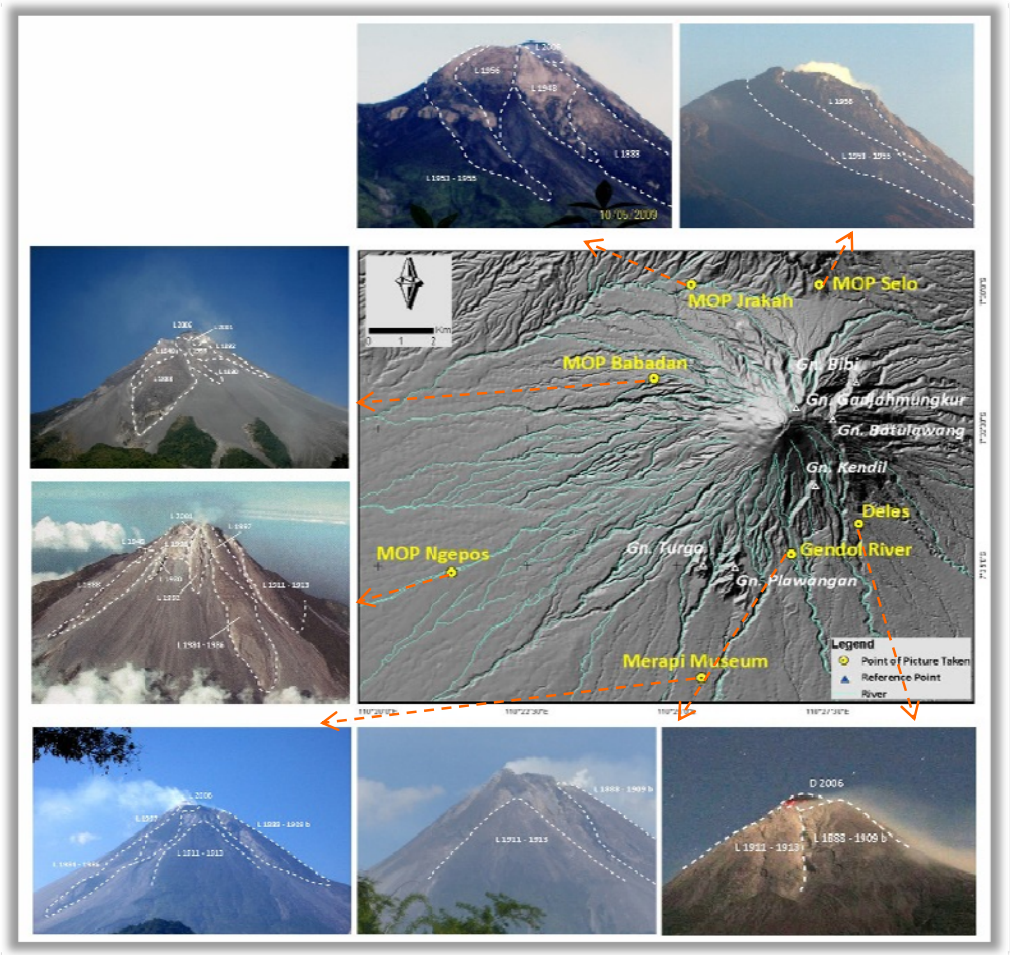


Figure 4-3. Pictures from Merapi sides with remnant of domes delineated (Source: Field work 2009)

### 4.2.3. Interview PIC at MOP

Interviewing PIC at every MOP was carried out to figure out procedures of EDM measurement (time, type of data, and series of measurement), recognition of dome remnants and morphologic changing during precursor of Merapi activities.

During field work activities, the author was able to meet Prof. Frank Lavigne, an expert in Volcanology. He underlined some important points regarding the nature of pyroclastic surges and flows, the importance of valley depth and valley morpho – arrangement and miss development of SABO DAM structure that change the morphology of valley and river channel.

## 4.3. Post – Field Work

Post field work activities were carried out to accomplish data process, visualization, analysis including DEMs generation and quality assessment, morphologic analysis for determining factors ascertain direction of Merapi – type eruption, prediction in direction

and affected area of Merapi – type eruption in the near future, proposed hazard map for Merapi – type eruption**,** layout and report writing.

### 4.3.1. DEMs Generation and Quality Comparison

Application in geo-science e.g. geology, geomorphology needs integration of terrain relief and features in form of spatial model (Rahman and Pilouk, 2008) and DEM is a very effective tool for terrain analysis since many terrain attributes e.g. as slope, aspect can be derived and displayed with the help of GIS (Bi *et al.*, 2006; Huggett, 2007). The quality of geomorphometry analysis, method for land surface analysis, is determined by the quality of DEMs input. Even the most sophisticated geomorphometric algorithm will be unable to rectify severe artifacts and errors in the input DEMs (Reuter *et al.*, 2009).

The most common form of DEM is grid DEM because of their simplicity and ease of computer implementation (I.D. Moore *et al.*, 1991, 1993f, Wise, 1998 in Wilson and Gallant, 2008). However, DEM derived products often contain blunder, systematic and random errors (Li *et al.*, 2005; Reuter *et al.*, 2009) which might not be detected in grid DEM. Sun shading, often called hill shade model or simple GIS operation, should be utilized to visually detecting those types of errors (Reuter *et al.*, 2009).

To be able to visually detect those types of errors, derived DEMs were developed into sun shading or hill shade model using Arc GIS 9.3 before editing and re – interpolation. 3D representation was developed from re – interpolated grid DEM into hill shade and TIN models by means of Arc Scene 9.3.

DEM quality comparison of input DEM could conceptually be carried out only for IFSAR DEM and ALOS DEM due to time range and significant accuracy difference between other topographic maps and DEM 2006 as reference.

#### 4.3.1.1. DEMs Generation

DEM generation in this research was conducted in two steps: DEMs preparation consist of coordinate system transformation, error recognition, editing and re – interpolation and development of 3D models, figure 4-4.

##### 4.3.1.1.1. DEM Preparation

DEM preparation was conducted to develop a dataset with particular coordinate system and correct representation of surface topography since the fundamental of morphologic analysis was based on parameters and objects extraction from DEMs (Pike *et al.*, 2009) in which observation of particular object was easier when they were referred in the same coordinate system (Anonymous, 2003).

Coordinate system is a fundamental issue when dealing with dataset from various institutions for observing changes of particular phenomena due to possibilities of miss positioning. Hence, unique geo – reference coordinate system must be utilized to make those physical phenomena easier to calculate or understood, frequently by conducting transformation from one coordinate system to another.

In this research, coordinate system UTM zone 49 south, reference datum WGS 1984 was used as geo-reference coordinate since most data available used it. Therefore, transformation from other coordinate systems was necessarily to develop single coordinate system for dataset e.g. transformation of TM coordinate system, Batavia datum (AMS topographic map 1964, later on called map 1935) and geographic coordinate system, ITRF 2000 (IFSAR DEM).

Generally speaking, there are three types of errors commonly occur in DEM derived products: blunder or gross error, systematic error and random error. Gross error in fact is a mistake e.g. wrong coded elevation contours. Systematic error usually occurs due to

procedure or system used to deliver DEM and this type of error could not be removed in the existing data. Random error usually refers as a random noise in data acquisition which commonly removes before the data has been published and filtering process is usually applied to remove this error (Li *et al.*, 2005; Reuter *et al.*, 2009).

Since data used in this research were existing data, only gross and random errors on DEM might be able to observe. Grid DEM was then built up into hill shade model to detect these errors.

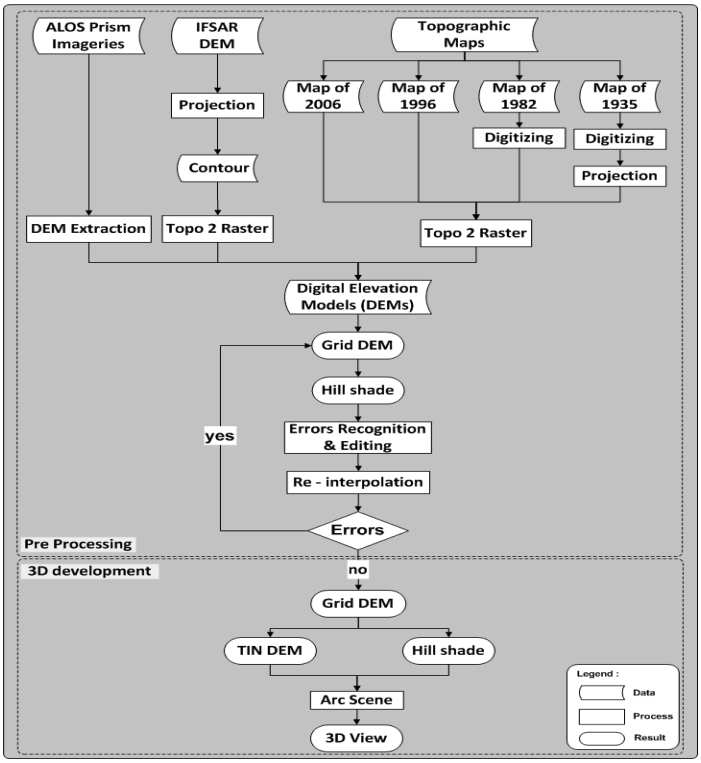


Figure 4-4. Workflow of DEM generation from various input data. The years of topographic maps represented were years of surface topographic represented, not the production date, refer to section 4.1.2 (source: own illustration)

DEM preparation from Topographic Maps

Contour lines of topographic maps are one of the most common resources to develop digital terrain models in most part of the World (Li *et al.*, 2005) before other techniques were developed e.g. photogrammetry and remote sensing. In this research, most of terrain representation from past 70 years could be achieved through topographical maps.

Digitization from scanned topographic maps, map 1935 and Map 1982, were conducted manually because low quality of lines obstacles automatic conversion using Arc Scan and result in segmented contour lines. In addition to, contour lines of summit area need to be digitized precisely due to their important visualization to study morphologic changes. Digital contour lines of map 1935 were then projected into dataset coordinate system.

Topo 2 Raster tools developed based on ANUDEM interpolation method (Arc GIS help) was chosen to convert contour lines into grid DEMs because it preserved actual representation of terrain shape e.g. ridges which is important in geomorphologic analysis (Fisher, 1998 in Reuter *et al.*, 2009), efficient in data processing, enforces sinks and defined output DEM resolution (Hutchinson and Gallant, 2000; Sinha, 2000 in Rahman, 2006; Yang *et al.*, 2005). The optimum resolution of ANUDEM interpolation, termed as a

rule of thumb, is $10^{-3}$ of the input map scale. For instance, the optimum output grid resolution of contour data scale 1:100.000 would be 100 m (Yang *et al.*, 2005).

To have optimum surface representation of morphologic changes from dataset, the output grid cell size chosen was based on the largest scale of topographic maps, map of 2006, which would produce 5 m grid cell size. Grid DEMs produced were then developed into hill shade models to recognize and edit the errors.

DEM preparation from IFSAR DEM

IFSAR DEM, together with Global Mapper 11, obtained from Intermap Technologies Inc. was DEM data in BIL format. Global Mapper 11 was utilized to convert and project data from original format into Arc GIS with specified dataset coordinate system.

Some noise in form of striped lines and void area were observed on DEM. However, filling the void area and filtering process might filter out true surface roughness and finish with over smooth DEMs (Reuter *et al.*, 2009) and affect the quality comparison process. Thus, to minimize striped lines around summit area, original IFSAR DEM was converted into contour lines before interpolated into grid DEM using Topo 2 Raster tools. This pre processed DEM was used in morphologic analysis whilst the original IFSAR DEM was used in DEM quality comparison.

DEM preparation from ALOS DEM

ALOS PRISM is one of three sensors carried by ALOS platform. PRISM sensor has been designed for mapping purposes with a specific aim towards Digital Elevation Model extraction. PRISM is capable of simultaneous stereoscopic acquisition of the observed landscape. This acquisition process makes automatic processing for DEM extraction easier (Bignone and Umakawa, 2008; Gonçalves, 2008).

DEM extraction from pair of ALOS PRISM Imageries nadir and forward was conducted using Ortho Engine in PCI Geomatics 9.1 by conducting these steps (PCI Geomatics helps):

1. Creating new project by choosing satellite orbital modeling for modeling method and defining the projection, datum and ellipsoid used in input and output file and in GCP. For pixel and pixel spacing used the spatial resolution of ALOS Prism image, 2.5 meter. In PCI Geomatics, projection UTM, datum and ellipsoid WGS 1984 was recognized as earth model E012, figure 4-5.
2. Reading generic image file for Nadir and Forward images, defining the orbit and sensor information from ALOS data users handbook (JAXA, 2008) and defining central of Nadir and Forward images from header file, figure 4-6.
3. Defining appropriate numbers of GCP's and ties points. Since DEM extraction was carried out throughout the scenes, the distribution of 9 tie points was scattered all over the images while distribution of about 81 GCPs was focus on Merapi area, total RMSE must be less than 1. Determination of GCPs elevation was derived from IFSAR DEM.

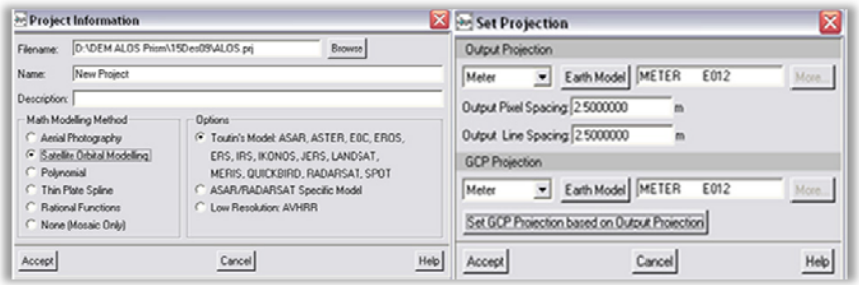


Figure 4-5. Creating project and set projection parameters

4. Model calculation through bundle adjustment by software default and extracting DEM from stereo model by creating epipolar image, forward as left image and nadir as right image before conducting automatic DEM extraction.
5. Import and build DEM from model output with the pixel size 5 m.

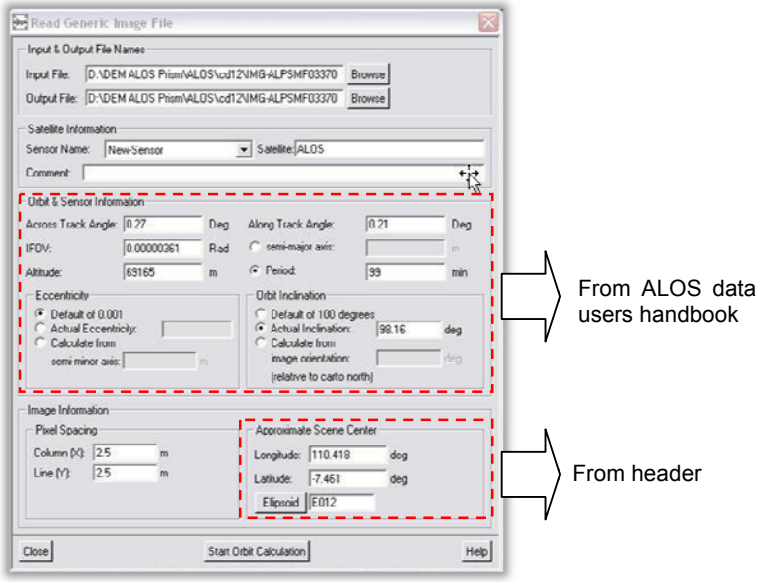


Figure 4-6. Setting orbital and sensor information and central of images

The result of DEM extraction was then converted into IMG format and projected into dataset coordinate system before finally cropped based on area of interest. Void area was then refined using IFSAR DEM by conducting these steps:

1. Reclassification of ALOS DEM into two classes, failed and non – failed area, conversion from raster to vector and deleting failed area.
2. Conversion from ALOS DEM and IFSAR DEM into contour lines, interval 25 m, using 3D analysis tools in Arc GIS.
3. Cropping failed area in IFSAR DEM using analysis tools to obtain the elevation of failed area.
4. Merging contour lines from ALOS DEM and IFSAR DEM and fill in the elevation of each contour line, elimination of zero value.
5. Grid DEM generation using Topo 2 Raster interpolation and developing TIN, hill shade and 3 D view of refined ALOS DEM.

However, the process of refining void area was only conducted for area around Merapi edifice and vicinity area because topographic condition of edifice has already changed due to activity in 15 June 2006.

#### 4.3.1.1.2. Development of 3D models

3D model was developed from re – interpolated grid DEMs by calculating hill shade and TIN models. By means of Arc Scene 9.3, 3D models were generated by using TIN as base height of hill shade.

### 4.3.1.2. DEM Quality Comparison

One of the DEM quality assessment goals is to fulfill the requirements of spatial data standards. DEM quality assessment could be carried out through visual and statistical assessment for one or multiple dataset. Visual methods provide first impression of DTM quality despite the fact that they are less objective than statistical one (Podobnikar, 2008).

Statistical methods are well accepted for quality assessment but they provide incomplete result and vice versa. Moreover, accurate representation of terrain shape is more important than absolute elevation accuracy (Geodata and Geoscience Australia, 2002) and the absolute accuracy of the elevation values in a sample is not the most important indicator of high quality DEMs (Reuter *et al.*, 2009). Thus, the combination of visual and statistical methods is needed to fulfill the weaknesses of one method to another.

In geomorphometry point of view, the accuracy of land – surface parameters and objects were the most consideration in which the DEM accurately resembles the actual shape and flow/deposition process, termed as *relative accuracy* or *geomorphological accuracy* of DEMs (Schneider, 1998; Wise, 2000 in Reuter *et al.*, 2009). For example, even elevation values are sampled very accurately e.g. LiDAR can achieve an accuracy of ± 0.15 m, the results of the geomorphometric analysis may still be poor e.g. because the DEM is too noisy; or the canopy is unfiltered.

Some visual methods for dataset quality assessment include initial observation of topographic representation of DEM and checking consistency of data set using a reference data for analysis i.e. better quality DEM, orthophoto, contour lines from map, etc (Podobnikar, 2008; Ping, 2003; Li *et al.*, 2005) by comparing a path drawn on each DEM or presenting terrain profile between two points (Podobnikar, 2008 and Trisakti and Pradana, 2007).

Most common statistical methods used to compared DEM quality was conducted by computing a mean error, indicator for a systematic error; root mean square error (RMSE), indicator for a random error after the systematic component has been eliminated, and range error (minimum/maximum error) (Podobnikar, 2008 and Li *et al.,* 2005). Amongst those parameters, RMSz errors is the most common descriptor used in statistical evaluation of DEM errors (Fisher and Tate, 2006; Yilmaz 2007 in Rodriguez – Gonzales, 2009; Li *et al.,* 2005 and Podobnikar, 2008).

In this research, DEM quality assessment was carried out by combining both visual and statistical methods of dataset using DEM 2006 as reference data because it has the highest accuracy among others (Li *et al*., 2005). The initial observations of topographic representation of morphologic features among DEMs were conducted visually for summit and vicinity area whereas the comparison of terrain profile and statistical assessments of input data were conducted only for IFSAR DEM due to enormous changes in topographic condition over acquisition date and vast accuracy gap between other input data with reference DEM, figure 4-7.

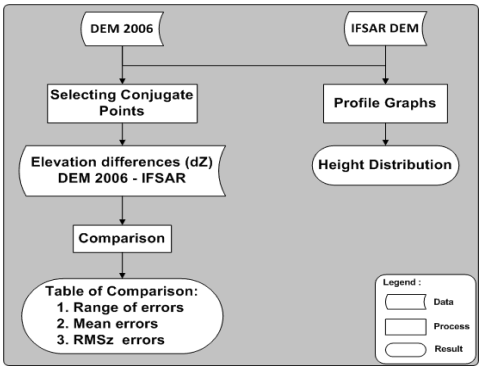


Figure 4-7. Workflow of DEM comparison of DEM 2006 and ALOS DEM to IFSAR DEM
(Source: own illustration)

Three transect lines were selected to observe height distributions between IFSAR DEM and DEM 2006 and fifteen conjugate points were chosen to calculate the statistical parameters showing the absolute elevation accuracy. Transect lines and conjugate points

were selected by avoiding the southwest, west and northwest parts of summit area owing to Merapi activities and avoiding vicinity area due to different surface representation. Transect lines and conjugate points distribution used in DEM comparison were displayed in figure 4-8.

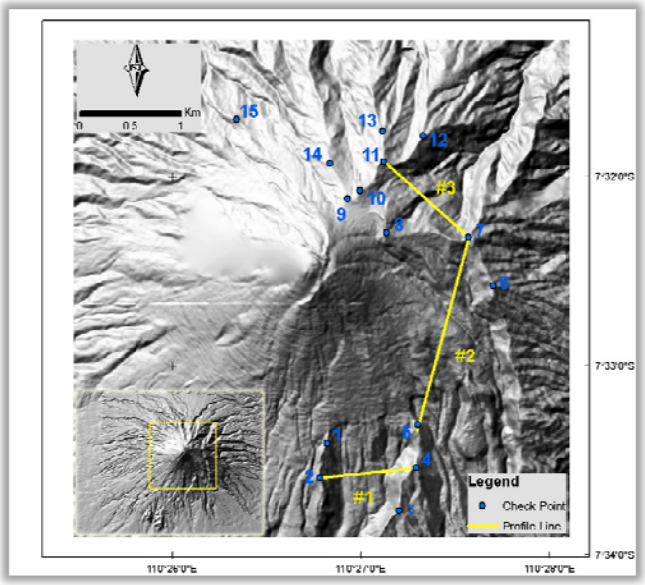


Figure 4-8. Points and lines distribution used in DEM comparison, overlying hill shade of DEM 2006 (Source: own illustration)

For absolute accuracy comparison using statistical parameter, identification coordinate X, Y of conjugate points were conducted using automatic field calculation in Arc GIS 9.3 before elevation values (Z) identified using point locator and cursor located value in ENVI 4.5. Three parameters of height differences were taken: range of z errors, z mean error and RMSz error. Range error is maximum and minimum value of z error among fifteen check points. Z mean error is mean error of all points and RMSz e is a global indicator of DEM quality calculated using equation 5 - 7 respectively.

$$R = e\ max - e\ min \quad \text{(Eq. 5)}$$

$$\mu = \frac{\sum e}{n} \quad \text{(Eq. 6)}$$

$$RMSz\ error = \sqrt{\frac{1}{n}\sum_{i=1}^{n} dzi^2} \quad \text{(Eq. 7)}$$

Where:

| | |
|---|---|
| $R$ | is range of errors |
| $\mu$ | is mean errors |
| $dzi$ | is elevation differences between IFSAR DEM to DEM 2006 |

### 4.3.2. Morphologic Analysis

Morphologic analysis of the study area was divided into five sections: utilization of EDM data for morphologic changes, morphologic features recognition and quantification of past time DEM, morphologic analysis of those features to determine direction of dome collapse in the past, reconstruction of Merapi – type eruption in the past and comparison of reconstruction results to those of historical data.

Morphologic factors that ascertain direction of dome collapse or Merapi – type eruption were then utilized for predicting direction of dome collapse in the near future based on recent summit topography after eruption 2006 (see Figure 4-9).

#### 4.3.2.1. EDM for morphologic changes

EDM data collected from every MOP were one of the resources to deliver morphologic changes in summit and flank area. Incomplete series of EDM data before Merapi eruption in 2006 and other supporting data e.g. coordinate of fixed prism prevented the utilization of those data to deliver morphologic changes due to 2006 activity. Thus, the best utilization for these data was distance changes after 2006 activity.

The distances from benchmark to fixed prisms were calculated from daily measurement before calculated into average distances per years. The distance changes were delivered as changes between year of 2006 and 2009.

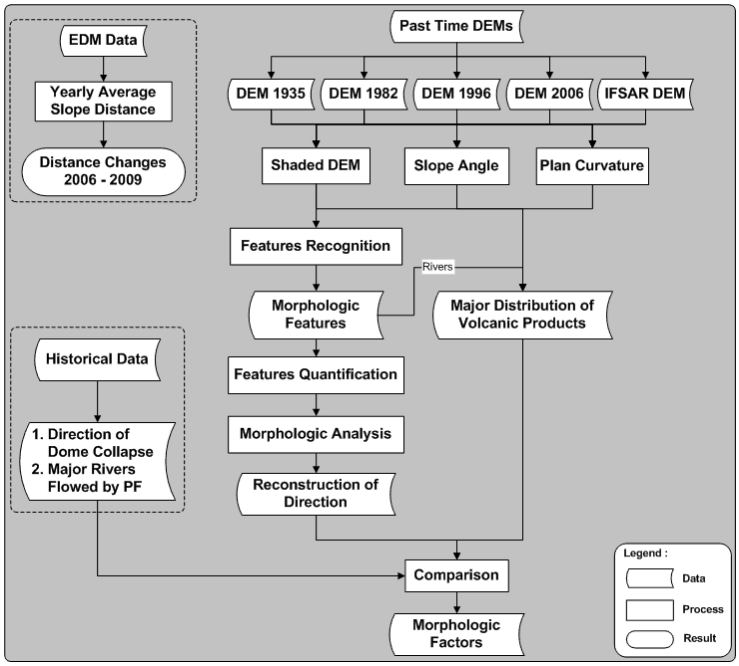


Figure 4-9. Workflow for morphologic analysis (Source: own illustration)

#### 4.3.2.2. Morphologic features recognition and quantification

Volcanic morphometric modeling provides reliable measurements of eruption edifice morphology and its derivatives which are important for constraining both aggradations and degradations models of volcanic landforms. For modeling process of aggradations and degradations of past time volcanic activity, morphometric parameters were determined (Rodriguez-Gonzalez *et al.*, 2009). The parameters taken mostly related to crater and their features (Corazzato and Tibaldi, 2006).

Morphologic features recognition and quantification from past time were carried out based on morphologic features observed on hill shades and 3D models of past time DEM: DEM 1935, DEM 1982, DEM 1996 DEM 2006 and IFSAR DEM. Summary of morphologic features and parameters used to quantify them was displayed in table 4-3.

Guided by studying the morphology of area; study by MVO, 2000; Rodriguez-Gonzalez *et al.*, 2009; Corazzato and Tibaldi, 2006 and expert opinion, the following morphologic features were identified, some of which were illustrated in figure 4-10:

##### 4.3.2.2.1. Summit Features

1. Crater rim: a circular crown of a volcanic cone with steep to very steep wall formed by explosion activity. As the volcanic activity was centered inside this features, it is most rapidly changed site on strato – volcano (Scarth, 1994). Tinkler, 1971 in Goudie,

1990 terms the ratio an ellipticity index to describe volcanic craters, where the short axis (b) represents the basic explosion width of the crater and the long axis (a) the tendency of the crater to elongate in the direction of some controlling factor.
Quantification of elongated degree of crater rim was performed by measuring major (a) and minor (b) axes using ellipse extension tools of Arc View 3.3 to calculate degree of ellipticity (e) using equation 8; whist crater rim perimeter was calculated automatically using Arc GIS field attribute.

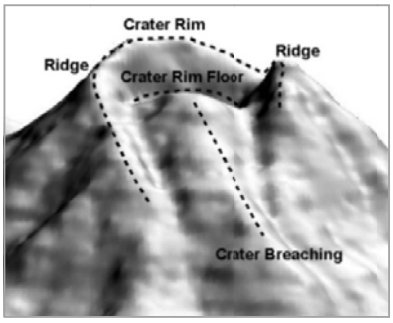


Figure 4-10. Illustration of some summit morphologic features (Source: own illustration)

$$e = 1 - \frac{b/2^2}{a/2^2} \quad \text{(Eq. 8)}$$

Eccentricity varies 0 ≤ e ≤ 1, where *e* = 0 is the case of a circle and represents a perfectly circular crater (A. Rodriguez – Gonzales, 2009) while value less than 1 represents elliptical crater rim (Corazzato and Tibaldi, 2006).

2. Crater breaching

Crater breaching or rim depression: low topographic area formed on crater rim (Corazzato and Tibaldi, 2006) in which direction of dome collapse might mainly flow toward its orientation since dome collapse was triggered by gravitational failure (Davidson and Silva, 1999).

Morphologic parameters used to quantify the crater breaching or rim depression were azimuth, shape, depth and width. Crater breaching azimuth is the azimuth of crater breaching which expressed as horizontal angle of the axis direction measured clockwise from north to the direction of major axis presenting a lower elevation in the major cone perimeter and the rim respectively, figure 4-11 (Corazzato and Tibaldi, 2006; Rodriguez-Gonzalez *et al.*, 2009).

Crater breaching was measured using distance and azimuth extension in Arc View 3.3 while its shape, depth and width were calculated from profile graph of cross section from adjacent ridges in Arc GIS 9.3.

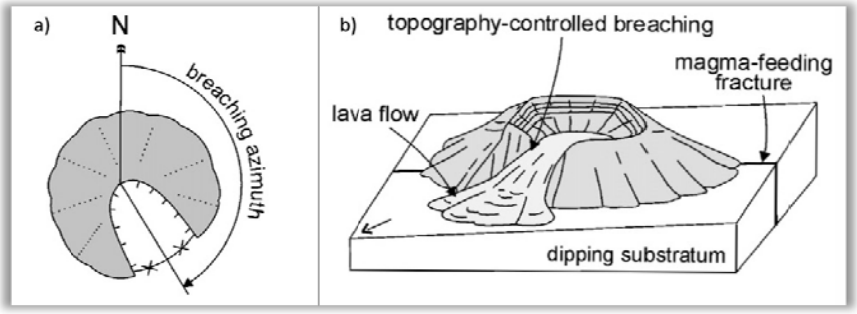


Figure 4-11. Crater breaching illustration, a) Crater breaching azimuth and b) topography controls breaching orientation (Source: Corazzato and Tibaldi, 2006).

3. Crater floor: area inside the crater rim representing area where the magma extrudes to the surface. Crater floor has formed as the result of ejection collapse material from explosive eruption and later on filled by some remnant of domes which not tore down during the eruption or developed after the eruption.
4. Adjacent ridges: ridges adjacent to crater breaching, important features since their presences could act as artificial barrier controlling direction of pyroclastic flow produced by dome collapse or Merapi – type eruption (CVGHM, 2006).

   Parameters used to quantify adjacent ridges were their relative positions and heights (Figure 4-10). Ridges position was determined by its relative direction to rim depression while their heights were calculated from cross section profile, maximum height - minimum height drawn in the profile.
5. Breaches: cracks on crater rim which might give preliminary judgment of the area altered by hydrothermal process making it more vulnerable to erosion by both long-term, slow-mass-wasting, glacial or fluvial processes and catastrophic failure (Davidson and Silva, 1999).

   Parameters measured for breaches were relative orientation, depth and width. Orientations of breaches, displayed as relative position to crater rim, were measured from north with central point on crater rim using distance and azimuth extension in Arc View 3.3 while its depth and width were calculated from profile graph of cross section along breaches.

Table 4-3. Morphometric parameters used to quantify features

| Features | Parameters | Description /unit | Proposed Methods |
|---|---|---|---|
| Crater | Shape | Ellipse parameters (a, b, *e*) | Ellipse extension |
| | Perimeter | Perimeter of rim /m | Shape length |
| Crater rim floor | Shape | Shape of rim floor | - |
| | Perimeter | Perimeter of rim floor/m | Shape length |
| Crater breaching | Orientation | Orientation of rim depression | Distance and azimuth extension |
| | Shape | U or V shape | Profile Graph from 3D |
| | Depth | The lowest point of depression | Cross section, Profile graph |
| | Width | Length of the depression /m | Cross section, Profile graph |
| Adjacent ridges | Position | Left or right sides of crater breaching | Cross section, Profile graph |
| | Height | The highest point of steep wall /m | Cross section, Profile graph |
| Breaches | Orientation | Orientation of major axis of rim | Distance and azimuth extension |
| | Depth | The lowest point of depression | Cross section, Profile graph |
| | Width | Length of the depression /m | Cross section, Profile graph |
| Remnant of domes | Shape | Dome or coulee | Shape Length |
| | Orientation | Orientation of major axis | Distance and azimuth extension |
| | Area | Covered area /$m^2$ | Shape Area |
| Drainage | Pattern | Basic drainage pattern | Flow direction and accumulation |
| Lineaments | Orientation | Azimuth | Rose Diagram |
| Major rivers | Name | Major rivers flowed by PF | |

(Sources: Corazzato and Tibaldi, 2006; A. Rodriguez – Gonzalez *et al*., 2009 and expert opinion)

6. Remnant of domes: parts of domes or coulees which not tore down during the activities and remain on or around crater rim. Dome is mounds of rock that accumulate around the vent and if they show some flow away from the vent, they are termed coulees (Goudie, 2004).

   The degradation process on most of strato volcano has underlining the effects of hydrothermal alteration by a sufficient heat flux from mature conduit. The consequence of this process is the rock volume affected by the system is altered and weakened, making it more vulnerable to erosion by both long-term, slow-mass-wasting, glacial or fluvial processes and catastrophic failure (Davidson and Silva, 1999).

   Remnant of domes in Merapi summit is one of critical points to consider when dealing with direction of dome collapse in the near future. Hydrothermal process from endogenic force, weathering and erosion process made remnant of old domes altered (Camus *et al*., 2000) and subsequent explosive eruptions or major dome

collapses might create new depressions that can differ from previous depressions in size and orientation (Young *et al.*, 2000). Thus, their relative position and estimated volumes must be clearly defined. However, volume estimation of remnants of domes was difficult to carry out owing to incomplete series of DEM before and after each eruption.

Remnant of domes was recognized based on their specific morphology and their delineations were carried out based on visual interpretation on hill shade and 3D models. For two recent DEMs: DEM 2006 and IFSAR DEM, recognition and delineation were carried out using combination of pictures of Merapi sides, recent sketches in MOPs and description from PIC in every MOP (refer to figure 4-3). Morpho – chronology of domes from historical data was used to verify the description.

Remnant of lava domes was amounted on hill shade view before checked in 3D model. The dimensions of remnants of domes calculated including their relative positions and areas, figure 4-12. Quantification of remnants of domes was carried out by their relative orientations toward crater rim and area covered. Initial positions of domes' remnants were delivered from table 3-2. Their orientations were relatively observed from center of crater rim to main axes and covered areas were automatically calculated from the attribute table.

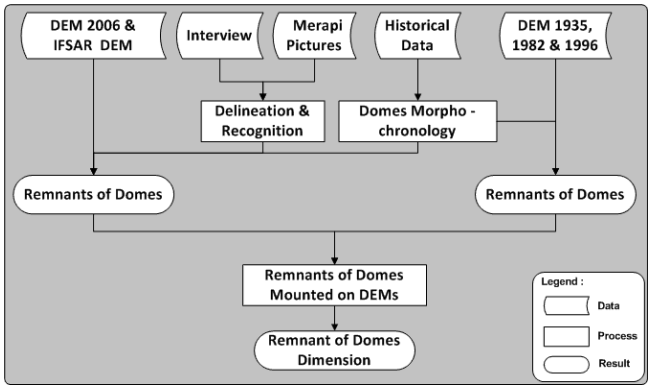


Figure 4-12. Workflow for remnant of domes (Source: own illustration)

#### 4.3.2.2.2. Vicinity Features

1. Drainage pattern reflects influence of such a factors as slope, rock, structural controls, etc that they are extremely helpful in the interpretation of geomorphic features and study of them represents one of the practical approaches to an understanding of structural and lithologic control of land form evolution (Thornbury, 1958). Disrupted of drainage pattern might be performed by fault scarps (Huggett, 2007).

   Basic drainage pattern of study area was derived from flow accumulation and flow direction from grid DEM 15 m pixel size because 5 m pixel results in too detail drainage pattern making hard to classify them. Drainage pattern and hill shade DEM were then utilized to define the lineaments and to digitize major rivers located down slope of crater breaching.

2. Lineaments: any linear features which perform straight lines or curves that resulted from tectonic origin (Huggett, 2007). Recognition of lineaments in study area were carried out by digitize them on hill shade overlain by drainage pattern.

   Parameter used to quantify lineaments was their relative orientation and distribution which calculated using distance and azimuth extension in Arc View 3.3 before drawn using Rozeta 2.0 (Pazera, 2004).

3. Major rivers: rivers located down slope of crater breaching which might be overflowed by pyroclastic flow hazard. These features were digitized on hill shade DEM overlain by drainage pattern and later on would be used to reconstruct major distribution of volcanic eruption products.

### 4.3.2.3. Morphologic analysis of features

Morphologic analysis of past time eruption in this research was divided into two steps: morphologic changes over 70 years and analysis of those morphologic features to determine factors that ascertain the direction of Merapi – type eruption.

#### 4.3.2.3.1. Morphologic changes over 70 years:

1. Computation of DEM difference
   Scales and resolution of input data were one of major problems when dealing with morphometric analysis of a dataset (Hutchinson and Gallant, 2000). In planar shape analysis, ratio combinations of area, perimeter length and axis length are used to quantify planar shape in specific geomorphometry (Goudie *et al.*, 1990).
   DEMs used in this research were computed from various scales and resolutions which might affect the result of morphometry features' quantification. To determine the ratio of area and perimeter among DEMs, conventional geomorphometry technique was utilized, using circle from a central point passing a reference point whereas ratio of distance was calculated by preserving distance between two reference points.
   The area and perimeter of the circle were derived automatically on field table attribute in Arc GIS before compared to DEM 2006 using equation 9. Percentage of area, perimeter and distance differences of DEM toward reference DEM were calculated using equation 10 and 11 before used for correcting area, perimeter and distance quantification value.
2. Correction of morphometry features' quantifications.
   Correction of morphometry features quantification was carried out by subtracting quantification values of features with percentage of area and perimeter correction as shown in equation 12.
3. Figure out the morphologic changes of features over 70 years.
   Morphologic changes over 70 years were carried out by observing morphology and corrected morphometry parameter of features which quantified in every DEM.

$$\Delta \text{ Area/Perimeter} = \text{Area/ Perimeter in DEM}_i - \text{Area/ Perimeter in DEM 2006} \quad \textit{(Eq. 9)}$$

$$\%\ \text{Area/Perimeter DEM}_i = \frac{\Delta\ \text{Area/PerimeterDEMi}}{\in \text{Area/PerimeterDEMi}} * 100\ \% \quad \textit{(Eq. 10)}$$

$$d = \frac{\Delta\ \text{Distance DEMi}}{\in \text{Distance DEMi}} \quad \textit{(Eq.11)}$$

$$c = \text{Quantification value} - \%\ \text{correction} * \text{quantification value} \quad \textit{(Eq. 12)}$$

Where:

$DEM_i$ is digital elevation model year i
$d$ is distance between two reference points drawn in a DEM
c is the correction value of $DEM_i$ to reference DEM

#### 4.3.2.3.2. Analysis of morphologic features

Morphologic analysis of features was conducted to determine the morphologic factor ascertain direction of dome collapse in the near future by studying past time eruptions. Morphologic changes of features from past 70 years were studied before deciding features that ascertain direction of dome collapse in the past.
As this study was focused on Merapi – type of eruption, pyroclastic flow produced by gravitational failure (Voight *et al*., 2000), morphologic features chosen as factors were the

one indicates low land area around Merapi edifice and the ones act as controlling factor directed pyroclastic flow hazard.

#### 4.3.2.4. Reconstruction of Merapi – type eruption in the past

Merapi activities are characterized by continuous growth of lava domes, interrupted by collapses and phases of quiescence (Camus *et al.*, 2000). Gravitational collapse of lava domes were then driven to several types of hazards i.e. tephra, pyroclastic flows and surges. Pyroclastic flows and surges are two end – member types of pyroclastic density current (Wilson and Houghton, 1999). Pyroclastic surges are distinguished from pyroclastic flow by contained material even though a continuum exists between them (Marti and Ernst, 2005).

Pyroclastic surge is a turbulent, low-density, high-velocity part of a pyroclastic density current. It is not so constrained by topography and can effect areas high on valley walls and even overtop ridges to enter adjacent valleys. Pyroclastic flow is a flow of volcanic material ranging from vesiculated, low-density pumice to unvesiculated, dense lava and clasts which tend to follow topographic lows, mostly restricted to valley floor (Nakada, 1999; Marti and Ernst, 2005) or depressions in the slope of volcano and spread out over the adjacent landscape (Zuidam, 1983).

Small nuees ardentes d'avalanche or Merapi – type eruption, reach only 1 – 3 km from the crater but the bigger one may reach a distance of 7 to 9 km (Zuidam, 1983). Pyroclastic material from Merapi-type dome failures is distributed usually in relatively narrow sectors defined by the approximately radial valley systems (Voight *et al*., 2000). Thus, the importance of valleys and their morpho – arrangement were needed to identify the area prone to pyroclastic flow (Frank Lavigne, personal communication).

Reconstruction in direction of Merapi – type eruption in the past was carried out to determine the direction of dome collapse and to identify major distribution of volcanic eruption products. Reconstruction of direction of dome collapse in the past was derived from analysis of morphologic factors ascertain the direction. Distribution of volcanic eruption products was accomplished based on morphology of flank area since height of barrier ridges, slope angle and gradient of ground surface greatly influence the flow directions. Topographical effect of break in slope on the flank of stratocone contributes to decoupling within two zones of pyroclastic flows: dense, gravity – driven pyroclastic flow and dilute, overriding turbulent gas – cloud surge of ash elutriate from the flow (Thouret, 1999).

Identification of the major distribution of volcanic eruptive product was conducted by free hand delineation on slope angle (°) overlying plan curvature, assistance by shaded DEM. Incomplete series of DEM before and after each eruption made consideration to include adjacent rivers, in addition to major rivers down slope of crater breaching, due to the nature of pyroclastic flows that often perform overbank flow (Frank Lavigne, personal communication). Overbank flows were produced from changing in valley (river) morphology either by volcanic products from previous activities or man-made structure i.e. SABO dam.

Slope would determine pyroclastic flow direction whist plan curvature performed the convergence and divergence of the flow.

1. Slope. Slope is a gradient maximum of height conveying the angle measured from horisontal line to tangent plane of a predifined point (Huggett, 2007; Klimanek, 2007). Slope is the means by which gravity induces flow of water and other materials so it has a great significance in hydrology and geomorphology (Gallant and Wilson, 2000). Verstappen and Van Zuidam in Zuidam (1983) suggested to devide the slope into seven classes as displayed in table 4-4 with expected terrain condition.

Slope angle (°) was calculated from grid DEMs using 3D analyst tool in ArcGIS 9.3 before reclassifiy into seven classses. The reclasified slope classes were then filtered to have smoother surface using low pass filter 3 x 3 in ArcGIS 9.3.

Table 4-4. Slope classes and expected terrain condition

| Classes | Slope angle (°) | Expected terrain condition |
|---|---|---|
| 1 | 0° – 2° | Flat or almost flat |
| 2 | 2°– 4° | Gently sloping |
| 3 | 4° – 8° | Sloping |
| 4 | 8°– 16° | Moderately steep |
| 5 | 16° – 35° | Steep |
| 6 | 35° – 55° | Very steep |
| 7 | > 55° | Extremely steep |

2. Plan curvatures. Curvature is the rate of change of a first derivative such as slope and aspect, usually in a particular direction. Surface curvature can be though of as the curvature of a line formed by intersection of a plane and topographic surface so a gentle curve has a small curvature value and a tight curve has a large curvature value (Gallant and Wilson, 2000). Plan curvature is one of the most frequently curvatures to be computed. Plan curvature measures the topographic convergence and divergence and the prosperity of the flow (Gallant and Wilson, 2000).

   A part from their use in modelling flow characteristic, curvature can be used to deliniate geomorphic units. A positive value of plan curvature indicates flow divergence on ridges and a negative value indicates the convergence or concentration of the flow on valleys (Hutchinson and Gallant, 2000; Li *et al.*, 2005; Gallant and Wilson, 2000), figure 4-13.

   The definition of plan curvatures along the path has a great influence to pyroclastic flow since it was responsible for local drainage into topographic lows (Legros and Kelfoun, 2000) and they may affected the area adjacent to their paths. Plan curvature of study area was calculated from grid DEMs pixel size 5 m using curvature tools in Arc GIS 9.3.

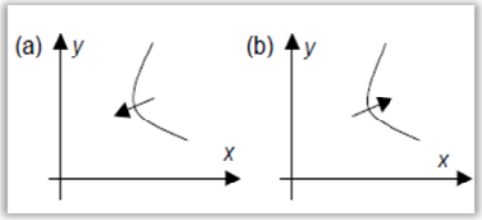


Figure 4-13. The sign of plan curvature a) positive, b) negative (Source: Li *et al.*, 2005).

### 4.3.2.5. Comparison of reconstruction results to those of historical data

Comparison of reconstruction results to those of historical data purposed to determine the validity of morphologic factors ascertain direction of Merapi – type eruption in past. This comparison was carried out by comparing directions of dome collapse and major distribution of volcanic eruption products resulted from reconstruction to those of historical data (table 3-1).

During 1935 to 2006, fifteen activities of Merapi had been recorded. Since this research was focused on Merapi – type eruption, direction of dome collapse pyroclastic flows adopted were the ones produce from new dome collapse for each period of eruption whilst some activities were eliminated to be used in comparison including:

1. Pyroclastic flows generated by fountain collapse or St. Vincent type e.g. eruption in 1961, 1972 and 1997.
2. Direction of dome collapse performed by changing in active sectors e.g. eruptions of 1948, 1953 – 1955, 1956, 1998, 2001 and 2006.
3. Activities without generation of pyroclastic flow e.g. eruption in 1940.

4. Eruption between 1961 and 1982 because no DEM available to quantify crater breaching dimension of rim 1961 in comparison to that of rim 1930.

Thus, historical eruptions used as a comparison limited to activities of years: 1942, 1943, 1984 – 1991, 1992 – 1993, 1994 and 1995.

### 4.3.3. Prediction of Affected Area and Improvement of Forbidden Hazard Zone

Geomorphology can contribute to geomorphic hazard zonation, both volcanic and non volcanic hazard (Thouret, 1999). Traditional methods of assessing the hazard zones associated with these events are based on reviews of historical records and field work to identify the limits of their deposits in the geological record. Predictions of future hazard zones are then based on interpolation and extrapolation of known data, perhaps supplemented by calibrated flow routing models (Stevens *et al.*, 2003).

Guided by studying historical eruption of Merapi in past two centuries, morphologic analysis of study area and previous study by Thouret *et al* (2000) and Charbonnier and Gertisser (2008, 2009), the predicted affected area by Merapi – type eruption in the near future and proposed hazard map of Merapi – type eruption were developed, figure 4-14.

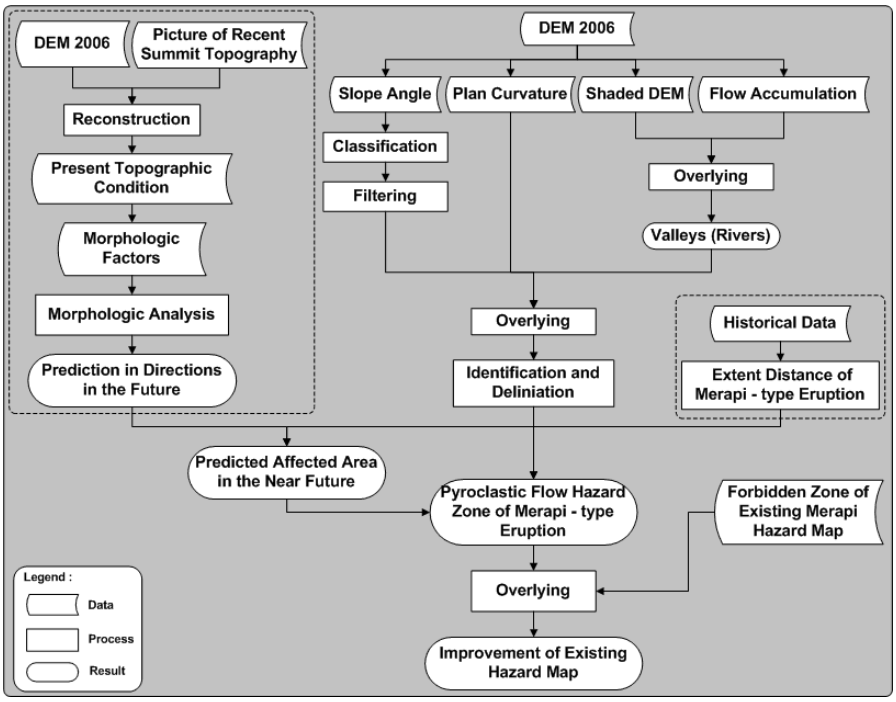


Figure 4-14. Workflow for predicting affected area and proposed hazard map (Source: own illustration)

#### 4.3.3.1. Predicted affected area in the near future

Revealing area prone to Merapi type eruption in the near future was separated into three parts: morphologic analysis to define direction of dome collapse; morphologic analysis to determine affected area by considering maximum extent distance from historical data (table 3-1); and delineation and identification of area prone to Merapi – type eruption in the near future.

##### 4.3.3.1.1. Morphologic analysis to define direction of Merapi – type eruption

Morphologic analysis was conducted by recognizing morphologic factors: crater breaching and its adjacent ridges and analyzing those factors to determine direction of dome collapse in the near future based on recent topographic condition.

Since absence of DEM after eruption 2006 prevented morphometric analysis of the factors, the analysis was finally conducted by reconstructing recent topographic condition using DEM 2006 and pictures of Merapi edifice and conducting visual interpretation of edifice morphography to determine direction of dome collapse.

#### 4.3.3.1.2. Morphologic analysis to determine affected area

Driven by gravity, pyroclastic flows seek topographically low areas of the volcano and tend to be channeled into valleys (Nakada, 1999). Local spatial changes in topography will cause changes in flow. As the slope angle increases, the flow will go faster and when slope angle decreases, very dense flows can be stopped as the basal friction becomes too high (Felix and McCaffrey, 2005). Pyroclastic flows slowed and thickened when traveling across a change in slope, from steeper to gentler slopes, when entering a channel and when passing through a constriction. For flows confined to the constricted channel, runout is longer than for comparable flows confined to the non constricted channel (Stinton and Sheridan, 2008).

The morphologic analysis to determine affected area by Merapi – type eruption was carried on DEM 2006 since DEM from ALOS Imageries, showing surface topography after eruption in June 2006, was failed to deliver recent topographic condition of study area due to thin cloud covered. The morphologic features utilized to predict area affected by Merapi – type eruption were slope and profile curvature since modeling simulation for pyroclastic flow was unable to conduct due to absence of recent DEM and time constraint.

Slope angle (°) of grid DEM 2006 was calculated using 3D analyst tools before classified into seven classes, as shown in table 4-4 and filtered using low pass filter 3x3 in Arc GIS 9.3 whereas plan curvature was calculated using curvature tools.

#### 4.3.3.1.3. Delineation and identification of affected area

Predicted affected area by Merapi – type eruption was carried by taking into account the direction of dome collapse, slope angle (°), profile curvature and historical data. Direction of dome collapse gave toward which pyroclastic flow hazard would affect flank area. Slope angle (°) and plan curvature gave impression of topographic barrier around volcanic cone and indication of overbank pyroclastic flow from main valleys (rivers) to adjacent valleys (rivers). Historical data gave the maximum extent area affected by dome collapse pyroclastic flow or Merapi – type eruption in the past.

Guided by numerical modeling of eruption in June 2006 developed by Charbonnier and Gertisser, 2009 and maximum extent area, delineation of the area was conducted free hand on slope angle (°) overlying plan curvature. From area delineated, villages prone to pyroclastic hazard were identified and the number of total inhabitants in those areas was calculated based on statistic data in 2008.

### 4.3.3.2. Proposed pyroclastic flow hazard zone of Merapi – type eruption

Previous study by Thouret *et al* (2000) portrayed hazard maps for Merapi volcano by differentiated hazards based on their recurrences and posed four eruption scenarios: first, Merapi – type dome growth based on quasi – continuous 'regular' eruptive activity and dome collapse scenario including small and moderate size of pyroclastic density current; second, mixed effusive/pelean based on 1930 – 1931 eruption; third, subplinian based on April 1872 eruption and fourth, worst – case scenario encompass flank failure of south southwest flank produce debris avalanche and direct blast parallel to avalanche caldera.

Two hazard zone maps was developed by Thouret *et al* (2000): hazard zone map for Merapi – type eruption scenario based on the 1961 – 1996 events (VEI 2-3), figure 4-15a, and hazard zone map for the subplinian eruption scenario based on the 1872 eruption

(VEI 4) and for the worst – case scenario, based on historical eruptions (VEI > 4), figure 4-15b.

Since specific focus of this research was dome collapse pyroclastic flow or Merapi – type eruption, first scenario developed by Thouret *et al* (2000) portrayed hazard zone beyond Merapi – type hazard. Moreover, changes in morphology of Merapi edifice, particularly crater breaching which toward southeast after eruption 2006 has changed some part of the portrayed hazard zone.

Proposed hazard zone in this research was delimited to pyroclastic flow produced from dome collapse or Merapi – type eruption and used to deliver detail area which may be affected by pyroclastic flows hazards in the near future as improvement of existing Merapi hazard map.

Proposed pyroclastic flow hazard zone of Merapi – type eruption was delivered from several steps: identification of extent distance from historical data and maximum distance for future eruption; morphologic analysis to develop proposed hazard zone and comparison to proposed hazard map to existing Merapi hazard map.

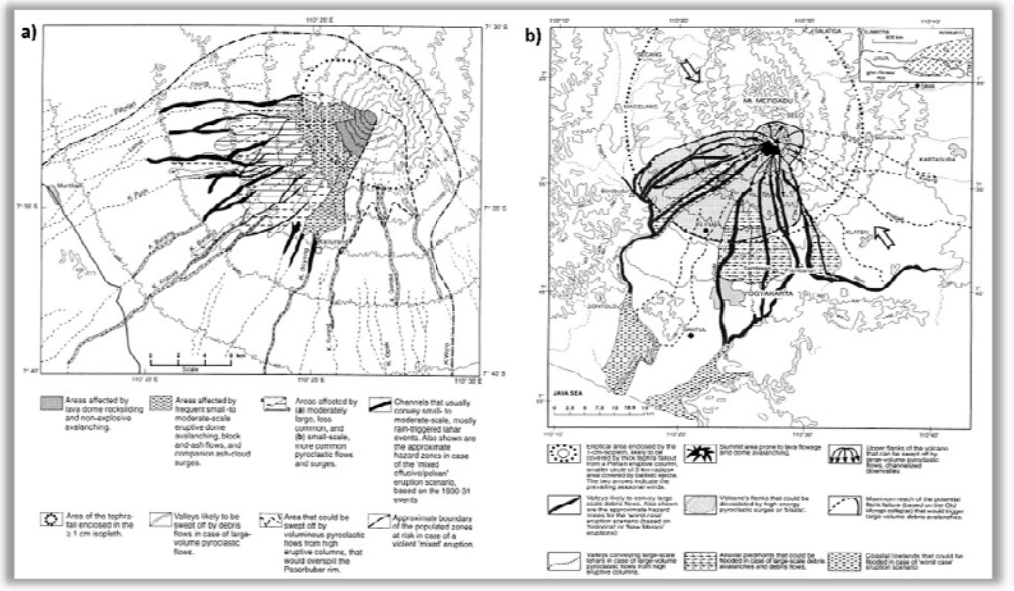


Figure 4-15. Two hazard zone maps proposed by Thouret *et al* (2000)

#### 4.3.3.2.1. Identification of pyroclastic flows' travel distances from historical data

Identification of pyroclastic flows extent distances was derived from sequence steps: identification of valleys (rivers) on the study area from flow accumulation (15m) overlying shaded DEM, identification of azimuth each valley (river) and distribution of extent distance of Merapi – type eruption on each valley (river) by using distance and azimuth tools in Arc GIS 9.3.

The extent distances of past time eruptions were delivered from table 3-1 and maximum distance of future eruption was delivered from predicted affected area. The maximum distance of future eruption was taken because morphology of valley and river channel down slope of crater breaching had been changed by volcanic products leading to father extent distance from eruption in June 2006, ± 7 km (Charbonnier and Gertisser, 2008).

#### 4.3.3.2.2. Morphologic analysis to develop pyroclastic flow hazard zone

Hazard zone for Merapi – type eruption was conducted by free hand delineation based on identification of extent distance and morphologic factors of slope angle (°) overlying plan curvature, assistance by shaded DEM, developed in previous section. Slope angle (°)

overlying plan curvature allow morphologic interrogation of study area e.g. presences of small (ridges) and large (caldera wall) topographic barrier around volcanic cone since they could allow deflection or directed the flow outward the opposite edge (Rolandi, 2009).

#### 4.3.3.2.3. Improvement forbidden zone of Merapi hazard map

Merapi hazard map scale 1: 100.000 was compiled by VSI in 1978. This hazard map is based on the lateral extent of the pyroclastic and lahar deposits from the 1930 and 1969 eruptions only with emphasize of macro hazard zonation toward west and southwest direction. The hazard zone divides the volcano's flanks and surrounding piedmont into three zones, without clearly stating the probability of type of hazard occurs (Thouret *et al.*, 2000), as shown in figure 4-16:

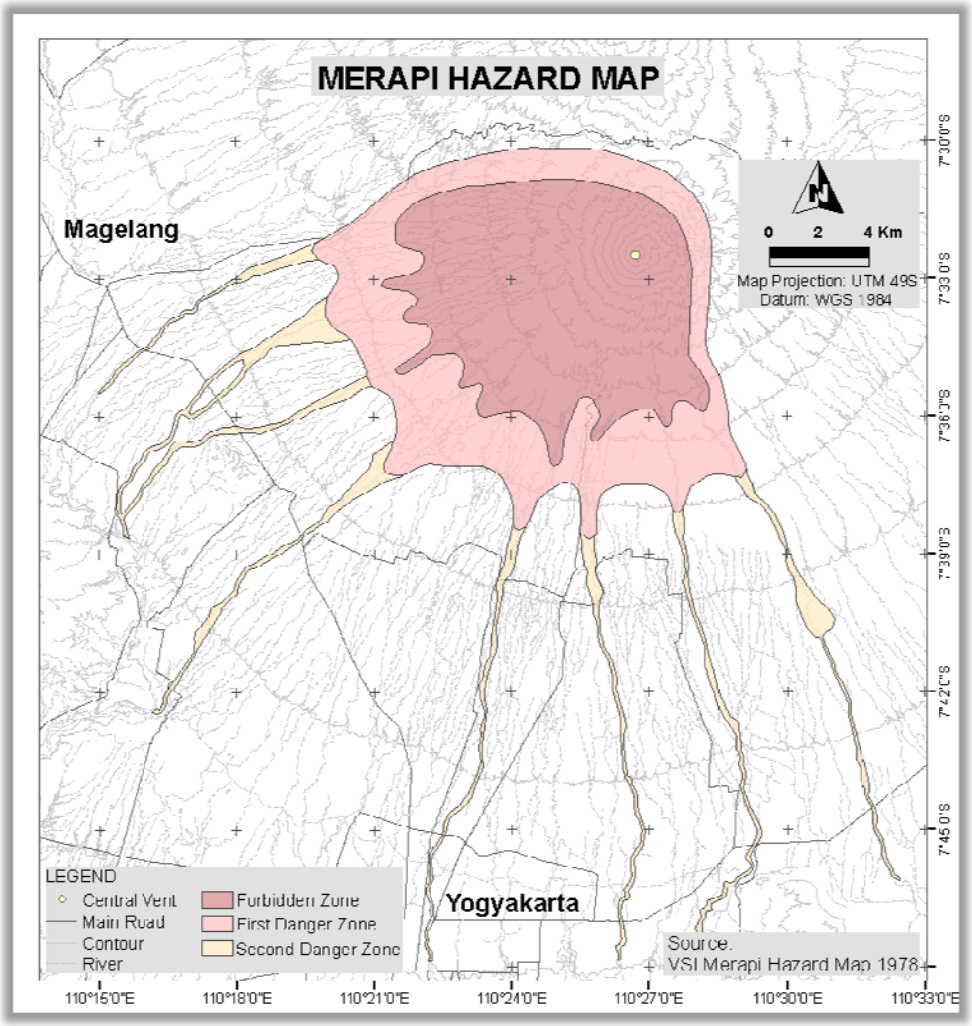


Figure 4-16. Three Merapi hazard zones (Source: VSI and BAKOSURTANAL)

1. The 'forbidden zone', above 1500 m altitude on the upper part of the volcano, is frequently affected by rockfall, pyroclastic flows, and tephra-fall, including ballistic ejecta.
2. The 'first danger zone' can be affected by tephra fall or lahars, should violent explosive eruptions occur. This area was thought to be beyond the reach of most pyroclastic flows and lava flows.

3. The 'second danger zone' corresponds to the radial valleys draining the volcano's flanks, particularly toward the west and south. Lahars and water floods can devastate the second zone as far as 30 km down valley from the summit

Most of Merapi historical eruptions were accompanied by pyroclastic flow hazard more often than any other volcanoes in the World (Thouret *et al.*, 2000) and the 61 reported eruptions since the mid-1500s killed about 7000 people (Lavigne *et al.*, 2008). Unfortunately, scientific view of Merapi has not automatically deliver inhabitants awareness about posed threaten hazards. Lack of knowledge in volcanic process, distance from active crater, visual obstacle between villages to active crater were thought to be the main reasons to develop inhabitants perception (Lavigne *et al.*, 2008). Furthermore, during the peak activity of Merapi, inhabitants also suffer from significant social and economic disruption and often decide to back to their village despite high possibility of hazard threaten (Sagala, 2007).

Improvement of existing hazard map was proposed to provide more reliable hazard zone for regular activity of Merapi, following recent trends of Merapi behavior after eruption 2006 since the volcano morphology have changed from the time of existing hazard map had compiled. Assessment of existing hazard map was carried out by overlying the proposed pyroclastic flows hazard and forbidden zone of hazard map and identifying the extent distance and area of proposed hazard zone and forbidden hazard zone. The distances were calculated by using measure distance tool whereas the areas were calculated automatically from table attribute in Arc GIS 9.3.

#### 4.3.3.2.4. Social and economic activity on forbidden hazard

Merapi flank is one of most densely populated volcanic areas. It is inhabited by almost 1.1 million people of which 440.000 are 440,000 are at relatively high risk in areas prone to pyroclastic flows, surges, and lahars (Thouret *et al.*, 2000). Overview of social and economic activities on forbidden zone was carried out to portray number of inhabitants on forbidden zone and current activities of inhabitants despite threat of the most dangerous and devastating hazards from the volcano. The overview of social and economic activities was delivered from previous studies, reports, spatial and statistic data combined with field work results both pictures and interviews.

# Chapter 5. DEM Generation and Quality Comparison

*This chapter provides result of DEMs preprocessing, DEM generation from dataset, DEMs quality comparison by initial observation, height distribution and statistical parameter and concluding remarks.*

## 5.1. DEM Generation

DEM generation was separated into two steps: DEM pre – processing and 3D models development from dataset.

### 5.1.1. DEM Preprocessing

DEM preprocessing was conducted to deliver proper surface representation as input data for morphologic analysis by editing gross and random error. Identification of those errors was performed on hill shade models since grid DEM unable to deliver them. Gross error of dataset was occurred on digital topographic maps, DEM 1996 and DEM 2006, whilst random error of dataset occurred from IFSAR DEM.

Editing for gross errors was limited to correction of wrong coded line elevations whilst refining terrace like paddy field either by adding supplementing contour with additional point elevation or degrading effective scale of DEM (Reuter *et al.*, 2009) were hardly to conduct because topographic condition had already changed and degrading the effective scale leading to less morphologic features representation. An example of gross error correction was displayed in figure 5-1.

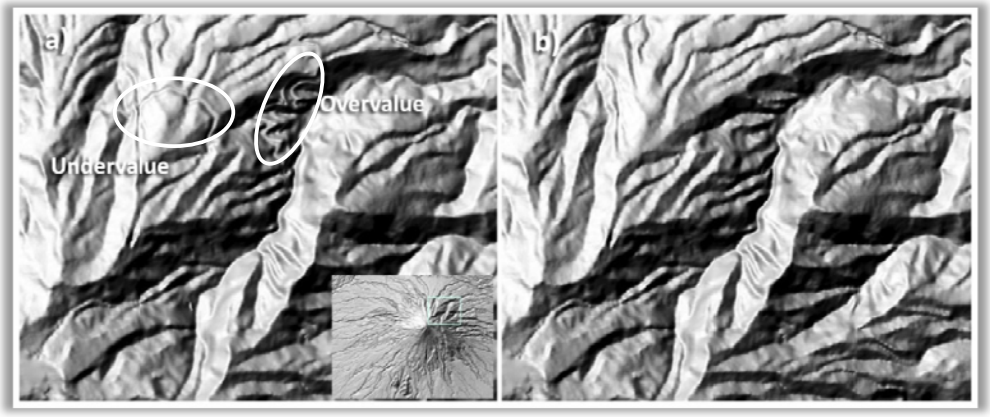


Figure 5-1. Gross error on DEM 1996, a) Undervalue and overvalue recognized on DEM, b) DEM after editing

Random error on IFSAR DEM was delivered from the nature of data capturing process. Since filling void area and filtering may affect DEM elevation, some striped lines on summit area was eliminated by re – interpolating the DEM using Topo 2 Raster interpolation method, see figure 5-2. The result of pre processing DEM would be used in morphologic analysis whereas original IFSAR DEM would be utilized in DEM quality comparison.

### 5.1.2. 3D Models Development

3D models of DEM were built from combination of hill shade and TIN by means of Arc Scene 9.3. Hill shade (illumination from southwest, 55°) and TIN models were built from grid DEM pixel size 5m using 3D analyst tools in Arc GIS. 3D models were used to assistance morphologic feature recognition to observe morphologic changes over 70

years. The results of 3D models were explained and displayed including some reference points: Gn. Turgo, Gn. Plawangan, Gn. Kendil and MOP Babadan.

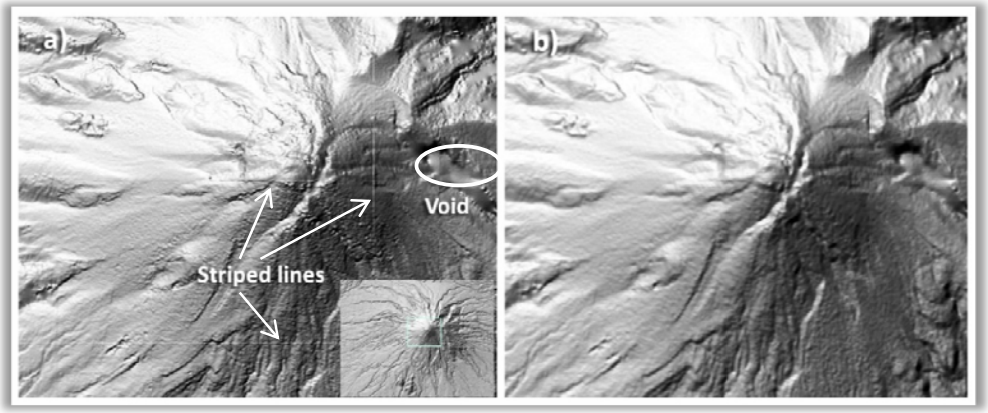


Figure 5-2. Random error on IFSAR DEM, a) striped lines and void area, b) DEM after editing

### 5.1.2.1. 3D Model of DEM 1935

3D modeling of DEM 1935 was built from AMS topographic map scale 1: 50.000 resulted from plane table survey. Digitalization process was conducted manually using point mode – on screen digitizing in preview scale of 1: 3000 to 1: 4000 since low quality of lines obstacles automatic conversion using Arc Scan tools.

Digital contour lines were then converted into grid DEM by Topo 2 Raster interpolation before built into TIN and hill shade. Combination of TIN and hill shade was assembled to build 3D representation of the area as shown in figure 5-3.

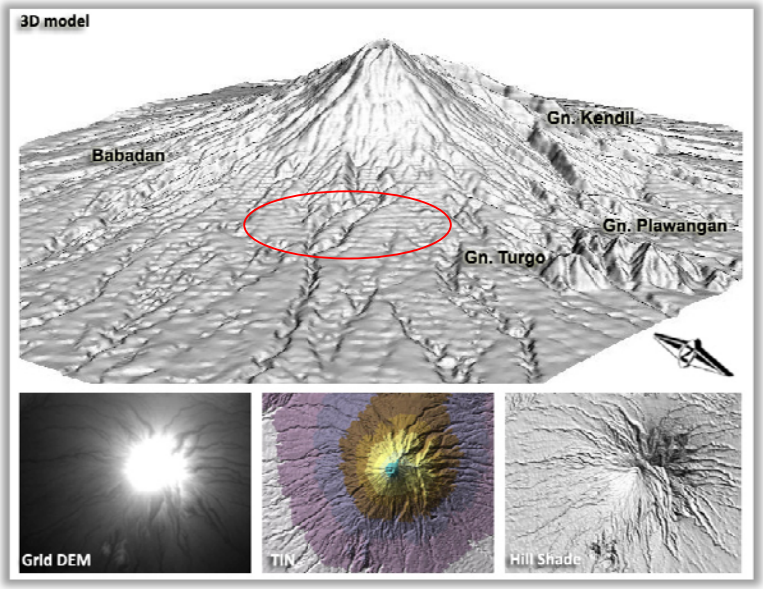


Figure 5-3. 3D model of DEM 1935

Some terraces like paddy field, red circle, could be spotted in vicinity area. These phenomena typically occurred from enclosed contour (Reuter *et al.*, 2009) that hardly to refine. Utilization of the data was carried out because rather difficult to find more reliable data to observe changes in summit morphology.

.

### 5.1.2.2. 3D Model of DEM 1982

The model was built from VSI topographic map scale 1:100.000 produced from aerial survey. Digitizing process was conducted manually using point mode – on screen digitizing, preview scale of 1: 3000 because poor quality of data in which contour lines were overlying the orthophoto in scanned format.

Digital contour lines were then converted into grid DEM by Topo 2 Raster interpolation before built into TIN and hill shade. Combination of TIN and hill shade was assembled to build 3D representation of the area as shown in figure 5-4.

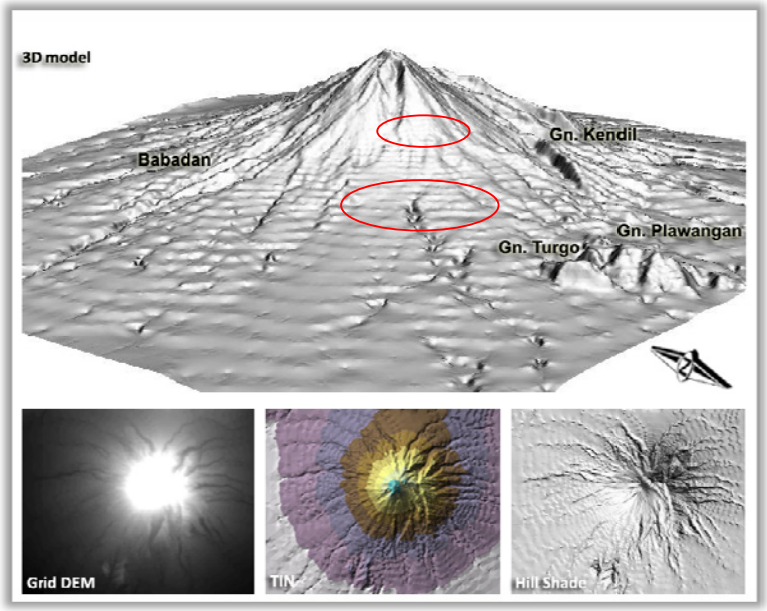


Figure 5-4. 3D model of DEM 1982

Similar to 3D model of 1935, some terraces some terraces also appear in the summit and vicinity area, red circles. Due to short of data available, this DEM was used to observe changes in summit morphology from last 70 years.

### 5.1.2.3. 3D Model of DEM 1996

3D model was built from BAKOSURTANAL digital contour of topographic map scale 1:25.000. The contour lines were converted to 5 x 5 m grid DEM before built into TIN and hill shade. 3D visualization was resulted from combination of TIN and hill shade as shown in figure 5-5.

Terraces in previous two DEMs were absent but volcanic cone was appeared as smooth surface, red circle, which might result from volcanic material covered or less detail topographic representation.

### 5.1.2.4. 3D Model of DEM 2006

The model was developed from SVT SABO digital contour of topographic map scale 1:5.000. The contour lines were converted to 5 x 5 m grid DEM before built into TIN and hill shade. 3D visualization was resulted from combination of TIN and hill shade as shown in figure 5-6.

Summit and vicinity area was clearly represented in the area that free of cloud covered despite some parts of summit and vicinity area covered by solfatara, red circles, which hinder observation of some morphologic features.

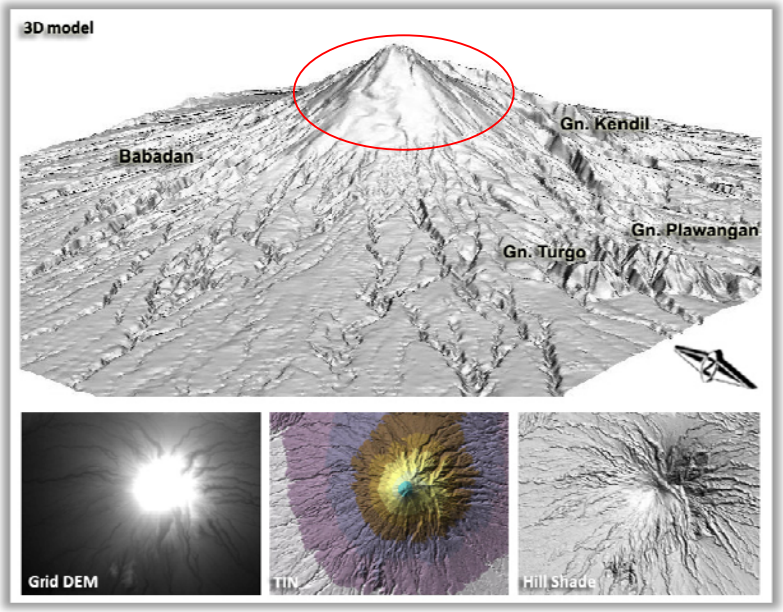


Figure 5-5. 3D model of DEM 1996

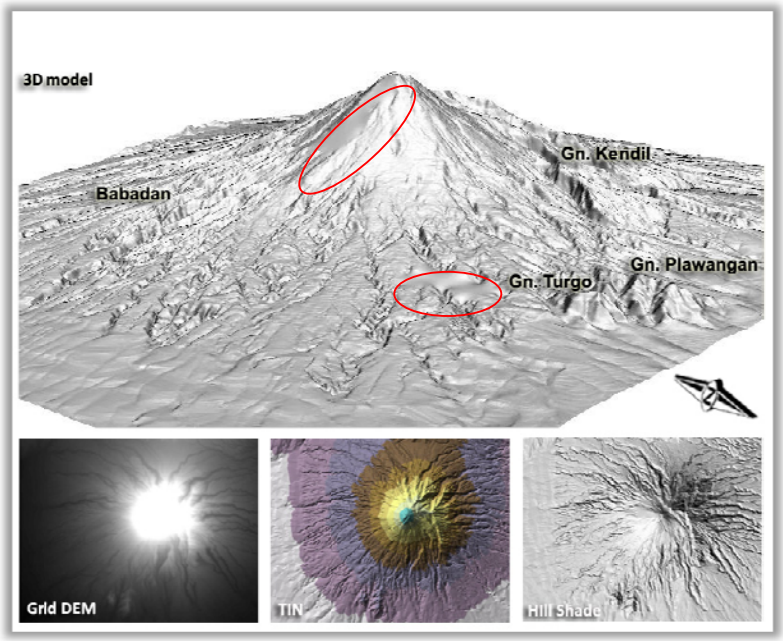


Figure 5-6. 3D model of DEM 2006

### 5.1.2.5. 3D Model of IFSAR DEM

3D model was built from DSM of Merapi in the beginning of June, just after 27 May 2006 earthquake and before the eruption. Re – interpolated grid DEM was built into TIN and hill shade. 3D visualization was resulted from combination of TIN and hill shade as shown in figure 5-7.

Vicinity area appeared as rough surface since IFSAR DEM was a digital surface model and upper slope of volcanic cone was covered by dense vegetation. However, summit area could be categorized as bare land that surface it represent is terrain representation (Li *et al*., 2005; technician expert of ExsaMap Asia, written communication).

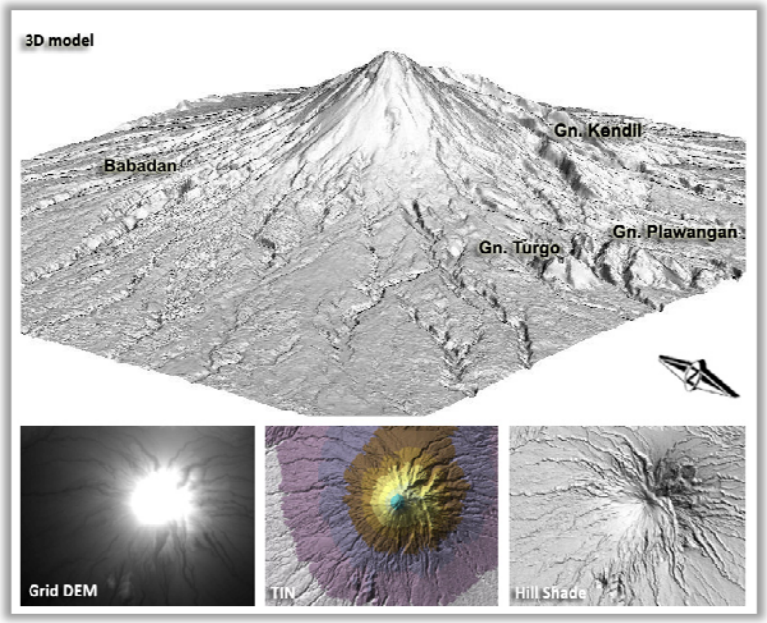


Figure 5-7. 3D model of IFSAR DEM

### 5.1.2.6. 3D Model of ALOS DEM

ALOS DEM was extracted from pairs of ALOS imagery portrayed in 12 September 2006, three months after last eruption in 2006. South, southwest and western part of study area was covered by thin cloud that prevents DEM extraction, figure 5-8a.

The result of DEM extraction was displayed in figure 5-8b, with a lot of void area both in summit and vicinity area. Void area surround volcanic cone was re – interpolated using IFSAR DEM in form of contour lines (interval 25m), but the edifice could not refined because summit topography had changed during the eruption 2006. TIN, hill shade and 3D model of ALOS, figure 5-9, were conducted from re – interpolated grid DEM.

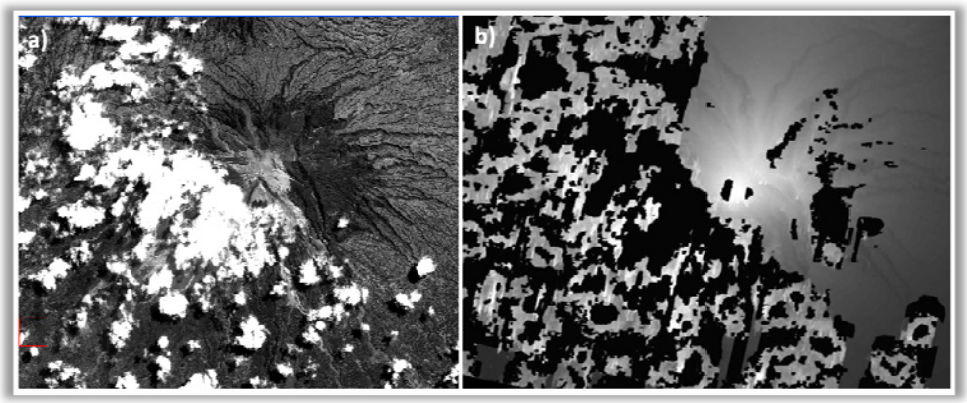


Figure 5-8. Study area in original scene of ALOS Prism Nadir Image (a) and extracted DEM (b)

The quality controls of DEM resulted by simple strategies of minimizing error during data acquisition, eliminating and reducing effect of errors and minimizing error introduced to surface modeling (Li *et al*., 2005) were partly carried out since the data used in this research were existing data. Eliminating and reducing effect of errors and minimizing their effect were accomplished through DEM preparation process and applied particular interpolation method. Hence, the quality of data input was mainly controlled by input data.

Initial interpretation of DEM input quality was carried out by observing their ability to convey morphology of the study area, especially morphologic features used in EM analysis, as shown in table 5-1.

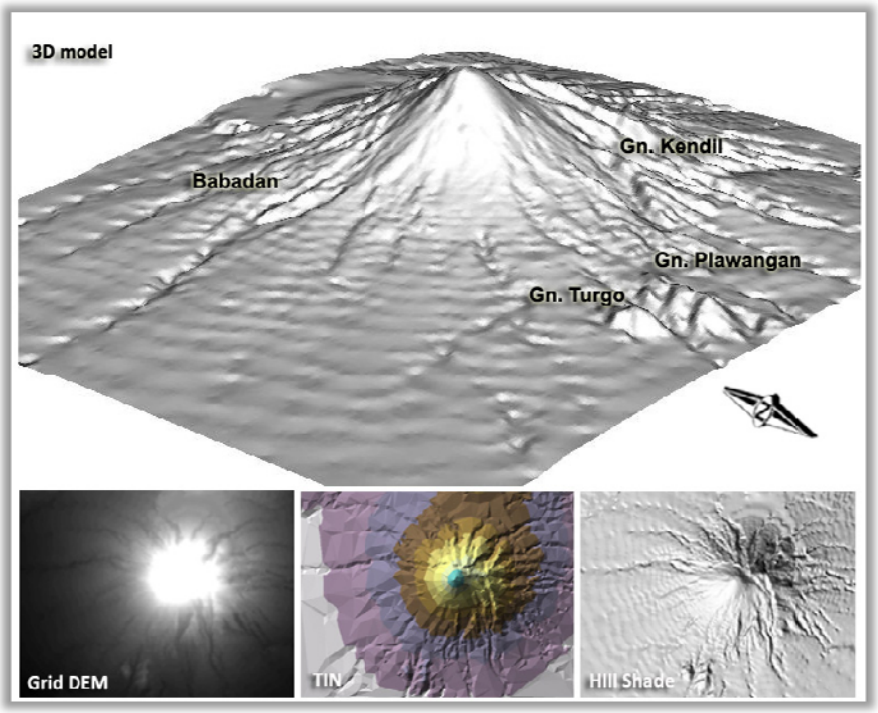


Figure 5-9. 3D model of ALOS DEM after refined

Table 5-1. Initial observation among DEMs

| | DEM 1935 | | DEM 1982 | | DEM 1996 | |
|---|---|---|---|---|---|---|
| | Summit | Vicinity | Summit | Vicinity | Summit | Vicinity |
| Representation of morphologic features | Good | Moderate | Moderate | Poor | Moderate | Good |
| | DEM 2006 | | IFSAR DEM | | ALOS DEM | |
| | Summit | Vicinity | Summit | Vicinity | Summit | Vicinity |
| | Good | Good | Good | Poor | Poor | Poor |

Initial interpretation of 3D models of DEMs above showed that accuracy of DEMs produced were mainly depend on quality of data source including techniques of data acquisition, scale of data representation and quality of original map as follows:

1. DEMs 1935 produced from plane table survey in scale 1:50.000 represented more detail topographic representation in summit area rather than DEM 1996 produced from photogrammetry technique in scale 1:25.000, refer to figure 5-3 and 5-5.
2. Poor quality of original map and small scale input data had led to less detail topographic representation as shown in figure 5-2.
3. DEM 2006 could give detail representation for both summit and vicinity area compared to other DEMs although solfatara and cloud often hindered edifice of active volcano. Cloud and solfatara were also the main obstacles to extract DEM from ALOS satellite imagery although it has higher accuracy than IFSAR DEM.
4. Terraces like paddy fields were often occurred in DEM derived from closed contours in which all elevation values inside the contours were assigned in the same value (Reuter *et al.*, 2009). Hence, they might affect morphometric quantification of particular features.

The scale of source data should guide the choice of resolution of generated DEMs and the scale of DEMs interpretation should match the natural scales of terrain dependent

applications (Goudie *et al.*, 1990; Hutchinson and Gallant, 2000). Land systems mapping may employ 1:50.000 base maps, or even smaller, whereas detailed morphological mapping and morphometric measurement require maps of 1:25.000 or larger with contour intervals of 10 m or less (Goudie *et al.*, 1990).

From initial observation, scale of 1: 25.000 seemed appropriate for studying vicinity area but scale 1: 5.000 or even larger were needed to study summit area. In addition to the scale, acquisition method needs to be considered since summit area of active volcano is a dangerous zone and it is often covered by cloud and solfatara. Until recently, ground survey and large scale aerial photograph could give better DEM representation rather than active remote sensing techniques e.g. IFSAR but they might restricted by dangerous of active volcano for ground measurement and by cloud or solfatara covered for aerial photographs. Thus, active remote sensing techniques should be taken into account to study volcano morphology despite expensive cost and technology used in these industries.

## 5.2. DEMs Quality Comparison

DEM quality comparison of this research was carried out to determine suitability of DEM produced from active remote sensing technique toward the one produced from passive technique. Since check points from DGPS could not be carried out due to topographic condition, DEM 2006 was used as reference to assess the quality of IFSAR DEM.

DEMs quality comparison was performed by combination of statistical and visual methods. Statistical methods used to compare DEMs through calculation of error range, mean errors and RMSz errors while visual methods were carried out through comparing height distribution of horizontal and vertical transect lines. Selection of points and transect lines were restricted to south - southeast – east – northeast – north of summit area and avoiding the vicinity area due to discrepancy of DSMs and DTM.

### 5.2.1. Visual Method for DEM Quality Comparison

Visual methods for comparing those three DEMs were carried out by comparing height distribution along transect lines drawn in those DEMs. The first and third transect lines were made horizontal along the elevation while the second transect line was made crossing the elevation. The height distributions of IFSAR DEM compared to DEM 2006 was displayed in figure 5-11.

From height distributions drawn in figure 5-11, visual interrogations of their distribution were carried out which enlighten some points in each line as follows:

1. Profile graph of transect line 1 showed almost similar trend of IFSAR DEM compared to reference DEM but in some point height differences could also easily observed. Distribution heights of IFSAR DEM along transect line 1 was somewhat smoother than those of reference DEM.
2. Very similar height distribution of transect line 2 with reference DEM could be easily observed in the profile graph. Height distributions of IFSAR DEM were smoother than those of reference DEM.
3. IFSAR DEM height distributions along transect line 3 displayed similar pattern although some serious height differences occur along the lines. Smoother height distribution was also observed along IFSAR transect lines rather than reference DEM.

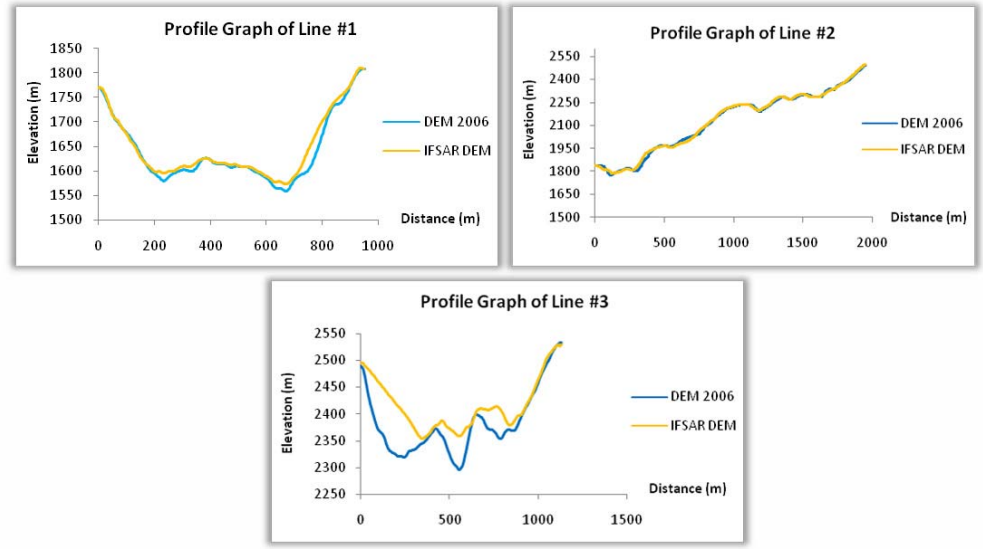


Figure 5-10. Height distribution along three transect lines

Smoother pattern in transect lines of IFSAR DEM compared to those of DEM 2006 was resulted from DEM accuracy. DEM 2006 were derived from contour interval 2.5 meter with accuracy 1/3 of contour lines (Li *et al.*, 2005) whereas IFSAR DEM type III has 3 meters accuracy (technician expert of ExsaMap Asia, written communication).

Different height distribution of profile lines 1 might result from volcanic ashes since IFSAR DEM was taken in the middle of Merapi activities and the transect line located very close to Merapi edifice. Serious height distribution along transect line 3 was resulted from pyroclastic flow material since this area were also affected by small pyroclastic flow during 2006 activity (CVGHM, 2006) before new crater breaching was formed toward southeast direction where transect lines 2 drawn. Thus, the height distributions of IFSAR DEM along transected line 2 were displaying actual distribution height compared to DEM 2006.

## 5.2.2. Statistical method for DEM Quality Comparison

Statistical parameters for elevation differences: error range, mean errors, and RMSz error were delivered from fifteen conjugate points in two DEMs. The conjugate points were the points which refer to the same natural object e.g. ridges, peak of hills. The elevation differences of IFSAR DEM to DEM 2006 (dz) were displayed in table 5-2 from which those three parameters were then calculated, as shown in table 5-3.

Table 5-2. Elevation differences and statistical parameters

| Id | $Z_{IFSAR\ DEM}$ (m) | $Z_{DEM\ 2006}$ (m) | dz (m) | $dz^2$ ($m^2$) |
|---|---|---|---|---|
| 1 | 1849.487 | 1854.025 | -4.538 | 20.591 |
| 2 | 1846.040 | 1837.809 | 8.231 | 67.744 |
| 3 | 1686.776 | 1681.738 | 5.039 | 25.387 |
| 4 | 1770.237 | 1769.140 | 1.097 | 1.203 |
| 5 | 1811.091 | 1808.167 | 2.924 | 8.552 |
| 6 | 2391.825 | 2389.276 | 2.550 | 6.500 |
| 7 | 2495.410 | 2487.804 | 7.606 | 57.844 |
| 8 | 2666.687 | 2658.219 | 8.468 | 71.707 |
| 9 | 2640.690 | 2644.198 | -3.508 | 12.305 |
| 10 | 2544.074 | 2533.343 | 10.731 | 115.163 |
| 11 | 2394.988 | 2392.858 | 2.130 | 4.537 |
| 12 | 2426.613 | 2423.489 | 3.123 | 9.754 |
| 13 | 2502.821 | 2497.063 | 5.758 | 33.156 |
| 14 | 2255.850 | 2248.555 | 7.295 | 53.223 |
| 15 | 2050.300 | 2049.026 | 1.274 | 1.622 |

Table 5-3. Statistical parameters

| Parameters | Value |
|---|---|
| $\Sigma dz^2$ | 489.288 $m^2$ |
| $\Sigma dz^2/n$ | 32.619 m |
| **Range** | **15.269 m** |
| **Mean ($\mu$)** | **3.879 m** |
| **RMSEz error** | **5.711 m** |

The statistical computation from elevation differences were resulted in 3.879 m of mean error, 15.269 m of range error and 5.711 m of RMSEz error. Thus, the absolute elevation of IFSAR DEM compared to references DEM was less acceptable since specification of IFSAR DEM vertical accuracy should be less than 3 m for DSM type III (Intermap, 2009).

IFSAR data delivered was the raw data, indentified from striped lines and void which may affect absolute elevation of check points. Thus, processed data of IFSAR DEM were needed to deliver better quality assessment.

## 5.3. Concluding Remarks

1. Initial interpretation among DEMs showed that DEM delivered from topographic map scale 1: 25.000 was appropriate to study morphology of vicinity area but larger scale, 1: 5000 or even larger was needed to deliver morphologic detail of summit area.
2. Different methods of deriving DEM play important rule in surface morphology's representation. Ground survey and aerial photogrammetry techniques were deliver better representation of topography rather than active sensor but limitation of those techniques leads to utilization of active remote sensing to study morphologic changes of summit area.
3. Visual assessment of height distribution showed that IFSAR DEM has similar height distribution along transect lines although it conveyed less detail topography compared to that of DEM 2006.
4. Statistic parameters showed that vertical accuracy of IFSAR DEM was less than the product specification, 3 m for DSM type III, with mean error 3.879 m, range error 15.269 m and RMSEz error 5.711 m.

# Chapter 6. Morphologic Analysis

*This chapter provides utilization of EDM data for morphologic changes, morphologic features recognition and quantification, morphologic analysis for verifying factor ascertain Merapi – type direction, reconstruction of Merapi – type eruption in the past using those factors, comparison of reconstruction results to historical data and concluding remarks.*

Morphologic analysis of morphologic features to determine direction of lava dome collapse in the near future was carried out through five main parts: EDM for morphologic changes, morphologic features recognition and quantification on past time DEMs, morphologic analysis to determine factors ascertain direction of Merapi – type eruption, reconstruction of direction of Merapi – type eruption in the past and comparison of construction results to that of historical data.

## 6.1. EDM for Morphologic Changes

Electronic distance meter (EDM) is one of monitoring tools utilized by MVO for ground deformation as precursor of Merapi activities. EDM measurement was divided into summit and observatory trilateration network. Since complete data was unable to conduct from MVO, observatory trilateration data was obtained directly from four MOPs: Kaliurang, Babadan, Jrakah and Selo.

Observatory trilateration network was developed from distance measurements of fixed prisms mounted on summit and flank area from benchmarks in every MOP, figure 6-1. Based on data observation and interview, every MOP has different number of fixed prisms to be measured independently, meaning no prism measured from two MOPs. Recently, Kaliurang has four prisms utilized to replace previous prisms that tore down during eruption in 2006; Babadan has six prisms; Jrakah and Selo have two prisms and other two fixed prisms from Deles. Since no MOP located in Deles, EDM data from Deles was unable to collect.

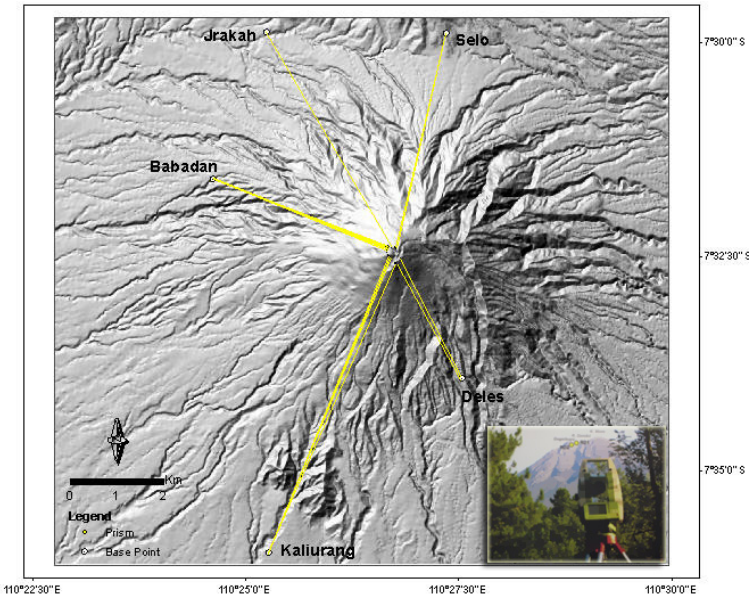


Figure 6-1. Sketch of Merapi observatory trilateration network, inset: EDM equipment (Reconstructed from MVO publication at Merapi Museum, taken at October 24th, 2009 and information from PIC at every MOP)

EDM data obtained were varied from one to other MPO for parameters measured and completeness (Table 6-1). EDM data started to be measured regularly after eruption 2006 regarding EDM instrument availability. From data observation, slope distances between benchmark and fixed prisms were the main parameter measured.

Table 6-1. Variable and completeness of EDM data from MOPs, complete: measured throughout the year

| No | Parameter | Kaliurang | Babadan | Jrakah | Selo |
|---|---|---|---|---|---|
| Variables | | | | | |
| 1 | Time | √ | √ | √ | √ |
| 2 | Atmosphere pressure | √ | √ | √ | √ |
| 3 | Temperature | √ | √ | √ | √ |
| 4 | Ppm | √ | √ | √ | √ |
| 5 | Horizontal angle | √ | | | |
| 6 | Vertical angle | √ | | | √ |
| 7 | Horizontal distance | √ | | | √ |
| 8 | Vertical distance | √ | √ | √ | √ |
| Data completeness | | | | | |
| 1 | 2006 | April – May | Feb – May , Aug | April – Sept | April – Dec |
| 2 | 2007 | Feb – Oct | Complete | April, June – Aug | Jan , Feb & June |
| 3 | 2008 | - | Complete | Complete | April, June – Dec |
| 4 | 2009 | April – Aug | Jan - Aug | Jan - Sept | Jan - Sept |

Construction of trilateration network needs beach mark coordinates, slope distances between benchmarks and fixed prisms and horizontal angle between two fixed prisms in the network. Construction of trilateration network in this study was difficult to carry out due to data availability. The best utilization of the EDM data available was distance changes from year 2006 to September 2009.

### 6.1.1. Distance Changes of Prisms in MOP Selo

In 2006, MOP Selo has only one prism to be measured and one additional prism was installed in 2007. The fixed positions of those prisms are: RS 1 in L 1956 and RS 2 in LUL or in block lava 1988 – 1909 a (see figure 6-7 as reference). The distance changes were computed from average slope distance in a year, table 6-2, before finally drawn into graphic in figure 6-2.

Table 6-2. . Slope distance and distance changes at MOP Selo

| Yearly Average Slope Distance | | | Distance Changes | |
|---|---|---|---|---|
| **Year** | **RS 1 (m)** | **RS 2 (m)** | **RS 1 (m)** | **RS 2 (m)** |
| 2006 | | 4824.908 | | |
| | | | **0.000** | **3.243** |
| 2007 | 4836.661 | 4828.151 | | |
| | | | -0.106 | -0.158 |
| 2008 | 4836.556 | 4827.993 | | |
| | | | -0.036 | -0.017 |
| 2009 | 4836.519 | 4827.976 | | |
| | | **Changes 2007 - 2009** | **-0.142** | **-0.175** |

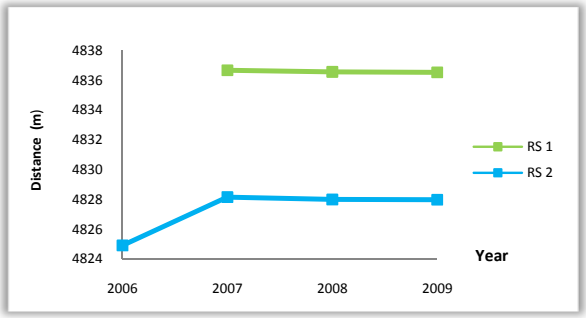


Figure 6-2. Distance changes of prisms at MOP Selo

During year 2006 – 2007, significant distance change of RS 2, 3.243 m, was observed whilst only small changes during 2007 – 2009, less than 0.2 m. The significant changes of slope distance during 2006 – 2007 were caused by Merapi activity in 2006.

### 6.1.2. Distance Changes of Prisms in MOP Jrakah

Jrakah has two fixed prisms which located in LUL (RJ 1) and L 1956 (RJ 2). The distance changes of those prisms during 2006 – 2009 were displayed in table 6-3 and figure 6-4. During 2006 – 2007, RJ 1 showed significant changes, -4.172 m, whilst RJ 2 showed only slightly distance changes, -0.110. Meanwhile, during 2007 – 2009, both RJ 1 and RJ 2 show slightly changes, 0.140 m for RJ 1 and 0.164 m for RJ 2.

Table 6-3. Slope distance and distance changes of prisms at MOP Jrakah

| Yearly Average Slope Distance | | | Distance Changes 2006 - 2009 | |
|---|---|---|---|---|
| **Year** | **RJ 1 (m)** | **RJ 2 (m)** | **RJ 1 (m)** | **RJ 2 (m)** |
| 2006 | 5616.363 | 5699.772 | | |
| | | | **-4.172** | **-0.110** |
| 2007 | 5612.190 | 5699.662 | | |
| | | | -0.098 | -0.111 |
| 2008 | 5612.092 | 5699.551 | | |
| | | | -0.042 | -0.053 |
| 2009 | 5612.051 | 5699.498 | | |
| | | **Changes 2007 - 2009** | **-0.140** | **-0.164** |

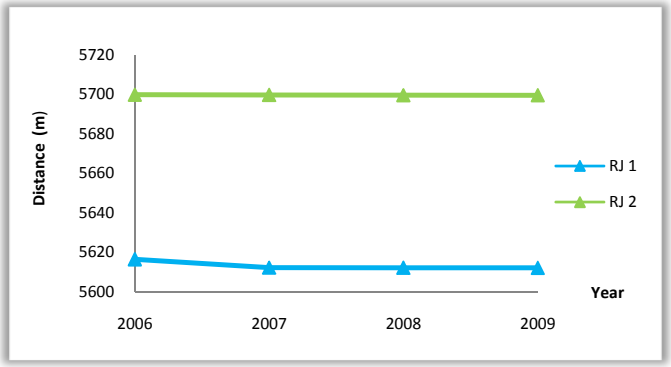


Figure 6-3. Distance changes of prisms at MOP Jrakah

### 6.1.3. Distance Changes of Prisms in MOP Babadan

Distance measurement at MOP Babadan has been started since 2003 with additional numbers of prisms measured. In 2006, three prisms had been installed to be measured from Babadan, RB 1 and RB 2 located in L 1948 and RB 3 located in L 1988. In 2007, an additional prism was installed in L 1948, named RB 4. RB 5 and RB 6 were installed in L 1888 at the beginning of 2009.

Average slope distance from 2006 to 2009 was displayed in table 6-4 from which distance changes of prisms were calculated, table 6-5. Table 6-5 showed that significant distance changes only occurred in RB 4, 0.6 m, whilst others less than 0.1 m. Figure 6-5 showed distance changes from 2006 to 2009 for RB 1 – RB 4.

Table 6-4. Slope distance of prisms at MOP Babadan

| Yearly Average Slope Distance | | | | | | |
|---|---|---|---|---|---|---|
| **Year** | **RB 1 (m)** | **RB 2 (m)** | **RB 3 (m)** | **RB 4 (m)** | **RB 5 (m)** | **RB 6 (m)** |
| **2006** | | 4425.176 | 4431.009 | | | |
| **2007** | 4424.618 | 4424.862 | 4430.661 | 4428.183 | | |
| **2008** | 4424.513 | 4424.768 | 4430.713 | 4429.518 | | |
| **2009** | 4424.649 | 4424.769 | 4430.691 | 4428.784 | 3832.450 | 3760.197 |

Table 6-5. Distance changes of prisms at MOP Babadan

| Distance Changes 2006 - 2009 | | | | | | |
|---|---|---|---|---|---|---|
| **Year** | **RB 1 (m)** | **RB 2 (m)** | **RB 3 (m)** | **RB 4 (m)** | **RB 5 (m)** | **RB 6 (m)** |
| **2006** | | | | | | |
| | **0.000** | **-0.315** | **-0.348** | **0.000** | | |
| **2007** | | | | | | |
| | -0.104 | -0.094 | 0.052 | 1.335 | | |
| **2008** | | | | | | |
| | 0.135 | 0.001 | -0.022 | -0.735 | 0.000 | 0.000 |
| **2009** | | | | | | |
| **Changes 2007 - 2009** | **0.031** | **-0.093** | **0.030** | **0.600** | **0.000** | **0.000** |

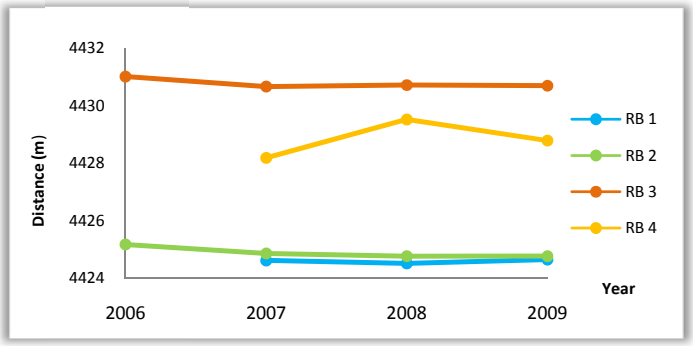


Figure 6-4. Distance changes of prisms at MOP Babadan

## 6.1.4. Distance Changes of Prisms in MOP Kaliurang

Before eruption 2006, MOP Kaliurang has two fixed prisms, RK 2 and RK 3 installed in Gegerboyo or L 1911 – 1913. 2006's activity had torn down those prisms making the observation of distance changes from 2006 to 2009 was unable to conduct.

Four new prisms RK 1 – RK 4 were installed in the Gegerboyo, adjacent to the new crater breaching toward southeast. RK 1 and RK 2 were installed in 2007 and RK 3 and RK 4 were installed in 2009. Slope distances and distance changes of those prisms during 2007 – 2009 were displayed in table 6-6 and figure 6-6 with the absence of data in 2008.

Table 6-6. Slope distance and distance changes of prisms at MOP Kaliurang

| Yearly Average Slope Distance | | | | | Distance Changes 2006 - 2009 | | | |
|---|---|---|---|---|---|---|---|---|
| **Year** | **RK 1 (m)** | **RK 2 (m)** | **RK 3 (m)** | **RK 4 (m)** | **RK 1 (m)** | **RK 2 (m)** | **RK 3 (m)** | **RK 4 (m)** |
| **2006** | | 7066.344 | 7045.745 | | | | | |
| | | | | | | | | |
| **2007** | 6579.374 | 6508.146 | | | | | | |
| | | | | | 0.662 | -0.962 | 0.000 | 0.000 |
| **2009** | 6580.036 | 6507.183 | 6755.287 | 6861.839 | | | | |
| | | | **Changes 2007 - 2009** | | **0.662** | **-0.962** | **0.000** | **0.000** |

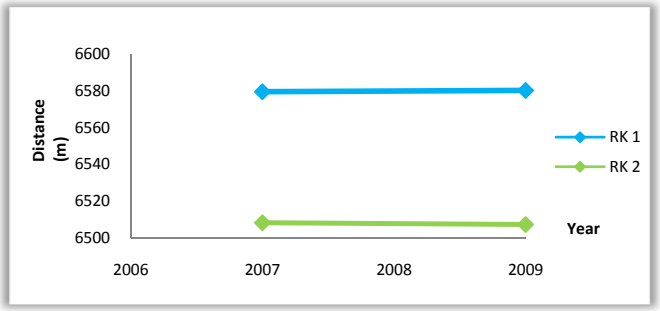


Figure 6-5. Distance changes of prisms at MOP Kaliurang

As we observed in table 6-6, distance changes of RK 1 and RK 2 conveyed significant changes in term of deformation, almost 1 m, during 2007 – 2009. Distance changes of RK 1 showed positive value whist distance changes of RK 2 showed negative value indicating reverse ground movement of the summit area.

Observation of EDM data showed that the slope distances often varied from day to day because EDM instrument was sensitive to changes in temperature, atmospheric pressure or humidity. No standard for time measurement made difficult to distinguish changes caused by magma activity or by instrumental bias except if trend of distance changes has continued. On the other hands, cloud covered, especially during monsoon and rainy season, made standardization for time measurement rather difficult to achieve.
Positive value of distance changes is an indication of ground deformation toward the direction of distance measurement and vice versa. Slope distance of prisms showed significant changes i.e. RS 2 (3.243 m), RJ 1 (-4.172 m) meaning magma extrusion caused deformation before, during and after eruption. Meanwhile, according to PIC at MOPs, during quiescence phase of Merapi e.g. from 2007 to 2009 usually no significant distance changes occur (± 10 cm) due to instrument bias, unless magma extrusion makes displacement in some parts of edifice. For instance, distance changes of three prisms: RB 4 (0.6 m), RK 1, (0.662 m) and RK2 (-0.962 m) indicates magma extrusion through conduit on south – southeast of Merapi edifice (Santoso *et al.*, 2009) and emphasize the instability of south flank – southeast flank.

Although distance changes were categorized significant during Merapi activities in term of ground deformation, they were difficult to be observed on DEM since their movements were less than a pixel size (5m). In case of enormous morphologic changing, there was a possibility of prism to tear down by dome collapse i.e. eruption in 2006. Thus, EDM data was less useable to observe morphologic changes of summit area.

## 6.2. Morphologic Features' Recognition and Quantification

Morphologic features recognition and quantification of past time DEMs were performed to conduct parametric analysis of features which plays important role in determining direction of dome collapse or Merapi – type eruption.

### 6.2.1. Morphologic features' recognition

Morphologic feature recognition was carried out to observe morphologic features in both summit and vicinity area that might reveal direction of Merapi – type eruption in the past. Features recognized were mainly the ones located in or around Merapi edifice with some additional features of vicinity area since direction of Merapi – type eruption was defined by summit topography.

Morphologic features recognition was conducted on past time DEMs: DEM 1935, 1982, 1996, 2006 and IFSAR DEM. Features from summit area able to identify were active crater rim, crater floor, crater breaching, adjacent ridges, breaches and remnant of domes. Features from vicinity area included drainage pattern, lineaments and major rivers.

#### 6.2.1.1. Morphologic features of summit area

Morphologic features of summit area on each DEM were observed and delineated on hill shade model with assistance of 3D model. Hill shade models were utilized for showing crater rims (green line: crater rim 1930, yellow line: crater rim 1961, dashed when inferred), crater floor (red lines), crater breaching (green dashed), breaches (purple dashed) and remnant of domes (blue lines, orange text indicating new domes) from

above, whilst 3D models viewed from southwest emphasized crater breaching, adjacent ridges, breaches and preliminary cracks as shown in figure 6-6 to figure 6-10.

#### 6.2.1.1.1. Summit area of DEM 1935

Observation on hill shade models of DEM 1935 showed active crater rim 1930 opened to west surrounded by steep rim wall with remnant of dome 1934 (coulee shaped) in the middle of depression, separated from surrounding rim wall by crater floor.

Adjacent ridges of crater breaching were located in the south and north of the depression forming artificial blocking channel toward west. South ridge was part of West dome (L 1911 – 1913) called *Gegerboyo*, peak point of *triangle rock*, and north ridge was L 1930. A crater breach, Br 1, was observed between Gegerboyo (L 1911 – L 1913) and East dome (L 1888 – 1909 b).

Some remnant of domes were able to observe in the summit area with various orientations, most of them were from remnants of East dome (L 1988, L 1888 – 1909 a, L 1888 – 1909 b and L 1906) and West dome (L 1911 – 1913) while others were formed after explosion 1930: L 1930, L 1931 and L 1934. Morphologic features of Merapi summit on DEM 1935 were displayed in figure 6-6.

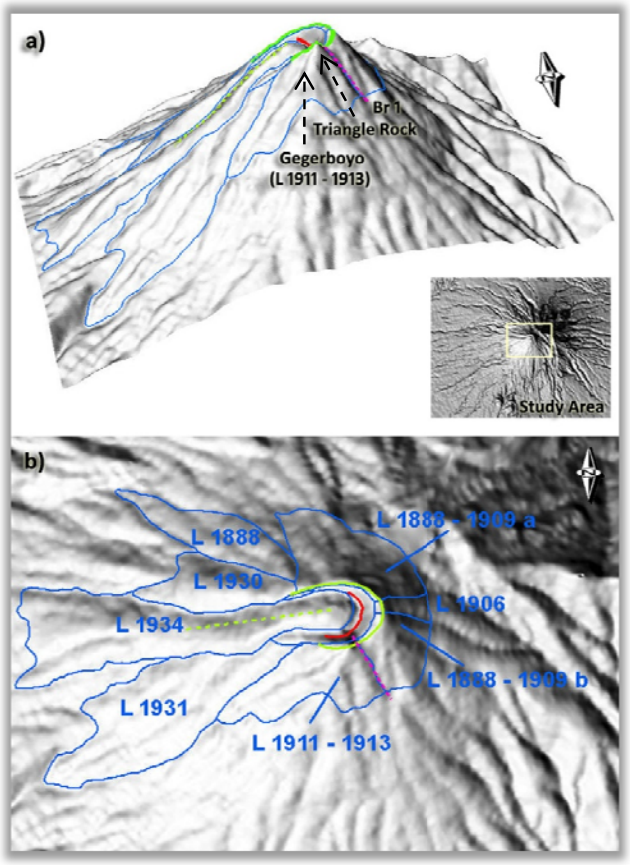


Figure 6-6. Morphologic features of Merapi summit on DEM 1935, not scaled. Inset: DEM 1935 of study area, a) Observed on 3D model, b) Observed on hill shade.

#### 6.2.1.1.2. Summit area of DEM 1982

Active crater rim of 1961 opened toward southwest and crater floor was covered by accumulative material of L 1940, L 1942 and L 1943. Crater breaching 1930 had filled by eruptive materials, leaving narrower depression compared to that of southwest.

Adjacent ridges of crater breaching 1961 were *Gegerboyo* (L 1911 – 1913) in south and narrow ridge of L 1934 in north, which also separated crater breaching 1930 and crater

breaching 1961. Triangle rock collapsed during the eruption of 1961 (Ratdomopurbo and Andreastuti, 2000) result in lower southern ridge. A breach, Br 1, was observed between Gegerboyo (L 1911 – 1913) and East dome (L 1888 – 1909 b). A preliminary crack, parallel to Br 1, was noticed between Br 1 and crater breaching.

Some remnants of domes were unable to recognize due to low topographic representation. Besides remnants of East and West domes, only L 1931 and L 1934 in west, accumulative dome of L 1940, L 1942 and L 1943 inside crater rim and L 1948, L 1953 – 1955 and L 1956 in north - northwest able to recognize whereas L 1957 – 1958 in west, part of L 1942 and L 1948 in southwest were unable to recognize. Morphologic features of Merapi summit on DEM 1982 were displayed in figure 6-7.

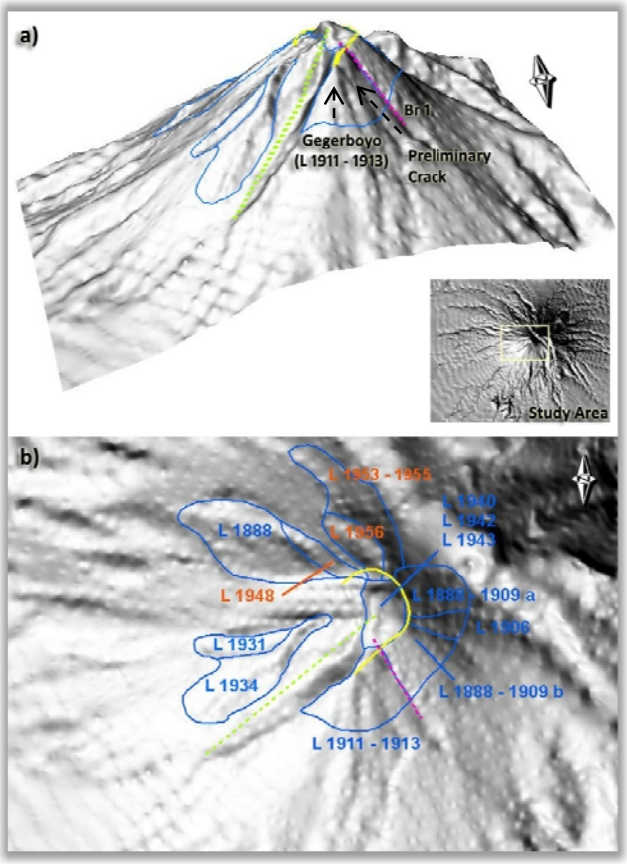


Figure 6-7. Morphologic features of Merapi summit on DEM 1982, not scaled. Inset: DEM 1982 of study area, a) Observed on 3D model, b) Observed on hill shade.

**6.2.1.1.3. Summit area of DEM 1996**

Summit area of DEM 1996 showed some changes from previous DEM. Crater floor was able to notice and crater breaching 1961 still opened to southwest direction, blocked by L 1992 – 1994 in southwest resulting little shifting of low land area more to south.

Adjacent ridges of crater breaching were Gegerboyo in south and L 1992 – 1994 in north. Two breaches, Br 1, between L 1911 – 1913 and L 1888 – 1909 b and Br 2, between L 1956 and L 1888 – 1909 a, were noticed. In addition to those breaches, two preliminary cracks: between Br 1 and crater rim breaching and between L 1953 – 1955 and L 1948 were recognized.

Some remnants of domes in summit area were delineated including remnant of East and West domes, L 1948, L 1953 – 1955 and L 1956 in north - northwest, small part of L 1930, L 1931/L1934, L 1957 in west, L 1984 – 1986 and L 1992 – 1994 southwest

direction and L 1992 in the summit. Morphologic features of Merapi summit on DEM 1996 were displayed in figure 6-8.

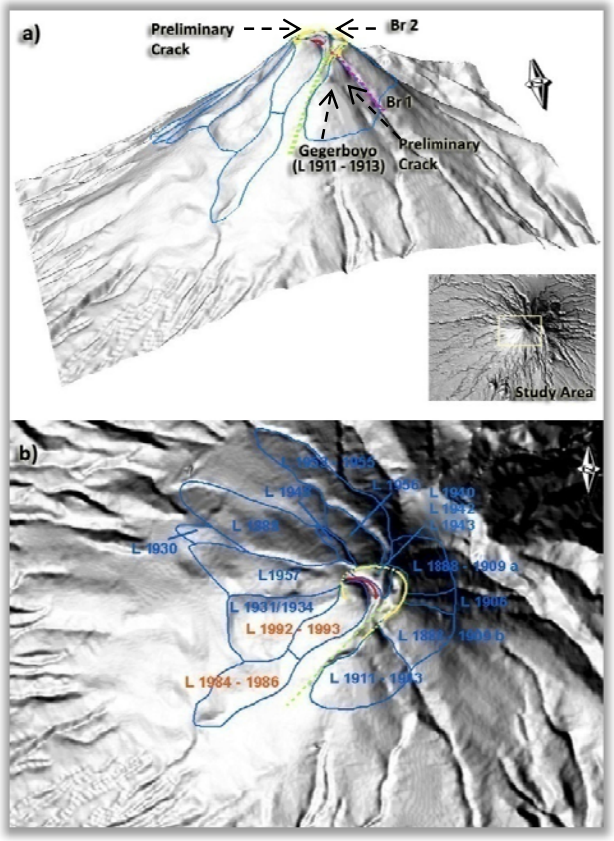


Figure 6-8. Morphologic features of Merapi summit on DEM 1996, not scaled. Inset: DEM 1996 of study area, a) Observed on 3D model, b) Observed on hill shade.

#### 6.2.1.1.4. Summit area of DEM 2006

Summit morphology of DEM 2006 showed small changes from DEM 1996, see figure 6-9. Crater rim of 1961, crater breaching, crater floor, adjacent ridges, preliminary crack and remnant of domes were relatively the same with those of summit 1996. An additional breach, Br 3, appeared between Br 1 and crater rim breaching where a preliminary crack was observed on DEM 1982 and 1996.

Solfatara covered southwest – west and northwest part of Merapi summit, preventing observation of some features e.g. crater rim of 1961, L 1997 – 1998, L 1930 and part of L 1888.

#### 6.2.1.1.5. Summit area of IFSAR DEM

Slightly changes in summit morphology of IFSAR DEM from DEM 2006 could be observed including two additional domes: L 2001 and the growing dome 2006 (D 2006) and new breach, Br 4, between L 1953 – 1955 and L 1948. Morphologic features of Merapi summit on DEM 2006 were displayed in figure 6-10.

According to MVO publication (2000), there were significant changes of summit morphology between DEM 1935 and DEM 1982 including changes of crater rim and crater breaching during Merapi activity in 1961. Reconstruction of summit morphology changes between year 1961 and 1982 was carried out by comparing picture from Merapi Museum to DEM 1982, as shown in figure 6-11.

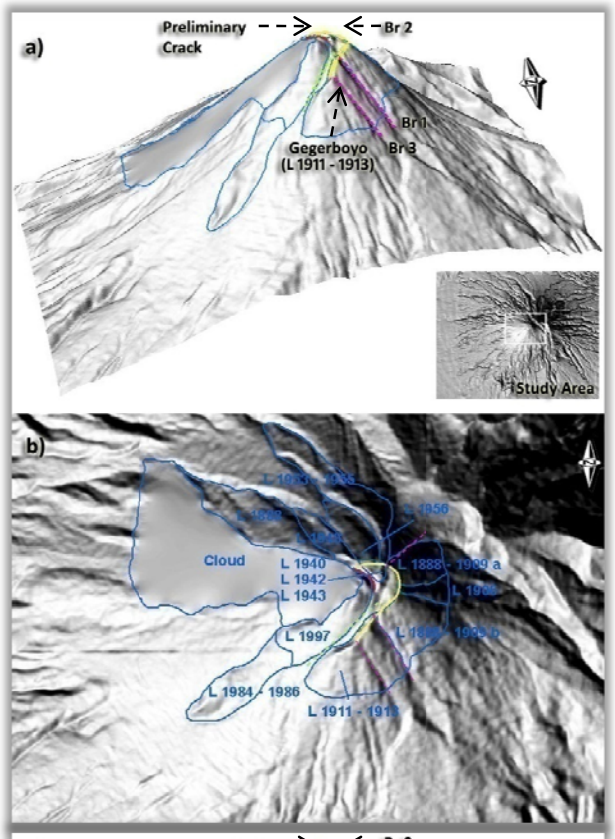


Figure 6-9. Morphologic features of Merapi summit on DEM 2006, not scaled. Inset: DEM 2006 of study area, a) Observed on 3D model, b) Observed on hill shade

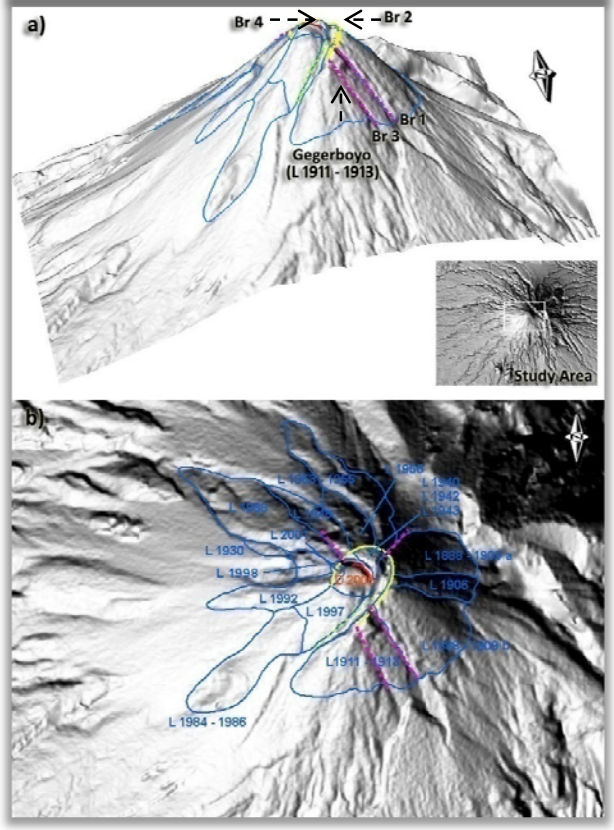


Figure 6-10. Morphologic features of Merapi summit on IFSAR DEM, not scaled. Inset: IFSAR DEM of study area. a) Observed on 3D model, b) Observed on hill shade.

Based on the reconstruction, there were slightly changes on morphography of Merapi summit between 1961 and 1982. In summit area of 1961, two crater breaching were observed, crater breaching of 1930 toward west and crater breaching of 1961 toward southwest. Pictures of summit in 1961 showed that crater breaching toward west was wider than that of southwest whilst crater breaching toward southwest was wider and deeper on DEM 1982. However, no morphometry parameters could be measured to compare which crater breaching had performed low land in summit area in 1961 so the low land of summit area during the interval time might be both or one of them.

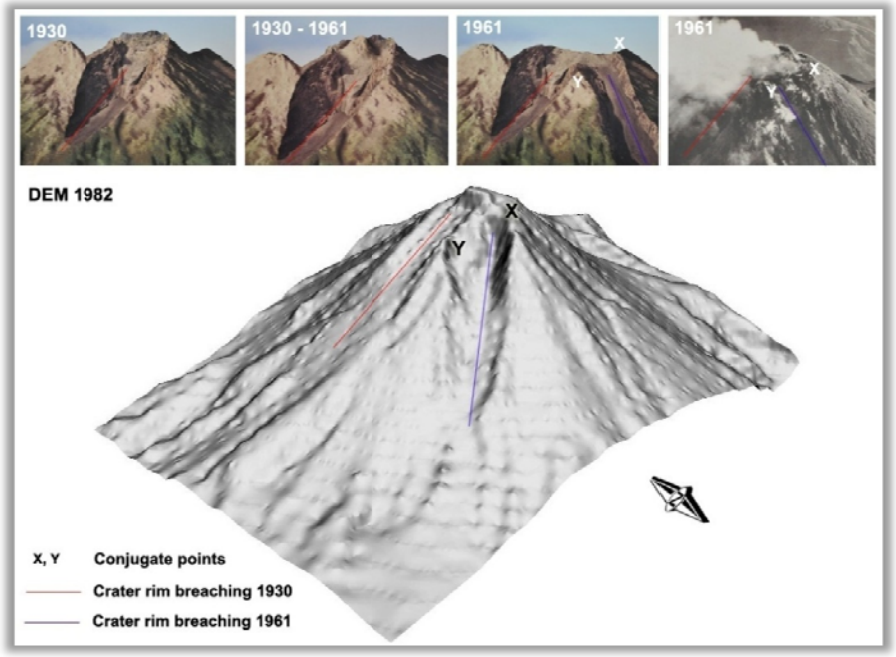


Figure 6-11. Reconstruction of summit morphology changes between 1961 and 1982. Pictures were captured from MVO publication in Merapi Museum, Kaliurang taken at October 24th, 2009.

#### 6.2.1.2. Morphologic features of vicinity area

Morphologic features of vicinity area observed including drainage pattern, lineaments and major rivers located down slope of crater breaching. Drainage patterns were derived from flow direction and flow accumulation whereas lineaments and major rivers were then visually observed and digitized on hill shade DEM overlaid by flow accumulation.

Three types of drainage pattern were able to observe: half circular radial on volcanic cone, sub dendritic/dendritic in southeast to northwest – north and parallel pattern ranging from south to northwest – north (see inset b of figure 6-12). Various numbers of lineaments and some major rivers located down slope of crater breaching were able to identify and digitized depending on visibility on the DEMs, figure 6-12.

### 6.2.2. Morphologic features' quantification

Morphologic quantifications of features recognized in previous section were conducted by applying morphometry parameters for each feature in past time DEM, table 4-3. Quantification process was carried out separately for every feature among DEMs.

#### 6.2.2.1. Morphologic features' quantification of summit area

Morphologic quantifications of summit area were carried out for all features located in the summit area including crater rim, crater floor, crater breaching, adjacent ridges, breach (es) and remnants of domes.

Crater rim

Crater rim quantification was based on elliptical parameters: major axis (a), minor axis (b) and eccentricity (e) using formula 8 and the perimeter was automatically calculated in field attribute on Arc Map 9.3.

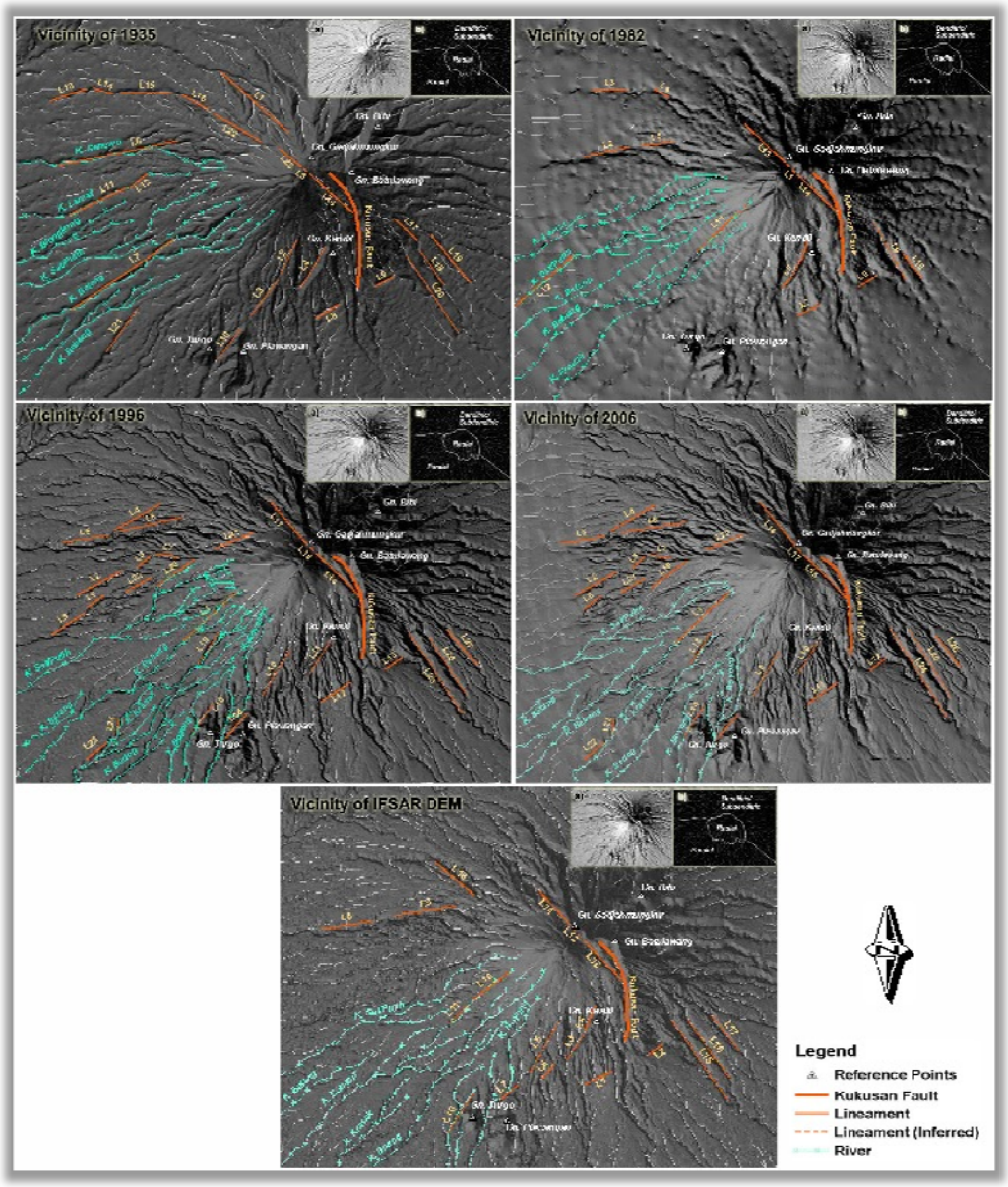


Figure 6-12. Morphologic features of Merapi vicinity area, hill shade (a) overlaid by flow accumulation (b)

Table 6-7. Quantification values of crater rim

| FEATURES | | DEM 1935 | DEM 1982 | DEM 1996 | DEM 2006 | IFSAR DEM |
|---|---|---|---|---|---|---|
| Crater rim | | | | | | |
| Shape | a | 780.171 | 950.998 | 680.088 | 594.447 | 645.767 |
| | b | 390.085 | 475.499 | 340.044 | 297.223 | 322.883 |
| | e | 0.866 | 0.866 | 0.866 | 0.866 | 0.866 |
| Perimeter (m) | | 1076.825 | 1022.234 | 980.073 | 735.267 | 967.483 |

Crater rim floor

Crater rim floor of Merapi summit called *Kawah Mati* which formed after eruption 1930. In present time, Kawah Mati was bordered by East dome in east, L 1940 in west and L 1956 in north.

Table 6-8. Quantification values of crater rim floor

| FEATURES | DEM 1935 | DEM 1982 | DEM 1996 | DEM 2006 | IFSAR DEM |
|---|---|---|---|---|---|
| Crater rim floor | | | | | |
| Shape | Curved line | - | Curved line | Curved line | Curved line |
| Perimeter (m) | 436.321 | | 225.875 | 185.995 | 152.190 |

Crater breaching

Crater breaching is low land area around Merapi edifice in which the horseshoe shape crater rim opens. Orientation of crater breaching was defined as azimuth of crater breaching major axis, calculated using distance and azimuth extension in Arc View 3.3. Dimension of crater breaching was calculated from cross section profile graph in Arc Map 9.3.

Table 6-9. Quantification of crater breaching

| FEATURES | DEM 1935 | DEM 1982 | DEM 1996 | DEM 2006 | IFSAR DEM |
|---|---|---|---|---|---|
| Crater Breaching | | | | | |
| Orientation | N 265 | N 228 | N 226 | N 226 | N 226 |
| Shape | U | U | U | U | U |
| Depth (m) | 105.980 | 111.736 | 102.397 | 107.945 | 97.860 |
| Width (m) | 396.000 | 407.131 | 213.029 | 215.595 | 162.807 |

Adjacent ridges

Adjacent ridges of crater rim depression were quantified by determining their relative position toward the depression and calculation of their height from profile graph of cross section in Arc Map 9.3. Positions of ridges were corresponding to the section 6.2.1.1.

Table 6-10. Quantification of adjacent ridges

| FEATURES | | DEM 1935 | DEM 1982 | DEM 1996 | DEM 2006 | IFSAR DEM |
|---|---|---|---|---|---|---|
| Adjacent ridges | | | | | | |
| # 1 | Position | S | S | S | S | S |
| | Height (m) | 105.980 | 111.736 | 32.496 | 15.768 | 18.366 |
| # 2 | Position | N | N | N | N | N |
| | Height (m) | 64.665 | 43.970 | 102.397 | 107.945 | 97.860 |

Breaches

Breaches orientation was calculated using distance and azimuth tools in Arc View 3.3 while their depth and width was calculated from profile graph of cross section in Arc Map 9.3. Numbers of breaches were corresponding to the section 6.2.1.2.

Table 6-11. Quantification of breaches

| FEATURES | | DEM 1935 | DEM 1982 | DEM 1996 | DEM 2006 | IFSAR DEM |
|---|---|---|---|---|---|---|
| Breaches | | | | | | |
| # 1 | Orientation | N 150 | N 150 | N 150 | N 150 | N 150 |
| | Depth (m) | 27.594 | 23.284 | 20.687 | 25.747 | 26.711 |
| | Width (m) | 133.462 | 137.186 | 142.476 | 142.378 | 144.498 |
| # 2 | Orientation | | | N 52 | N 52 | N 52 |
| | Depth (m) | | | 39.994 | 30.116 | 50.451 |
| | Width (m) | | | 121.571 | 88.558 | 88.977 |
| # 3 | Orientation | | | | N 148 | N 148 |
| | Depth (m) | | | | 69.818 | 79.911 |
| | Width (m) | | | | 134.022 | 144.498 |
| # 4 | Orientation | | | | | N 323 |
| | Depth (m) | | | | | 27.016 |
| | Width (m) | | | | | 104.345 |

Remnant of domes

Remnant of domes in the summit area varied among DEMs. Their relative orientations were calculated using distance and azimuth extension in Arc View 3.3 and areas covered were calculated automatically in field attribute on Arc GIS 9.3.

Table 6-12. Quantification of remnants of domes

| FEATURES | | DEM 1935 | DEM 1982 | DEM 1996 | DEM 2006 | IFSAR DEM |
|---|---|---|---|---|---|---|
| Remnant of Domes | | | | | | |
| # L 1888 | Shape | Coulee | Coulee | Coulee | Coulee | Coulee |
| | Orientation | N 300 | N 300 | N 300 | N 300 | N 300 |
| | Area | 196839.155 | 233093.689 | 217777.396 | 159807.755 | 204111.470 |
| # L 1988 – 1909 a | Shape | East dome | East dome | East dome | East dome | East dome |
| | Orientation | N 77 | N 77 | N 77 | N 77 | N 77 |
| | Area | 135559.296 | 102380.440 | 96157.852 | 67034.232 | 111680.926 |
| # L 1888 – 1909 b | Shape | East dome | East dome | East dome | East dome | East dome |
| | Orientation | N 129 | N 129 | N 129 | N 129 | N 129 |
| | Area | 266651.771 | 99977.581 | 105865.515 | 109079.795 | 199176.221 |
| #L 1906 | Shape | Coulee | Coulee | Coulee | Coulee | Coulee |
| | Orientation | N 98 | N 98 | N 98 | N 98 | N 98 |
| | Area | 33415.508 | 35558.090 | 25439.005 | 27729.894 | 56170.346 |
| #L 1911 – 1913 | Shape | West dome | West dome | West dome | West dome | West dome |
| | Orientation | N 183 | N 183 | N 183 | N 183 | N 183 |
| | Area | 247159.092 | 160890.026 | 165244.911 | 167990.586 | 209632.066 |
| #L 1930 | Shape | Coulee | - | Coulee | - | Coulee |
| | Orientation | N 284 | | N 289 | | N 286 |
| | Area | 190818.991 | | 27578.159 | | 14328.801 |
| #L 1931 | Shape | Coulee | Coulee | - | - | - |
| | Orientation | N 237 | N 240 | | | |
| | Area | 511076.681 | 56713.776 | | | |
| # L 1934 | Shape | Coulee | Coulee | - | - | - |
| | Orientation | N 265 | N 256 | | | |
| | Area | 601132.394 | 178369.543 | | | |
| # L 1940, L 1942, L 1943 | Shape | - | Dome | Dome | Dome | Dome |
| | Orientation | | Central | Central | Central | Central |
| | Area | | 79581.503 | 24939.370 | 13040.189 | 12209.238 |
| # L 1948 | Shape | | Coulee | Coulee | Coulee | Coulee |
| | Orientation | | N 314 | N 314 | N 314 | N 314 |
| | Area | | 46841.955 | 15974.823 | 47353.289 | 64162.051 |
| # L 1953 – 1955 | Shape | - | Coulee | Coulee | Coulee | Coulee |
| | Orientation | | N 334 | N 334 | N 334 | N 334 |
| | Area | | 151347.111 | 151713.658 | 148650.675 | 143134.497 |
| # L 1956 | Shape | - | Coulee | Coulee | Coulee | Coulee |
| | Orientation | | N 336 | N 336 | N 336 | N 336 |
| | Area | | 68038.035 | 64344.984 | 66220.098 | 55733.565 |
| # L 1957 | Shape | - | - | Coulee | - | - |
| | Orientation | | | N 281 | | |
| | Area | | | 180120.801 | | |
| # L 1984 – 1986 | Shape | - | - | Coulee | Coulee | Coulee |
| | Orientation | | | N 232 | N 232 | N 232 |
| | Area | | | 130054.731 | 121051.113 | 167495.177 |
| # L 1992 | Shape | - | - | Coulee | - | Coulee |
| | Orientation | | | N 268 | | N 268 |
| | Area | | | 91887.173 | | 83208.954 |
| # L 1997 | Shape | - | - | | Coulee | Coulee |
| | Orientation | | | | N 228 | N 228 |
| | Area | | | | 104519.711 | 73548.160 |
| # L 1998 | Shape | - | - | - | - | Coulee |
| | Orientation | | | | | N 225 |
| | Area | | | | | 28748.252 |
| # L 2001 | Shape | - | - | - | - | Coulee |
| | Orientation | | | | | 277 |
| | Area | | | | | 6585.875 |
| # L 2006 | Shape | - | - | - | - | Dome |
| | Orientation | | | | | Central |
| | Area | | | | | 38709.967 |

### 6.2.2.2. Morphologic features' quantification of vicinity area

Morphologic features recognition of vicinity area was carried out for all features located in the vicinity area including drainage patterns, lineaments and major rivers.

Drainage pattern

In general, three types of drainage patterns were observed in Merapi vicinity area including half circular radial drainage pattern along volcanic cone, dendritic/sub dendritic drainage pattern in north – northwest to southeast and parallel drainage pattern in south to northwest (see figure 6-12b).

Lineaments

Lineaments in vicinity area except for Kukusan Fault were recognized and delineated on hill shade DEM. Their relative orientations were defined as an azimuth before drawn to Rose Diagram using Rozeta en. Numbers of lineaments from one DEM, refer to figure 6.3, were not correlated with the same number on another DEM.

Table 6-13. Quantification values of lineaments orientation

| FEATURES | DEM 1935 | DEM 1982 | DEM 1996 | DEM 2006 | IFSAR DEM |
|---|---|---|---|---|---|
| Nr. Lineaments | | | | | |
| # 1 | N 131 | N 133 | N 227 | N 256 | N 243 |
| # 2 | N 207 | N 257 | N 242 | N 242 | N 233 |
| # 3 | N 216 | N 273 | N 229 | N 223 | N 218 |
| # 4 | N 212 | N 303 | N 240 | N 242 | N 199 |
| # 5 | N 131 | N 261 | N 260 | N 260 | N 209 |
| # 6 | N 257 | N 207 | N 257 | N 261 | N 218 |
| # 7 | N 235 | N 246 | N 280 | N 281 | N 225 |
| # 8 | N 243 | N 248 | N 237 | N 233 | N 262 |
| # 9 | N 242 | N 241 | N 134 | N 213 | N 234 |
| # 10 | N 216 | N 151 | N 210 | N 212 | N 221 |
| # 11 | N 243 | N 142 | N 212 | N 235 | N 140 |
| # 12 | N 226 | N 225 | N 236 | N 237 | N 140 |
| # 13 | N 247 | N 229 | N 236 | N 221 | N 140 |
| # 14 | N 291 | | N 224 | N 210 | N 147 |
| # 15 | N 268 | | N 208 | N 135 | |
| # 16 | N 302 | | N 134 | N 140 | |
| # 17 | N 135 | | N 142 | N 135 | |
| # 18 | N 143 | | N 134 | N 215 | |
| # 19 | N 138 | | N 213 | N 234 | |
| # 20 | N 145 | | N 234 | N 247 | |
| # 21 | N 215 | | N 246 | N 238 | |
| # 22 | N 301 | | N 241 | N 232 | |
| # 23 | | | N 236 | N 194 | |
| # 24 | | | N 190 | N 147 | |
| # 25 | | | N 147 | N 146 | |
| # 26 | | | N 146 | N 140 | |
| # 27 | | | N 140 | | |

Major Rivers

Major rivers recognition was carried out to determine rivers located down slope of crater rim breaching. Regarding the nature of pyroclastic flow which not flows toward a river channel but affect broader sector, the delineation of major rivers was utilization for much broader area.

Table 6-14. Major rivers located down slope of crater breaching

| FEATURES | DEM 1935 | DEM 1982 | DEM 1996 | DEM 2006 | IFSAR DEM |
|---|---|---|---|---|---|
| Rivers | | | | | |
| # 1 | Senowo | Blongkeng | Sat/Putih | Sat/Putih | Sat/Putih |
| # 2 | Lamat | Sat/Putih | Batang | Batang | Batang |
| # 3 | Blongkeng | Batang | Bebeng | Bebeng | Bebeng |
| # 4 | Sat/Putih | Bebeng | Krasak | Krasak | Krasak |
| # 5 | Batang | Krasak | Bedog | Bedog | Bedog |
| # 6 | Bebeng | | Boyong | Boyong | Boyong |

## 6.3. Morphology Analysis of Features

Morphology of Merapi edifice is developed by collapse, rebuilding and changing vent location through time as complex evolution that is controlled by the interplay of

aggradation and degradation. The morphologic analysis of features from past time DEM was carried out by observing morphology changes over 70 years especially in Merapi summit and morphologic analysis for determining the factors ascertain direction of dome collapse.

### 6.3.1. Morphology Changes over 70 Years

The observation of morphologic changes of Merapi edifice was conducted by computation of DEM differences, correction of morphometric features quantification and observing morphologic features' changes over times.

#### 6.3.1.1. Computation of DEM differences

Scale and resolution of input data in this research were varies, which might affect morphometric quantifications of features. To have correct morphometric quantification of area, perimeter and distance, their differences among DEMs were calculated by using DEM 2006 as reference.

The computation of area and perimeter difference was conducted by drawing a circle from a specific central point (X: 439333.3094 m; Y: 9165725.6489 m) that passing a reference point, named Gn. Batulawang whilst distance computation was conducted by drawing lines from Gn. Kendil to Gn. Batulawang, showed in figure 6-13. The area, perimeter and distance differences of DEMs to DEM 2006 were calculated using formula 9 to 11, see table 6-15.

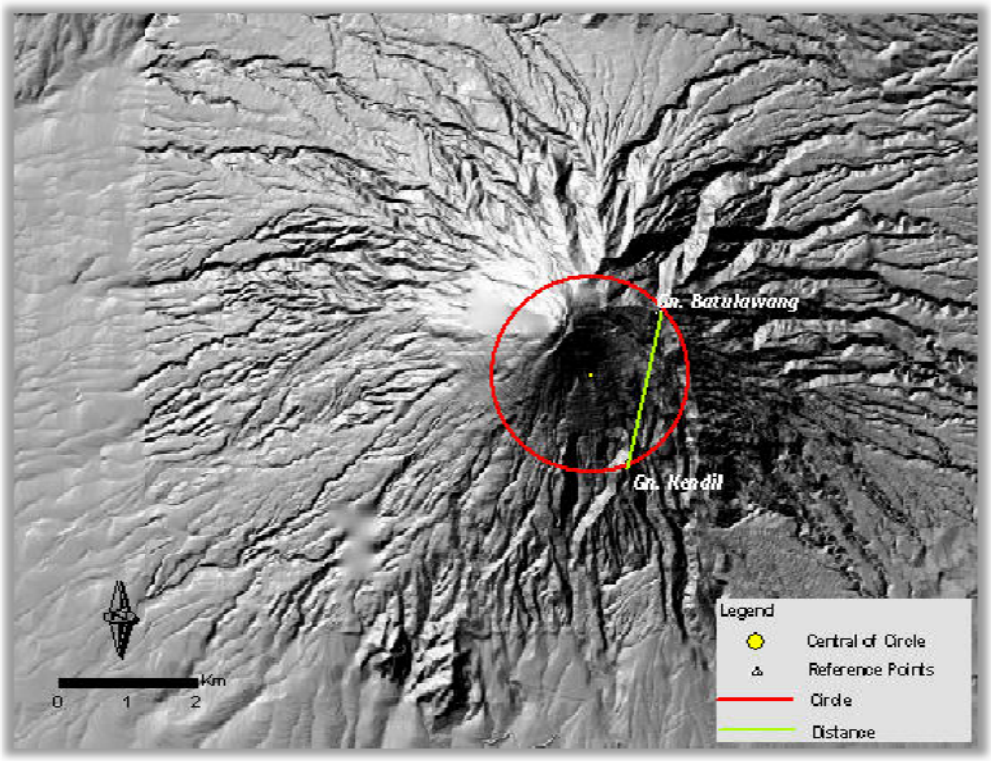


Figure 6-13. Circle and line used in DEM differences computation overlying DEM 2006

As shown in the table 6-15, the differences of DEMs to DEM 2006 were less than one percent except for DEM 1935 which deliver -15.47% for area, -7.46% for perimeter and -1.26% for distance differences. These differences might result from coordinate and datum transformation from Transverse Mercator, datum Batavia to UTM, datum WGS 1984.

### 6.3.1.2. Correction of Morphometric Quantification Values

Correction of morphometric quantification values was established for some features in summit area using formula 12, as follow:

- Percentage of area was used to subtract area of remnants of domes
- Percentage of perimeter was used to subtract perimeter of crater rim and crater floor
- Percentage of distance was used to subtract the width of crater breaching and breaches.

Table 6-15. Area, perimeter and distance differences among DEM

| | DEM 2006 | DEM 1935 | DEM 1982 | DEM 1996 | IFSAR DEM |
|---|---|---|---|---|---|
| Area | 6186215.8672 | 5357613.0013 | 6131459.8835 | 6188658.0519 | 6198044.6451 |
| Perimeter | 8816.9315 | 8205.2270 | 8777.8242 | 8818.6717 | 8825.3570 |
| Distance | 2300.7950 | 2272.2247 | 2279.2843 | 2300.2802 | 2296.4891 |
| Δ Area | | -828602.8659 | -54755.9837 | 2442.1847 | 11828.7779 |
| Δ Perimeter | | -611.7045 | -39.1073 | 1.7402 | 8.4255 |
| Δ Distance | | -28.5703 | -21.5108 | -0.5149 | -4.3059 |
| % Area | | -15.47 | -0.89 | 0.04 | 0.19 |
| % Perimeter | | -7.46 | -0.45 | 0.02 | 0.10 |
| % Distance | | -1.26 | -0.94 | -0.02 | -0.19 |

#### 6.3.1.2.1. Corrected area of remnants of domes

Corrected areas of remnants of domes were calculated using formula 12 using DEM 2006 as reference. The result of correction process was displayed in table 6-16.

Table 6-16. Corrected area of remnants of domes on every DEM

| Remnants of Domes | DEM 1935 | DEM 1982 | DEM 1996 | DEM 2006 | IFSAR DEM |
|---|---|---|---|---|---|
| L 1988 | 227282.095 | 235175.293 | 217691.456 | 159807.755 | 203721.930 |
| L 1988 - 1909 a | 156524.757 | 103294.732 | 96119.906 | 67034.232 | 111467.787 |
| L 1988 - 1909 b | 307891.857 | 100870.414 | 105823.738 | 109079.795 | 198796.099 |
| L 1906 | 38583.516 | 35875.635 | 25428.966 | 27729.894 | 56063.147 |
| L 1911 - 1913 | 285384.460 | 162326.827 | 165179.701 | 167990.586 | 209231.989 |
| L 1930 | 220330.858 | | 27567.276 | | 14301.455 |
| L 1931 | 590119.270 | 57220.249 | | | |
| L 1934 | 694102.906 | 179962.443 | | | |
| L 1931 - 1934 | | | 166462.757 | | |
| L 1940, L 1942, 1943 | | 80292.193 | 24929.529 | 13040.189 | 12185.937 |
| L 1948 | | 47260.270 | 15968.519 | 47353.289 | 64039.600 |
| L 1953 - 1955 | | 152698.691 | 151653.788 | 148650.675 | 142861.329 |
| L 1956 | | 68645.638 | 64319.592 | 66220.098 | 55627.199 |
| L 1957 | | | 180049.721 | | |
| L 1984 - 1986 | | | 130003.409 | 121051.113 | 167175.518 |
| L 1992 | | | 91850.912 | | 83050.152 |
| L 1997 | | | | 104519.711 | 73407.796 |
| L 1998 | | | | | 28693.387 |
| L 2001 | | | | | 6573.306 |
| L 2006 | | | | | 38636.090 |

#### 6.3.1.2.2. Corrected perimeters of crater rim and crater rim floor

Corrected perimeters of crater rim and crater rim floor were calculated using formula 12 toward reference DEM. The result of correction was displayed in table 6-12.

Table 6-17. Corrected perimeters of crater floor and crater rim floor

| | DEM 1935 | DEM 1982 | DEM 1996 | DEM 2006 | IFSAR DEM |
|---|---|---|---|---|---|
| Crater rim | 1157.103 | 1026.788 | 979.880 | 735.267 | 966.557 |
| Crater rim floor | 468.849 | - | 225.830 | 185.995 | 152.045 |

#### 6.3.1.2.3. Corrected width of crater breaching and breaches

Corrected width of crater breaching and breaches were calculated using formula 12. The result of correction was displayed in table 6-13.

As the percentages of correction for every DEM, except for DEM 1935, was less than one percent for all parameters: area, perimeter and distance, there were no significant effects

on trends of morphologic changes of those features. Inconsistent remnants of domes' areas were mainly caused by aggradation and degradation processes in which some eruptive materials covering the older one and their differentiation were difficult to carry out due to lack of data series.

Table 6-18. Corrected width of crater breaching and breaches

| | DEM 1935 | DEM 1982 | DEM 1996 | DEM 2006 | IFSAR DEM |
|---|---|---|---|---|---|
| Crater Breaching | 400.979 | 410.973 | 213.077 | 215.595 | 163.112 |
| Breaches | | | | | |
| # 1 | 135.140 | 138.481 | 142.508 | 142.378 | 144.769 |
| # 2 | - | - | 121.598 | 88.558 | 89.144 |
| # 3 | - | - | - | 134.022 | 144.769 |
| # 4 | - | - | - | - | 104.541 |

Correction of other values related to elevation were not carried out i.e. crater breaching depth because huge time gaps to reference DEM and their quantifications were only needed to be compared to other values on the same DEM e.g. depth of crater breaching were compared to depth of breaches in order to define the lowest topographic area on Merapi edifice that moment.

### 6.3.1.3. Morphologic Changes

Observation of morphologic features, especially those in Merapi edifice from over 70 years, was carried out to determine features which ascertain the direction of dome collapse in the past, regarding the low land area around crater rim. From the observation, morphologic changes of features were underlined:

#### 6.3.1.3.1. Summit area

Dynamic morphologic changes of features in summit area from section 6.2 were summarized as follows:

1. Crater rim
   Crater rim form described using eccentricity parameter (e) derived from major and minor axes of ellipse. As the eccentricity value less than 1, the crater rim form represents ellipse (Corazzato and Tibaldi, 2006).
   Quantification of crater rim shape showed eccentricity parameter of Merapi in past 70 years approximately about 0.866 meaning Merapi has ellipse shape with a low land area in crater rim, described by crater breaching azimuth or known as horse shape crater rim (MVO, 2000). Perimeter of crater rim 1930 was longer than that of crater rim 1961. Crater rim 1961 shows a tendency to decrease, except on DEM 2006 because some part of crater rim could not be observed.
2. Crater floor
   Crater floor is the area where the magma extrudes to the surface. Crater floor perimeter of Merapi has a tendency to decrease during 70 years by some remnant of domes which not tore down during the eruption or developed after the eruption, except for DEM 1982 in which crater floor was absent due to low accuracy of input data. Decreasing in perimeter of crater floor indicated the possibility of Merapi central vent to be blocked and increased of lithostatic pressure of the magma. Thus, changing in active sector toward lower land area may perform for future eruption.
3. Crater breaching
   Crater breaching showed the low land area around the summit. The orientations of crater breaching tend to shifting in past 70 years. Crater rim of 1930 had oriented toward west (N 265) and crater rim of 1961 had oriented toward southwest (N 228 – N 226). Crater rim of 1961 in DEM 1982 had orientation of N 228 and N 226 in DEM 1996, DEM 2006 and IFSAR DEM meaning the major axis of the crater breaching

was changing during the time. The depth and width of crater breaching of rim 1961 was being likely to decrease by aggradations of eruptive material.

4. Adjacent ridges

   Adjacent ridges of crater breaching were act as controlling factors, which function as artificial barrier directed Merapi – type eruption. Morphologic changes in adjacent ridges of crater breaching 1935 could not be observed due to absence of DEM after 1935 and before 1961, but changes of crater rim 1961's adjacent ridges could be well observed through series of DEM 1982 – IFSAR DEM. Height of south ridge tended to decrease significantly in vice versa of north ridges. As observed in 3D model of DEMs in figure 6-7 to 6-10, the northern part of crater rim 1961 was blocked by remnant of domes which lifting north ridges while south ridge tended to decrease by hydrothermal process of Merapi activities.

5. Breach (es)

   Breaches or cracks on Merapi summit might give preliminary judgment of area altered by hydrothermal process. Numbers of breaches varied from one DEM to another, depending on topographic representation on DEM's. A breach, Br 1 with orientation N 150 appeared constantly from DEM 1935 to IFSAR DEM. Br 2, orientation N 52, appeared on DEM 1996 to IFSAR DEM. Br 3 was observed in DEM 2006 and IFSAR DEM after a preliminary crack was ob served in its position on DEM 1982 and 1996. Br 4 was observed in IFSAR DEM with orientation of N 148. Position of those breaches could be observed in figure 6-6 to 6-10.

   The positions of breaches: Br 1, Br 3 and Br 4 were related to the fractures which are sub vertical and produce hot gases, essentially water vapor and SO2, suggesting that they may be connected to the magma (Beauducel *et al.*, 2000; Tiede *et al.*, 2007), compared figure 6-10 to figure 6-14.

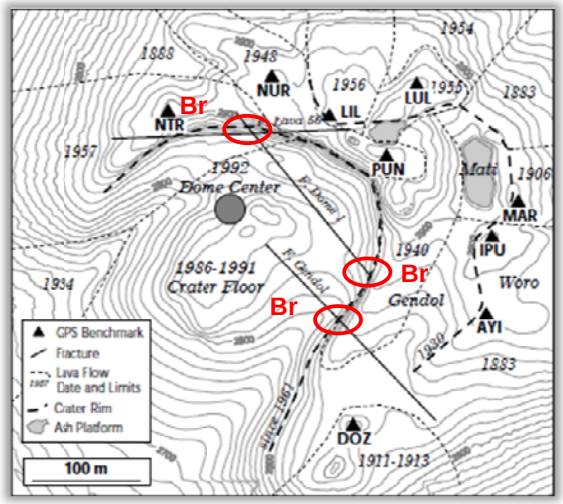


Figure 6-14. Map of Merapi summit indicating fractures (Source: Beauducel *et al.*, 2000).

6. Remnant of domes

   Remnant of domes in Merapi summit varied from time to time depending on Merapi activities in between DEMs. Some remnant of domes was unable to recognize on DEM 1982 due to low accuracy of input data and on DEM 2006 since some southwest – west – northeast part of summit were covered by solfatara. Development of domes has been affecting the low land area in Merapi summit since they could block the direction of pyroclastic flow. Remnant of domes in Merapi summit was displayed in form of rose diagram, figure 6-15.

Rose diagram showed quantitative frequency and distributions of dome remnants around Merapi edifice. Distribution of remnants of domes in last 70 years was toward north, west, northwest and southwest while no remnants of domes toward south, southeast and east part of edifice meaning no activities toward those directions during last 70 years. Distribution of dome remnants on DEM 1996 and IFSAR DEM showed that the northwest, west and southwest of Merapi edifice were somewhat blocked by dome remnants which not tore down during the eruption and changed the low land area on crater rim because they changed the depth of crater breaching by lifting or lowering adjacent ridges.

On the other hand, hydrothermal process of magma extrusion has weakened the older dome remnants in south, southeast and eastern part of Merapi edifice and led to possibility to collapse during Merapi activities both explosion and effusion in the future.

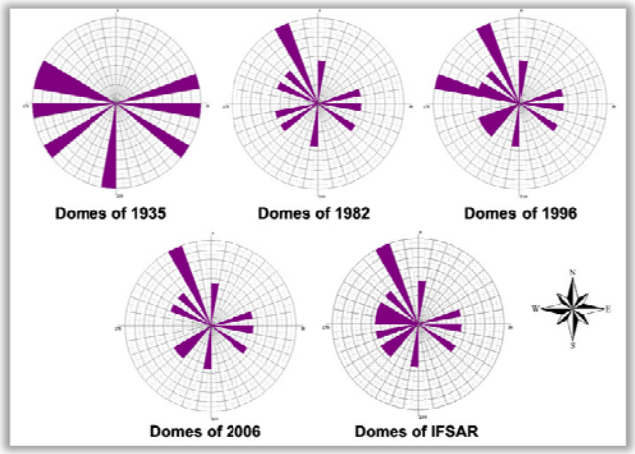


Figure 6-15. Rose diagram of remnants of domes drew among DEMs.

#### 6.3.1.3.2. Vicinity Area

Morphologic features observed in vicinity area were showing slightly changes during 70 years, except for major river flowed by pyroclastic flow because they were identified based on their position to crater breaching in every DEM.

1. Drainage patterns

   Disrupted of drainage pattern might be performed by fault scarps (Huggett, 2007). On study area half circular radial drainage pattern of volcanic cone was separated from dendritic/sub dendritic pattern in eastern part of the cone by a somma rim which is claimed as part of avalanche caldera, named Kukusan Fault (Camus *et al*., 2000). Dendritic/sub – dendritic drainage pattern in north to southeast part of vicinity area indicated unconsolidated sediments and on homogeneous igneous rocks where there are no structural controls. Parallel drainage pattern from south to northwest part indicated moderate to steep slope with strong structural control (Zuidam, 1983; Huggett, 2007).

   Differentiation of drainage pattern was performed by different process acting on surface. Eastern part of volcanic cone separated by somma rim of Kukusan Fault was identified free from Modern Merapi activity in which no pyroclastic flows were flowed over the somma rim after it developed in middle Merapi period (Camus *et al*., 2000) whilst southwest to northwest part were constantly flowed by volcanic material from Merapi activity.

2. Lineaments
   Most of lineaments observed in vicinity area were belongs to the two major structures named avalanche caldera and hyperbolic fault, figure 3-4 in Camus *et al* (2000). Avalanche caldera rim curves trough Senowo River, passing through eastern part of hyperbolic fault and Pasar Bubar crater rim and down to Kukusan fault (Camus *et al*. 2000). Part of this avalanche caldera was able to observe when passing Senowo river and down to Kukusan Fault. Hyperbolic fault curves from west, in between Senowo and Lamat rivers, passing through eastern part of volcanic cone and down to western part of Gn. Kendil ended at Gn. Turgo. Hyperbolic fault was hardly to observe except small part in western part of Gn. Kendil.
   Numbers of lineament orientations in every DEM were drawn in form of rose diagram, figure 6-16. Trends of lineament orientations were more to southwest and southeast.

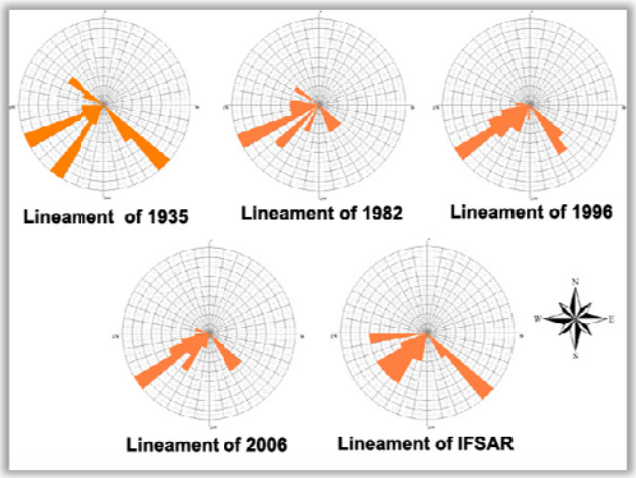


Figure 6-16. Rose diagram for lineament orientations among DEMs

3. Major rivers
   Major rivers and river morpho - arrangement identified on vicinity area varied depending on position of crater breaching.

### 6.3.2. Analysis of morphologic features

Morphologic analysis of features was conducted to determine the morphologic factor ascertain direction of dome collapse in the near future by studying past time eruptions. As this study was focused on Merapi – type of eruption, pyroclastic flow produced by gravitational failure (Voight *et al*., 2000), morphologic features chosen as factors were the one indicate low land area around Merapi edifice and the one which directed pyroclastic flow hazard.

From six morphologic features observed in the past time DEM: crater rim form, crater floor, crater breaching, adjacent ridges, breaches and remnant of domes, three features were chosen to predict the direction of dome collapse in the past. Those three factors were: crater rim form, crater breaching and adjacent ridges. Crater rim form showed a basic form of crater rim, horseshoe, with low land area around edifice represented by crater breaching whilst adjacent ridges were acting as controlling factors directed the eruptive product. Thus, the main morphologic features that play the most important rules in determining the direction of dome collapse were crater breaching and its adjacent ridges.

## 6.4. Reconstruction of Merapi – type eruption in the past

Reconstruction of direction of Merapi – type eruption in the past was carried out to assess usefulness of morphologic factors to ascertain direction of Merapi – type eruption in the past. The result of this assessment would be used to predict direction of Merapi – type eruption in the near future based on topographic condition after eruption 2006.

Direction of Merapi type eruption in the past was constructed based on two main factors observed in summit area: crater breaching and its adjacent ridges while major distribution of volcanic eruptive product was reconstructed based on direction of Merapi – type eruption and guided by morphologic analysis of slope angle (°) overlying plan curvature, assistance by shaded DEM, combined with rivers identified from section 6.2.1.2.

Since adequate data to reconstruct each eruption was absent, the reconstruction process of direction and major distribution of volcanic eruptive products was separated in between DEMs in hands.

### 6.4.1. Reconstruction of Merapi – type eruption 1935 – 1982

Reconstruction of eruption between 1935 and 1982 was derived from morphologic analysis of DEM 1935. The crater breaching of horse shoe shape rim 1930 oriented to west direction (N 265) and the adjacent ridges controlled the direction of eruption toward west with possibilities toward northwest and southwest when lava dome grew overtopping the rim and produced moderate to large pyroclastic flow. The major distribution of volcanic material resulted would toward Senowo, Lamat, Blongkeng, Sat/Putih and Batang as shown in figure 6-17.

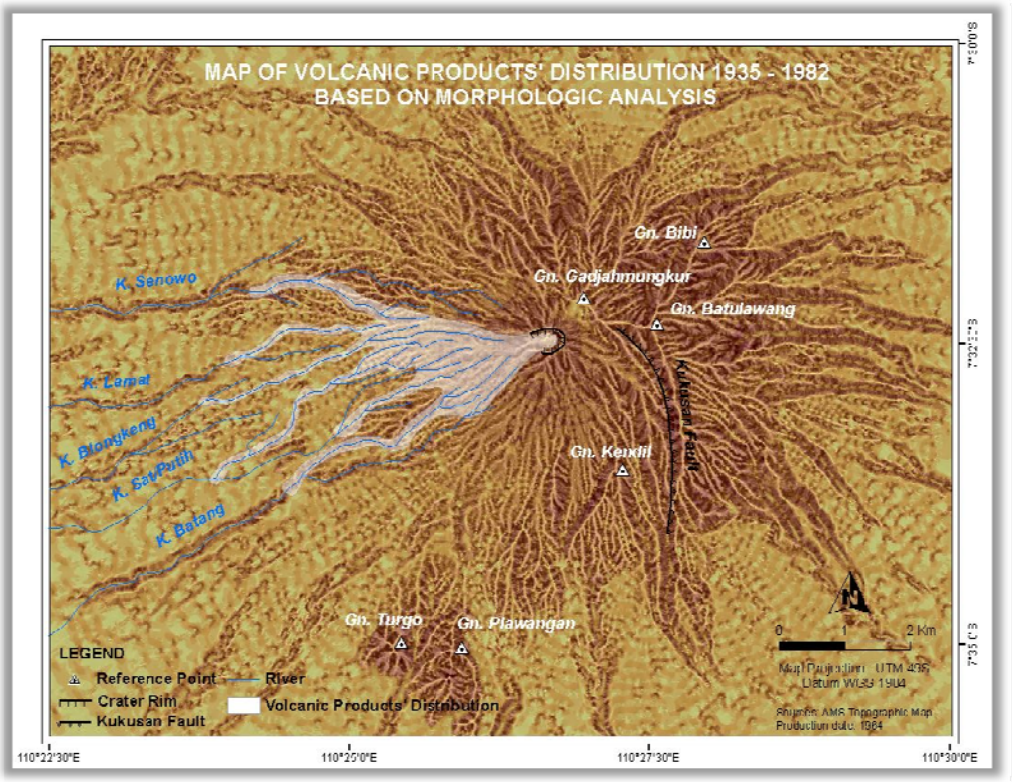


Figure 6-17. Major distribution of volcanic eruptive products between 1935 and 1982

### 6.4.2. Reconstruction of Merapi – type eruption 1982 - 1996

Eruption activates in between 1982 and 1996 was delivered from morphologic analysis of DEM 1982. Orientation of crater breaching on this DEM was toward southwest (N 228) with south ridge higher than north ridge. Hence, the direction of dome collapse was presumed to shift from northwest – west – southwest to west – southwest which directing the eruptive material straight to the rivers located down slope: K. Krasak, K. Bebeng and K. Batang with some extent to Sat/Putih and Blongkeng since crater rims of 1935 and 1982 was separated only by L 1931 and L 1934, as shown in figure 6-18.

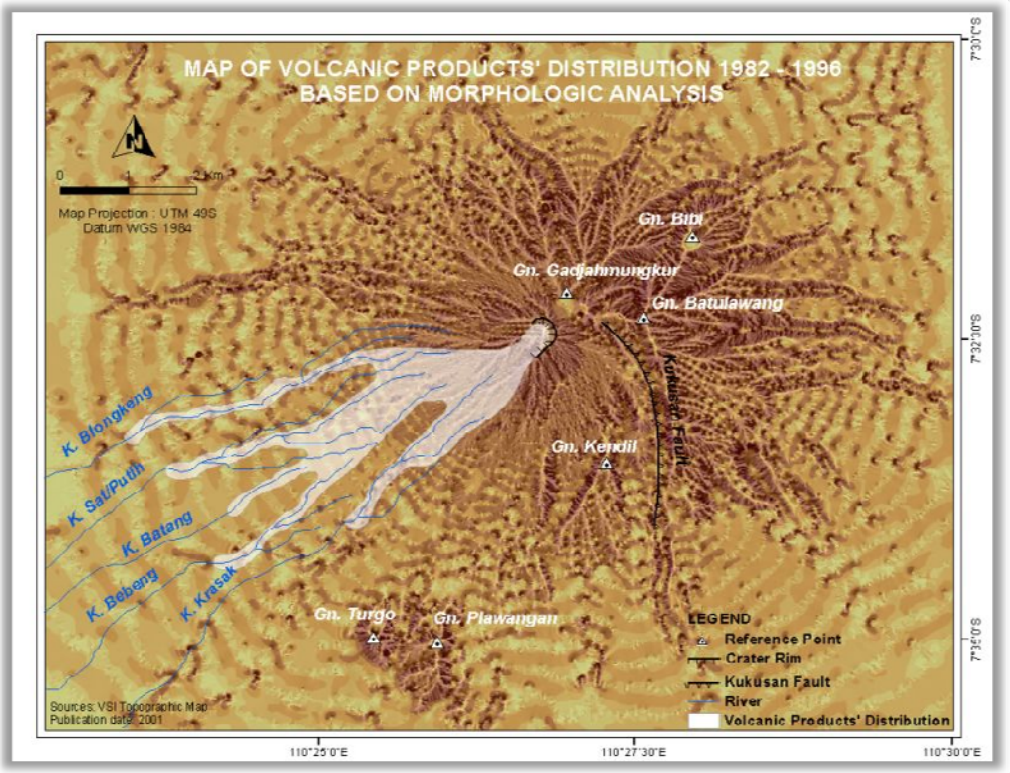


Figure 6-18. Major distribution of volcanic eruptive products between 1982 and 1996

### 6.4.3. Reconstruction of Merapi – type eruption 1996 – 2006

DEM 1996 was utilized to reconstruct direction Merapi activities between 1996 and 2006 through morphologic analysis of crater breaching and its adjacent ridges. Crater breaching orientation was slightly shift more to south direction, from N 228 to N 226 and south ridge was lowered, in vice versa to north ridge. Thus, Merapi – type eruption slightly shifted toward west – southwest – south direction to produce pyroclastic flow on mainly Krasak and Bebeng rivers with extent to Sat/Putih, Batang, Bedog and Boyong as displayed in figure 6-19.

Table 6-19. Reconstruction of Merapi – type eruption in the past using morphologic analysis

| DEMs | Eruptions | Direction | Major Distribution (Rivers) |
|---|---|---|---|
| # 1935 | | | |
| | 1935 – 1982 | Mainly : W and NW – SW | Senowo, Lamat, Blongkeng, Sat/Putih, Batang |
| # 1982 | | | |
| | 1982 – 1996 | Mainly: SW and W | Blongkeng, Sat/Putih, Batang, Bebeng, Krasak |
| # 1996 | | | |
| | 1996 – 2006 | Mainly : SW and W – S | Sat/Putih, Batang, Bebeng, Krasak, Bedog, Boyong |
| # 2006 & IFSAR | | | |

*Note: E: east, SE: southeast, S: south, SW: southwest, W: west, NW: northwest, N: north*

The results of reconstruction processes including the direction of eruptive activities and major distribution of volcanic eruptive products were summarized in table 6-19. From the result, shifting in trends of Merapi – type eruption from northwest – west – southwest to west – southwest – south could be figured out.

Shifting trends of Merapi – type eruption from 1982 – 1996 to 1996 – 2006 was revealing fact that same crater rim, rim 1961, could produce different direction of Merapi – type eruption because changes in adjacent ridges by remnant of domes, in this case north ridge lifted by L 1984 – 1986 and L 1992 – 1993, (figure 6-8 as reference).

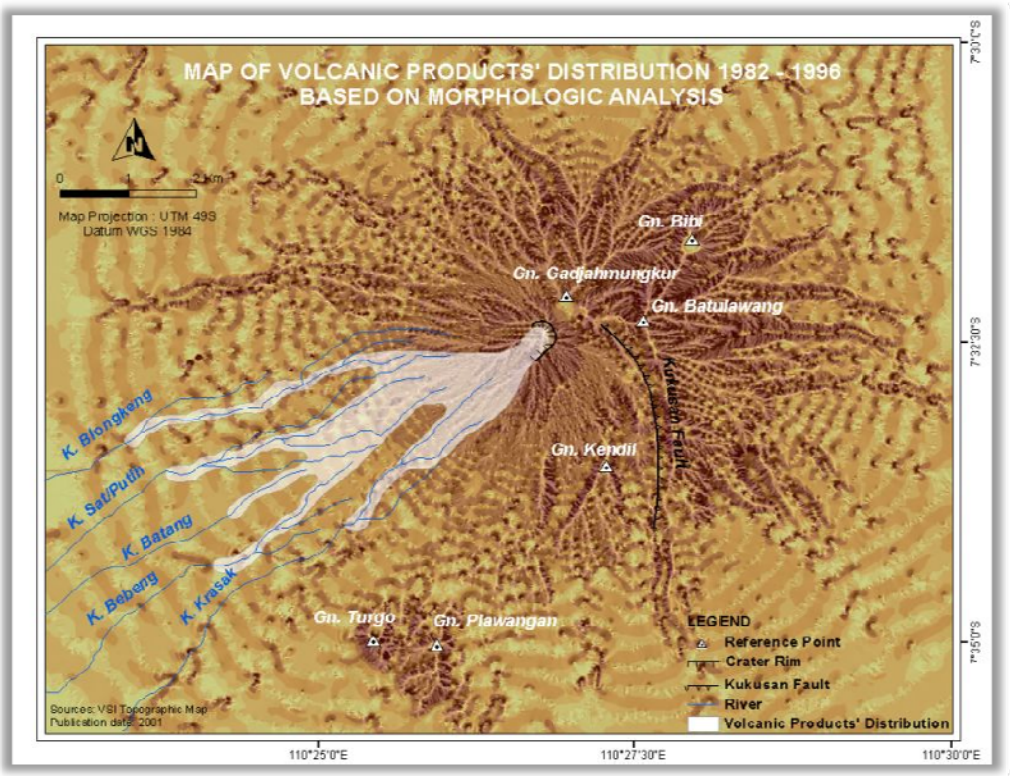


Figure 6-19 Major distribution of volcanic eruptive products between 1996 and 2006

## 6.5. Comparison of Reconstruction Results to Historical Data

Comparison of reconstruction result from morphologic analysis to those of historical data was aimed to assess validity of morphologic factors ascertain direction of Merapi – type eruption in the past. The assessment was accomplished through comparing directions and major rivers flowed from reconstruction and those of historical data (table 3-1).

In comparison process, some Merapi activities from past 70 years were eliminated because of several reasons: first, they were not representing Merapi – type eruptions; second, direction of dome collapse changed because of changing in active sectors; and third, no DEM data representing changes of morphologic factors observed. Thus, historical eruptions used were eruptions in 1942, 1943, 1984 – 1991, 1992 – 1993, 1994, 1995, 14 January 1997 and 2001. The comparison result was displayed in table 6-20.

As showed in table 6-20, directions and rivers flowed of Merapi – type eruptions from historical data were included in range of reconstruction results established by morphologic analysis, except eruption 1994 and 1995.

Eruption in 1994 and 1995 showed direction of Merapi – type eruption toward southwest, southwest – south and south. Based on historical data, in section 3.5.5, during the activity

of 1994 – 1998, some of volcanic material deposit built up against south crater wall allowing pyroclastic flows jumped to south flank (Boyong valley). This fact was strengthened by morphologic analysis of adjacent ridges on DEM 1996 that showed lifting of northern ridge by L 1984 – 1986 and L 1992 – 1993, figure 6-8 as reference. Hence, changes in adjacent ridges of crater breaching 1961 had occurred during activities of 1984 – 1986 and 1992 – 1993.

Table 6-20. Comparison of reconstruction results to those of historical data

| Eruption | Morphologic analysis | | Historical data | |
|---|---|---|---|---|
| | Direction | Major Rivers | Direction | Major rivers |
| **# 1935 – 1982** | NW – W – SW | Senowo, Lamat, Blongkeng, Sat/Putih, Batang | | |
| 1942 | | | NW, W | Senowo, Blongkeng |
| 1943 | | | SW | Batang |
| **# 1982 – 1996** | W – SW | Blongkeng, Sat/Putih, Batang, Bebeng, Krasak | | |
| 1984 – 1991 | | | W – SW | Sat/Putih |
| 1992 – 1993 | | | W – SW | Sat/Putih |
| 1994 | | | SW, SW – S, S | Bebeng, Krasak, Bedog, Boyong |
| 1995 | | | SW, S | Krasak, Boyong |
| **# 1996 - 2006** | W – SW – S | Sat/Putih, Batang, Bebeng, Krasak, Bedog, Boyong | | |
| 1997 (14 Jan) | | | SW, SW– S | Bebeng, Krasak, Bedog |

*Note: S: south, SW: southwest, W: west, NW: northwest*

Incomplete series of DEM's before and after the eruption prevented observation of more specific summit morphology and lava dome position of each eruption. Thus, specific directions, major rivers flowed and quantitative validation for Merapi – type eruption were unable to conduct.

Although quantitative validation was unable to carry out due to lack of data series, reconstruction of direction of Merapi – type eruptions and major rivers flowed using those morphologic factors could be accepted with limitation that those factors were able to define direction of Merapi – type eruption but restricted to lava dome growth inside active crater rim.

## 6.6. Concluding remarks

From studying morphologic changes of Merapi edifice using EDM data, DEMs and historical data, some remarks could be underlined:

1. Distance changes derived from slope distance between benchmarks and fixed prisms were less usable for morphologic changes of Merapi summit area due to relative small changes during the activity, less than 1 pixel size (5 m) of DEM, and possibility of the prisms to tear down during the eruption. Utilization of the distance measurement more reliable for precursors of Merapi activity.
2. Significant differences of morphometric quantification values: area, perimeter and distance were observed from DEM data which posed coordinate system transformation so correction of morphometry quantification values needs to be carried out for this type of data.
3. Morphologic analysis of summit and vicinity area showed dynamic changes of Merapi summit by aggradation and degradation processes including: changing direction of crater rim breaching from west to southwest and lifting of northern ridge of crater breaching by remnant of domes which affecting the direction of Merapi – type eruption; increasing numbers of breaches that could give initial view of fractures on Merapi summit which interconnected to magma extrusion and might perform weak zone around the edifice; and old dome remnants in south, southeast and east direction of Merapi edifice as a critical point to monitor due to possibility of collapse during Merapi activity in the near future.

Main structure on Merapi vicinity: part of avalanche caldera, observed as Kukusan Fault had performed topographic barrier to direct pyroclastic flows from Merapi activities. Therefore, pyroclastic flows will never flow over this somma rim in case that the direction of dome collapses toward southeast, east or northeast.

4. Morphologic analysis was able to reconstruct direction of Merapi – type eruption and major distribution of volcanic eruptive product in the past. Hence, utilization of those factors: crater breaching and its adjacent ridges for direction's reconstruction and slope angle (°) overlying plan curvature assistance by shaded DEM for major distribution of volcanic eruptive products, to predict direction of Merapi – type eruption and major rivers flowed in the near future could be achieved, restricted to lava dome growth inside active crater rim.

# Chapter 7. Predicted Affected Area and Improvement of Forbidden Hazard Zone

*This chapter provides predicted affected area in the near future by morphologic analysis of recent summit topography and vicinity area; proposed hazard zone for Merapi – type eruption through travel distance from historical data and morphologic analysis, improvement of existing Merapi hazard map, social and economic activities on forbidden zone and concluding remarks.*

## 7.1. Predicted Affected Area

Predicted affected area for eruption in the near future was accomplished by defining the direction of Merapi – type eruption through analysis of crater breaching and its adjacent ridges, morphologic analysis of slope angle, plan curvature, shaded DEM combination to determine the affected area and delineation and identification of affected area.

### 7.1.1. Morphologic Analysis to Define Direction of Merapi – Type Eruption

Representation of recent summit topographic condition was needed to observe two morphologic factors ascertain direction of dome collapse in the near future. Since DEM after eruption in 2006 were unable to give appropriate and comprehensive view of summit and vicinity area, the recent topographic condition was reconstructed from 3D model of DEM 2006 and pictures of southwest – south and southeast of Merapi edifice, as shown in figure 7-1.

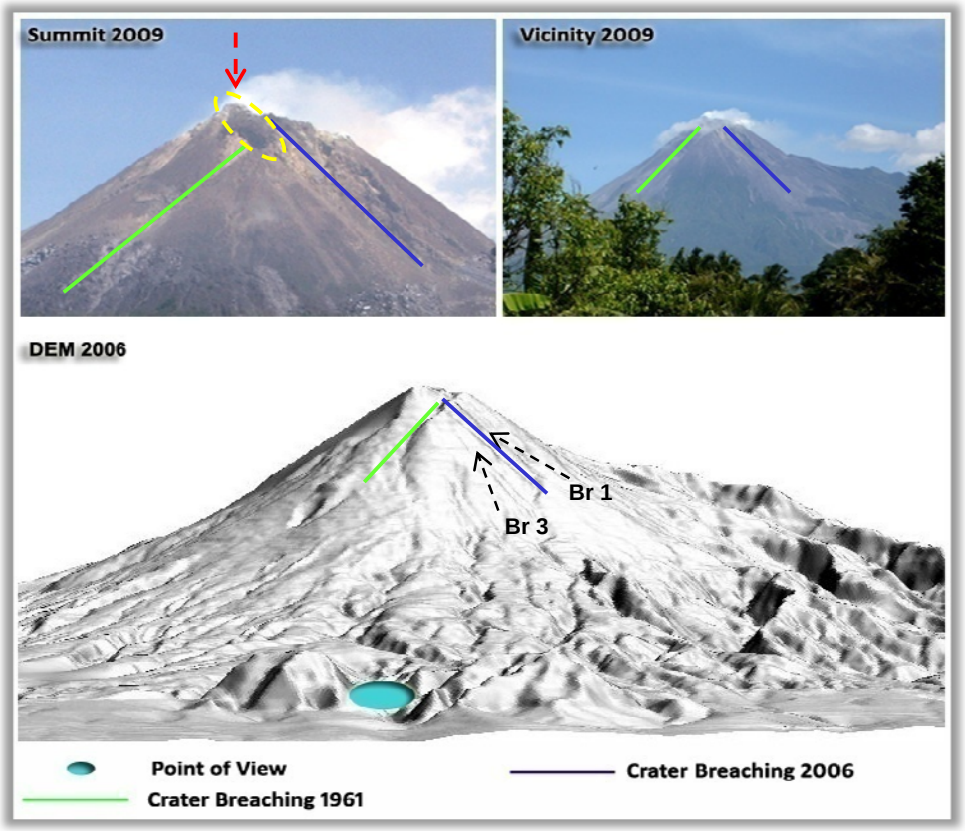


Figure 7-1. Reconstruction of recent topographic condition, after eruption 2006

Based on visual interpretation of figure 7.1, topography of Merapi edifice had changed. The crater breaching 1961 was replaced by new crater breaching, crater breaching 2006, performed by eruption 2006. Some volcanic materials, pointed out by yellow dashed circle, have blocking path from central vent (red dashed arrow) to crater breaching 1961. The crater breaching 2006 were previously observed as breaches, Br 1 and Br 3, which were actually fractures, refer to figure 6-9, 6-10 and 6-14.

By interrogatting the morphography of Merapi summit, identification and analysis of morphologic factors ascertain direction of dome collpase in the past: crater breaching and its adjacent ridges was carried out.

### 7.1.1.1. Crater Breaching

Crater breaching is the lowest topographic area on crater rim. By initial interpretation, we can observe that the lowest area was located in crater breaching 2006 with a sliding surface (white dashed circle), figure 7-2. The central vent of Merapi in which solfatara appeared was located in the top of this crater breaching. If the new lava dome emerges from central vent, the dome instability will lead to Merapi – type eruption toward southest, N 148 – N 150 (paralel to azimuth of Br 1 Br 3).

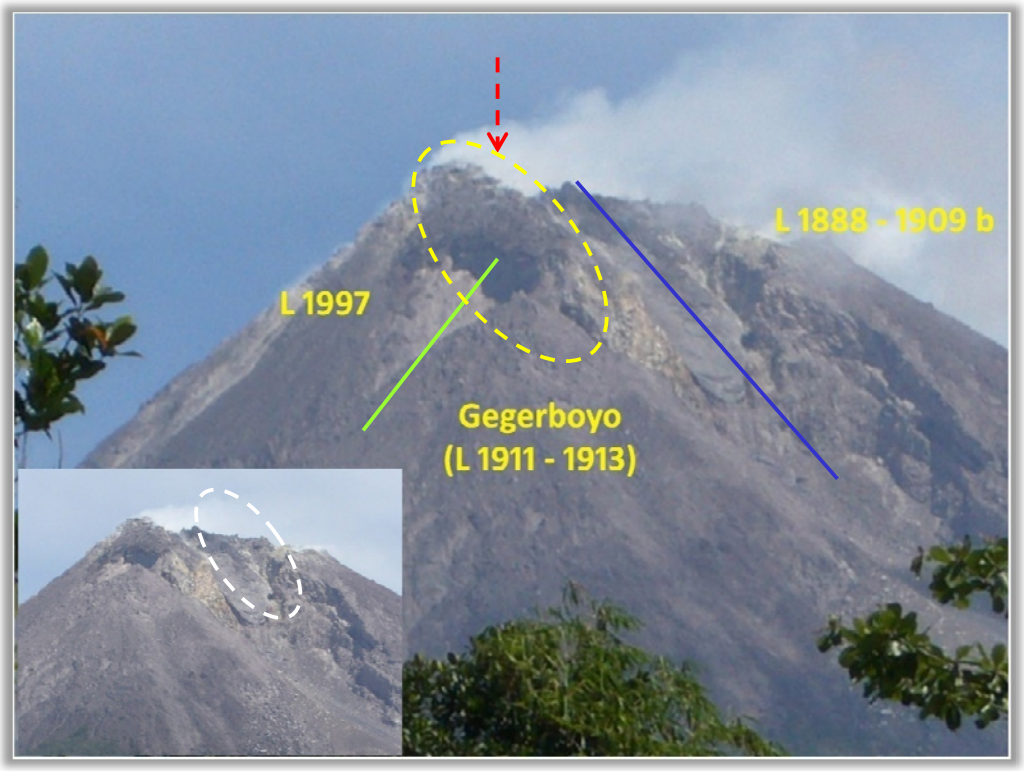


Figure 7-2. Merapi Summit pictured from south, inset: sliding surface, taken at 18th December 2009

### 7.1.1.2. Adjacent Ridges

Adjacent ridges of crater breaching 2006 are remnant of dome: L 1997 and volcanic material in west side, Gegerboyo (L 1911 – 1913) in south side and L 1888 – 1909b in east side. The west ridge has someone higher topography compared to east ridge. This topographic condition will directing dome collpase toward southeast and flow Gendol valley (river) and its adjacent valleys (rivers).

On the other side, large volume of lava dome growth through central vent may also caused collapase of volcanic material (yellow dashed circle) blocked path to crater

breaching 1961. Hence, the south and southwest direction of Merapi will also be threathen by Merapi – type of eruption (Subandriyo *et al*., 2009) in addition to major direction of dome collpase toward southeast. However, in this research, the affected area was identified and deliniated only based on recent morphology of Merapi edifice in which Merapi – type eruption will flow through direction of crater breaching 2006.

### 7.1.2. Morphologic Analysis to Determine Affected Area

Morphologic analysis of study area was conducted to reveal the area which may be affected by Merapi – type eruption by considering the prediction in direction of dome collapse in the near future. The morphologic analysis was utilized in DEM 2006 since the recent DEM from ALOS Imageries was failed to deliver recent topographic condition of study area due to thin cloud covered. Moreover, model simulation for pyroclastic flow was prevented by inavailability of recent DEM, after eruption 2006, and time constrain.

Morphologic analysis of study area was conducted for two factors: slope angle (°) and plan curvature. Slope angle (°) reveals terrain condition and paths in which pyroclastic flows tend to flow whereas the plan curvature indicate the divergence and convergence of the flow.

Free hand delineation of area which may affacted by pyroclastic flows based on the direction circumstances in which the direction toward southest (N 148 – 150) as direction of crater breaching 2006 and maximum distance affected by Merapi – type eruption in the past, 8 km, 27 – 28 November 1961 eruption (table 3-1 and figure 7-5).

Slope angle (°) was calculated from grid DEM pixel size 5 m and classified into seven classess, see table 7-1 whereas plan curvature calculated from grid DEM pixel size 5 m by means of curvature tools in Arc GIS 9.3, as shown in the figure 7-3 a and b. Slope angle (°) was then overlying plan curvature with 40% transparency to observe the flow path of pyroclastic flow before conducted free hand digitizing, figure 7-3 c.

Table 7-1. Slope angle (°) classification

| Classes | Expected Topographic Condition | Total pixel | Percentage (%) |
|---|---|---|---|
| 1 | Flat or almost flat | 82361 | 1.18 |
| 2 | Gently sloping | 550917 | 7.88 |
| 3 | Sloping | 1797447 | 25.71 |
| 4 | Moderately steep | 1725640 | 24.68 |
| 5 | Steep | 1692006 | 24.20 |
| 6 | Very steep | 1063034 | 15.20 |
| 7 | Extremely steep | 80563 | 1.15 |
| | **Total pixel in study area** | **6991968** | **100.00** |

From table 7-1,we can observe that study area has dominated by sloping to very steep slope, approximately 25%, followed by gently sloping topography, flat or almost flat area and extremely steep topography. As shown in figure 7-3 a, the extremely steep slope dominates southeast, east and northeast part of volcanic cone in which avalanche caldera rim located.

Plan curvature values were ranging from -28.54 to 20.57. Low or minus values indicates the divergence of flow whilst high or positive values indicates convergence of the flow. The low value of plan curvature were dominating south (Gn. Kendil), east (avalanche caldera/Kukusan Fault), northeast (Jurang Nganjang) and north (down slope of Pasar bubar crater rim).

### 7.1.3. Deliniation and Identification of Affected Area

Guided by slope angle (°), plan curvature and previous study by Charbonnier and Gertisser, 2009, deliniation of predicted affected area was perfomed. Free hand deliniation was based on the slope angle (°) overlying the plan curvature, assistance by shaded DEM, by considering major rivers located downslope of crater breaching 2006,

(Gendol river and its adjacent rivers) and simulation model of Merapi – type eruption in 2006 developed by Charbonnier and Gertisser, as shown in figure 7-4.

Delineation of predicted affected area showed that pyroclastic flow flowed downslope crater breaching toward southeast before finally blocked by Gn. Kendil and hills across it and performed overbank flow to bury Kaliadem tourism object before descents Gendol river at south flank of volcanic cone.

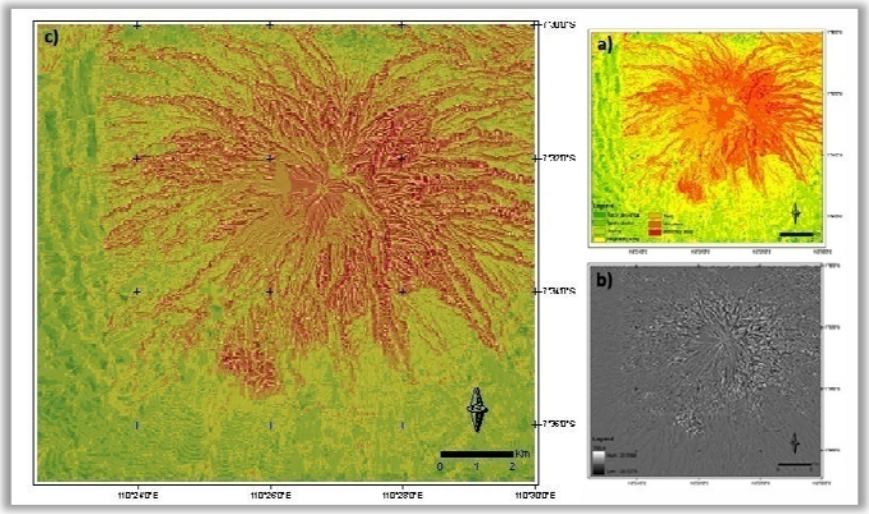


Figure 7-3. Classified slope angle (°) (a), plan curvature (b) and slope angle (°) overlaying plan curvature (c)

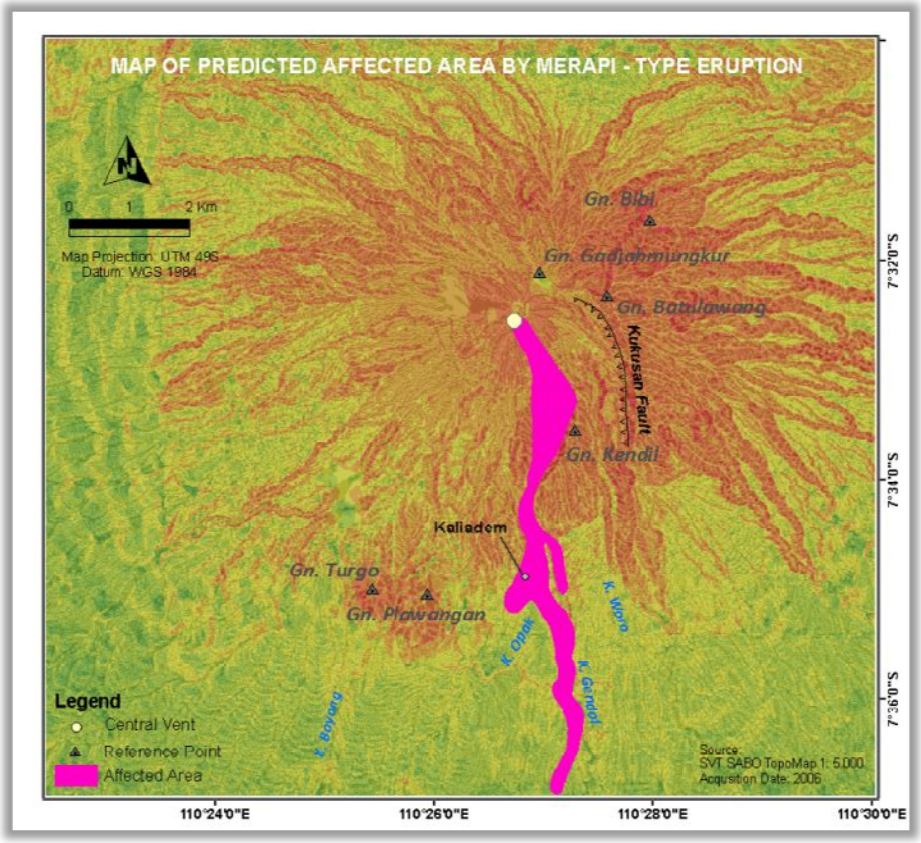


Figure 7-4. Map of predicted affected area delineated on slope angle (°) overlying plan curvature

Identification of affected area was conducted by overlying the predicted area with administrative boundary and detemination of numbers of inhabitants in those areas. The number of inhabitants in village level was delivered from statistic data in 2008, as shown in the table 7-2.

Table 7-2. Identification of affected area and number of inhabitants (source: statistic data, 2008)

| No | Sub – district | Village | Number of inhabitants |
|---|---|---|---|
| 1 | Pakem | Hargobinangun | 7384 |
| 2 | Cangkringan | Umbulharjo | 4263 |
| 3 | Cangkringan | Kepuharjo | 2818 |
| 4 | Cangkringan | Glagaharjo | 2795 |
| | | Total | 17260 |

The main sub – district affected by pyroclastic flow would be Pakem and Cangkringan with total number of inhabitants is 17.260 people in four villages Hargobinangun, Umbulharjo, Kepuharjo and Glagaharjo. Number of inhabitants may not reflect the actual number of people that may affected by pyroclastic flow hazard but still the increasing number of population in the hazard area should taken into account to deliver proper mitigation program during Merapi activity in the future.

## 7.2. Proposed Hazard Zone for Merapi – Type Eruption

Proposed hazard zone for Merapi – type eruption was carried out by interrogating the extent distance reached by dome collapse pyroclastic flow in the past, morphologic analysis to determine the area which likely to be affected by the hazard and evaluation of Merapi hazard map using proposed hazard zone.

### 7.2.1. Identification of Pyroclastic Flows Travel Distances from Historical Data

Identification of extent distance was conducted based on azimuth of valleys (rivers) delineated from flow accumulation overlying shaded DEM and extent distance from historical data, as shown in figure 7-5.

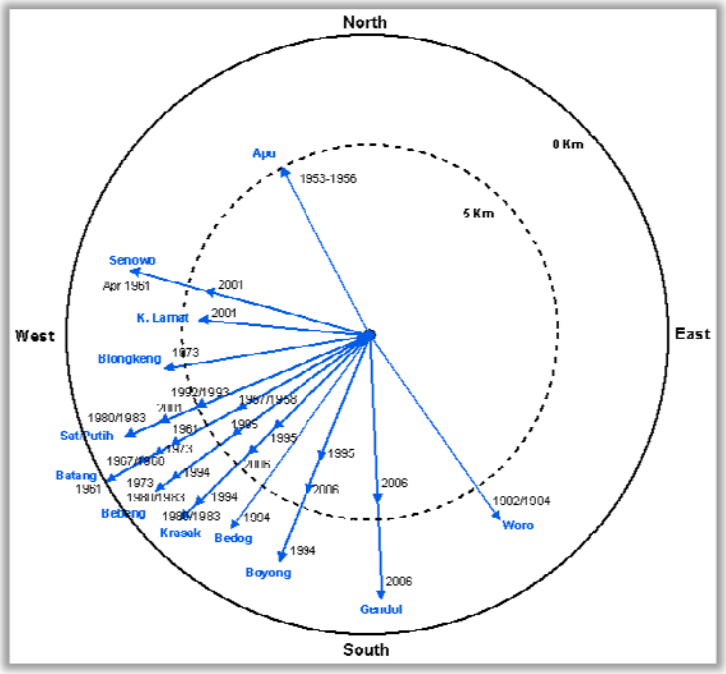


Figure 7-5. Azimuth and travel distance of Merapi – type eruptions over past 70 years

Travel distances of Merapi – type eruption in figure 7-5 showed in the past two centuries it was mainly toward west – southwest and southeast directions with maximum travel distance to Batang as far as 8 kilometer while east and northeast of volcanic cone were free from pyroclastic flows hazard.

### 7.2.2. Morphologic Analysis to Determine Pyroclastic Flows Hazard Zone

By interrogating slope angle (°) overlying plan curvature, assistance by shaded DEM and travel distance of Merapi – type eruption in the past (figure 7-5), free hand delineation of proposed hazard zone for Merapi – type eruption was conducted, see figure 7-6.

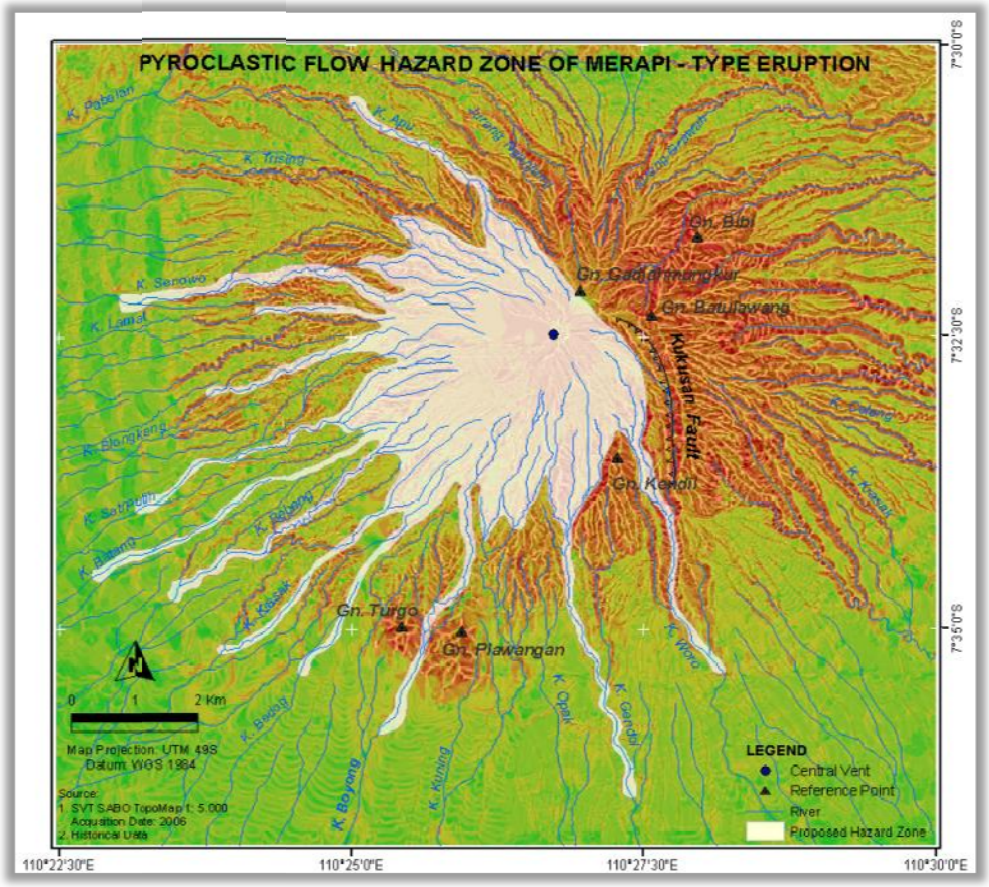


Figure 7-6. Proposed pyroclastic flow hazard zone of Merapi – type eruption

The pyroclastic flow hazard zone was delineated by considering the travel distance of previous eruption and morphology of flank area. Hence, some areas which have higher elevation would likely be free from pyroclastic flows' hazards of Merapi – type eruption i.e. eastern part of Kukusan Fault, Gn Kendil and its adjacent ridges, Gn. Plawangan and Gn. Turgo.

### 7.2.3. Improvement Forbidden Zone of Merapi Hazard Map

Improvement of forbidden zone of Merapi hazard map by pyroclastic flow hazard zone was carried out to assess the fitness of the hazard map regarding recent trend of Merapi eruption toward southeast. The assessment was established by overlying pyroclastic flow hazard zone with digital hazard map, digitalization by Bakosurtanal based on hardcopy of Merapi hazard map published by VSI, see figure 7-7.

In general, the proposed pyroclastic flow hazard zone was still in range of forbidden zone of Merapi hazard map, except for northern (K. Apu) and southern (K. Gendol) parts in which proposed pyroclastic flow hazard zone exceeds the forbidden zone to first danger zone. The extent distance of proposed pyroclastic flow hazard zone in northern part is measured as far as 1.42 km with 2.2 hectare covered area while southern part is measured as far as 0.43 km with 0.9 hectare of covered area.

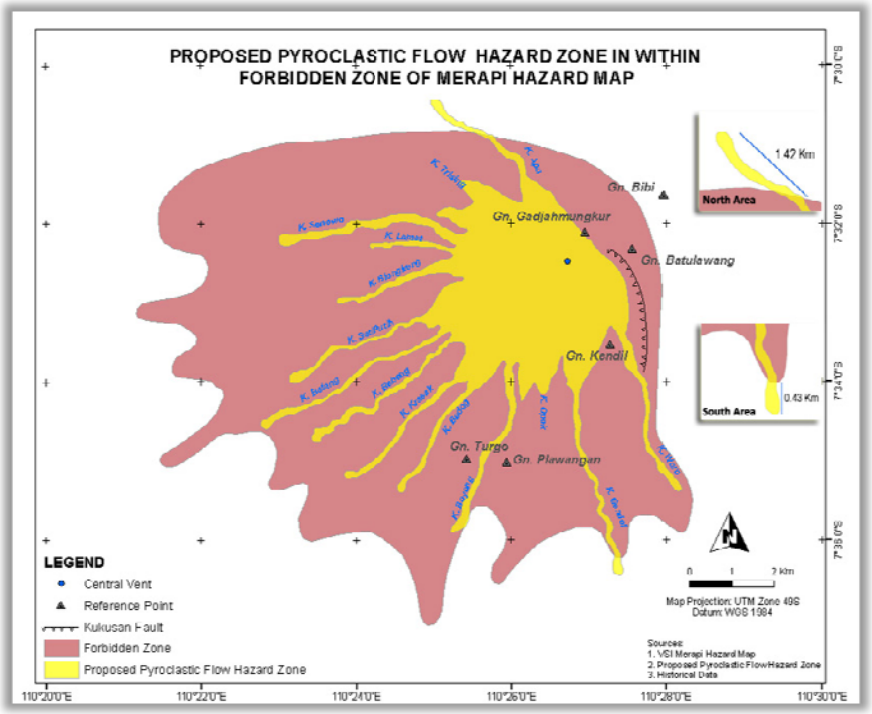


Figure 7-7. Proposed pyroclastic flow hazard zone in within forbidden zone of Merapi hazard map

Existing hazard map seems to give less detail representation and includes areas which have higher elevation i.e. eastern part of Kukusan Fault as the areas which likely to be affected by pyroclastic flows and less detail in river channels prone to pyroclastic flows. Although forbidden zone of existing hazard map is also likely to be affected by other types of hazards, namely tephra-fall, including ballistic ejecta that may affect areas outside proposed pyroclastic flow hazard zone, pyroclastic flows hazard produced from Merapi – type eruption is the most frequent hazard occurred in Merapi (Thouret *et al.*, 2000). Moreover, historical data also showed that intensity of Merapi eruption has been decrease from VEI 4 to ≤ VEI 3 meaning Merapi – type eruption would probably dominate eruption in the near future.

Proposed pyroclastic flow hazard zone should not be used for permanent or temporal activities due to high intensity of hazard threaten while the area between the proposed hazard zone and existing hazard zone could be used for temporal activity during day time by considering Merapi activity.

## 7.3. Social and Economic Activities on Forbidden Hazard Zone

Merapi flank area is a dense populated area, with around 1.1 million people live on, of which 440.000 are at relatively high risk in areas prone to pyroclastic flows, surges, and lahars (Thouret *et al.*, 2000). On forbidden zone of Merapi hazard map, which frequently affected by pyroclastic flows, surges and tephra fall, about 132.000 people inhibit four districts, dispersed in 38 villages, table 7-3.

Table 7-3. Numbers of inhabitants on forbidden zone of Merapi hazard map (sources: statistic data 2008)

| Province | Districts | Number of Villages | Inhabitants |
|---|---|---|---|
| Yogyakarta Province | Sleman | 8 | 51,994 |
| Central Java Province | Boyolali | 9 | 23,781 |
| Central Java Province | Magelang | 18 | 48,458 |
| Central Java Province | Klaten | 3 | 7,661 |
| | **Total** | 38 | 131,894 |

Historical records show that Merapi has had at least thirteen major eruptions with human casualties since 1006 (Thouret *et al.*, 2000; Dove, 2008). Thirteen events were large enough to cause at least 7000 deaths (Thouret *et al.*, 2000), and the deadliest eruption in historical times occurred in 1672, leaving a reported 3000 people dead (Dove, 2008).

Merapi activities also caused permanently resettlement of inhabitants i.e. resettlement of Gendeng which destroyed by eruption in 1961 (Voight *et al.*, 2000), Turgo villages partly destroyed by eruption in 1994, Klakah villages by eruption 1953 – 1955, see figure 7 – 8. On the other hand, fertile soil provided by volcanic eruptive products has invited people to live or work during day time on increased risk of Merapi forbidden hazard zone. The inhabitants mainly work related with tourism, agriculture, forestry, livestock and sand mining (Sagala, 2007) despite their understanding that living on Merapi flank area will risk their lives and they insist to stay on Merapi flank since their livelihoods depend on it.


Figure 7-8. Resettlement of Klakah Village, Boyolali due to Merapi activities (Source: field work 2009)

### 7.3.1. Tourism

Beautiful view of mountainous landscape is attractively credited for tourism industry ranging from hiking, camping, sightseeing and glowing lava dome and lava tour, figure 7 - 9. Three hiking tracks of Merapi includes: Selo, Babadan and Kaliurang, as far Selo was the favorite one due to less steep slope track. One of camping area around Merapi flank is Kaliadem, the area which devastated by overbank pyroclastic flow in 2006. Sightseeing of volcanic landscaping can be done from tower in Kaliurang and Museum Merapi Ketep Pass, on the way to Boyolali. Recently, glowing lava dome and lava tour becomes one of most favorable activities during Merapi activities i.e. during 2001 activity; tourist had waiting for seeing the glowing lava from MOP Babadan (PIC at MOP Babadan, personal communication).

The tourism activities on Merapi flank area should considering Merapi activities especially for hiking, camping and lava tour because they may dangerous. Lack of knowledge about volcanic process and its' threaten hazard will lead to higher vulnerability of community.

Figure 7-9. Lava tour on Gendol valley, inset: an escape bunker where 2 people buried by pyroclastic flow (Source: field work 2009)

### 7.3.2. Agriculture

The land use around Merapi can be described as high-intensity, low-technology, and subsistence tropical agriculture with a year-round tropical growing season that is typically divided into a wet season, October to March, and a dry season, April to September (Wilson *et al.*, 2007). In the higher elevation, people often farm tobacco, tea and coffee plants, wild raspberries and clove, figure 7-10. Agriculture of Merapi flank area is one of economic structure to support economic activity of inhabitants.


Figure 7-10. Agricultural activities on Merapi flank (Source: field work 2009)

### 7.3.3. Forestry

On foot slope of volcanic cone, most of landscape is covered by forest area; of which Merapi National Park exist. Merapi National Park has purposed to support the areas around by conserving biodiversity, land and water and tourism. Total area on Merapi flank has 6615.89 hectares and most of it (40.28%), located in Magelang district, 22.18 % in Boyolali district and 12.99% in Klaten district, Central Java province whereas 24.55% located in Sleman district, Yogyakarta Province, figure 7-11 (Spatial Planning Directorate, 2008).

Zonation of Merapi National Park is purposed to limit people activities in dangerous zone, but a part of Merapi National Park can be utilized by inhabitants surrounding for their activities i.e. for grassing and sand mining. Boundary's reconstruction of Merapi National Park is still in progress, thus, sometimes local people or tourist could go into active volcanic zone which is considerably dangerous when Merapi is active.


Figure 7-11. Merapi National Park and local people activities inside it
(Source: Merapi National Park and field work 2009)

### 7.3.4. Livestock

Livestock are mainly kept to produce meat for domestic consumption. Typical farm animals include cows, oxen, sheep, goats, chickens, and ducks. There appears to be limited milking of animals in the region, and that which occurs is centered mainly on Kaliadem (Wilson *et al.*, 2007).

During Merapi activity, inhabitants usually relocated into temporary shelter and leaving their house and livestock unprotected. Every day, some people are going back to feed their livestock and often they become pyroclastic flow victims, for instance during Merapi activities in 1961, 12 people trapped by pyroclastic flow with six killed and the other 6 severely injured when returning home despite repeated warning by MVO (Voight *et al.*, 2000).

### 7.3.5. Sand Mining

Merapi volcano offers favorable conditions for lahar generation, due to three main factors: abundant pyroclastic depositions, high rainfall intensity (commonly 40 mm in 2 hours) from the tropical monsoon climate and very dense drainage systems (Lavigne and Thouret, 2003). Thirteen rivers surrounding Merapi have experienced lahars, from the Apu River on the northwest, to the Woro River on the southeast (Lavigne et al., 2000).

Volcanic depositions' transportations of lahars provide numerous sediments along river channels and invite people to mine sand, figure 7-12. Sand mining activities on rivers down slope volcanic cone exposes people who work on this industry to lahars in monsoon seasons (Lavigne *et al.*, 2000). Lavigne et al (2000) reported 41 casualties and enormous damage of property by lahars, some of which also affect sand miners and truck drivers for instance on 11 December 1994, two truck was trapped by small lahars occurred upstream from Bebeng Dam 4.

Figure 7-12. Sand mining activity at Boyong River (Source: field work 2009 and Google image)

Forbidden zone of Merapi hazard map is, in reality, not a inhibited area. The fact that this area provides fertile soil making government attempts to forbid community to cultivate and finally seatle this area seems to be fall shorted. For instances, in north flank of Merapi, some people has cultivated in the higher slope, only 2 – 2.5 km from active crater rim. They feel safe because this area never affected by pyroclastic flow for almost 53 years (PIC at MOP Selo, personal communication). Thus, socialization of volcanic process and availability of more reliable hazard map are needed to develop awareness and community perception.

Detail of forbidden zone proposed by pyroclastic flow was developed to provide more reliable pyroclastic hazard zone which then could fill the gaps between scientific point of view and inhabitants' perceptions, to eliminate casualties. Furthermore, the revision of existing hazard map following recent trend of Merapi activity ensuing dynamic changes of Merapi eruption behavior is on a great demand since this map is used to provide guidelines for mitigation plans and long term landuse planning.

## 7.4. Concluding Remarks

Some remarks could be concluded regarding the predicted area that might affected by dome collapse pyroclastic flow as follows:

1. Recent crater breaching has opened toward southeast (N 148 – N 150), in which 2 breaches on crater rim, Br 1 and Br 3, was observed in previous DEM. Hence, the direction of dome collapse will be likely toward southeast and would produce pyroclastic flows hazard on the south – southeast of Merapi flank.
2. Morphologic analysis of slope and plan curvature, assistance by shaded DEM, and maximum travel distance of Merapi – type eruption in the past reveals four villages will probably be affected by pyroclastic flow hazard in the near future, with more than seventeen thousand inhabitants.
3. Morphologic analysis of slope and plan curvature, assistance by shaded DEM, and travel distance of Merapi – type eruption in the past discovers that proposed pyroclastic flow hazard zone exceeds the forbidden zone to first danger zone, in northern part (K. Apu) is measured as far as 1.42 km with 2.2 hectare covered area while southern part (K. Gendol) is measured as far as 0.43 km with 0.9 hectare of covered area.

   The existing hazard map seems to give less detail representation, includes areas with higher elevation as area to be likely affected by pyroclastic flow and not gives detail of river channels prone to pyroclastic flows. Thus, detail of forbidden zone by purposed pyroclastic flow hazard zone could be used to provide more reliable forbidden zone in regular activities of Merapi and to fill the gaps between scientific point of view and inhabitants' perceptions, in eliminating the casualties.
4. The improvement of exiting hazard map by giving detail hazard map and by ensuing dynamic changes of Merapi eruption behavior is on a great demand since this map is used to provide information for local communities to increase their awareness of volcanic hazard and guidelines for landuse planning and for evacuation in mitigation phase during Merapi activities. Proper evacuation plan should be effectively organized because almost 132.000 inhabitants live on the forbidden zone which might be affected by pyroclastic flow hazard in the near future.

# Chapter 8. Conclusion and Recommendation

*This chapter defines achievements of this research n as well as contribution of this research for present circumstances related to Merapi – type hazard. The recommendation is also presented for future research regarding Merapi hazards.*

## 8.1. Final Conclusion

In general, this research could satisfy the general research objectives addressed in first chapter. The purposed of this research is to study morphologic changes of Merapi edifice related to Merapi – type eruptions in the last 70 years. Study of morphologic changes was carried out by incorporating series of DEMs before conducting morphologic analysis to determine morphologic factors ascertain direction of Merapi – type eruption in the past. Those factors were then utilized to reveal the direction of Merapi – type eruption in the near future and the predicted affected area as well.

Related to specific research objectives addressed, some conclusions could be highlighted as follows:

**Morphologic changes of Merapi edifice related to Merapi – type eruption**

Study of morphologic changes on Merapi edifice was carried out on a series of digital elevation models (DEMs) from past 70 years. Some morphologic changes related to Merapi – type eruptions could be observed in this research were trend of crater breaching changes from west (N 265) – southwest (N 228 – 226) and southeast (N 148 – 150); crater floor and adjacent ridges were dynamically changed by remnant of domes and affected direction of Merapi – type eruption; and breaches appeared on Merapi edifice could give preliminary judgment of fractures related to magma activity.

**Forecasting the direction dome collapse in the near future based on morphologic analyses of past time eruptions**

There are some morphologic features observed in both summit and vicinity area which might contribute to ascertain direction of Merapi – type eruption. Summit features incorporate crater rim form, crater floor, crater breaching, adjacent ridges, breaches and remnant of domes whilst vicinity features include drainage pattern, lineaments and major rivers. From summit features, crater breaching and its adjacent ridges were the main factors that ascertain the direction of Merapi – type eruption. The extent area affected by Merapi – type eruption was blocked by Kukusan Fault in eastern part of volcanic cone to direct the flow toward southeast - south.

**Identification of areas prone to Merapi – type eruptions in the near future and improvement forbidden zone of Merapi hazard map**

Morphologic analysis of slope angle (°) and plan curvature, maximum travel distance and previous study was able to identify the area which would likely be affected in the near future. The area prone to Merapi – type eruption was on south – southeast flank, along Gendol River and its adjacent rivers. The predicted affected area was covering four villages inhibited by more than seventeen thousands people.

Morphologic analysis of slope angle (°) and plan curvature, assistance by shaded DEM, and travel distance of previous eruptions was exposed that existing hazard map gives too general forbidden area, includes higher elevation as part of area prone to pyroclastic flows and not clearly represents river channels prone to pyroclastic flows. Overlaying proposed pyroclastic flow hazard zone and existing hazard map also shows extent area of proposed hazard zone to forbidden zone in northern part (K. Apu) measured as far as 1.42 km with 2.2 hectare covered area while southern part (K. Gendol) measured as far

as 0.43 km with 0.9 hectare of covered area. Thus, detail of forbidden zone is needed to provide more reliable forbidden zone in filling gaps between scientific point of view and inhabitants' perceptions and awareness of volcanic hazard to eliminate casualties. Moreover, improvement of Merapi hazard map is on a great demand since this map used as guidelines for landuse planning and for evacuation in mitigation phase during Merapi activities considering 132.000 inhabitants living in forbidden hazard zone.

**Comparison of accuracy and efficacy of different type of input data**

Initial interpretation reveals that scale 1: 25.000 was appropriate to study morphology of vicinity area and scale 1: 5.000 (pixel size 5 m) or even larger is needed to study morphology of summit area. Digital elevation model produced from ground survey (DEM 1935) and photogrammetry (DEM 2006) give better topographic representation rather than the one produced from active remote sensing technique but those methods have been started to lose their ability to deliver most up to date topographic representation. However, assessment of IFSAR DEM to DEM 2006 through three statistical parameters, mean error (3.879 m), range error (15.269 m) and RMSEz (5.711 m) showed that absolute vertical accuracy of this data less than its product specification although it delivers similar height distribution.

Besides addressed research objectives, an additional discovery revealed is the usefulness of trilateration network to study summit morphology. Trilateration network in form of EDM data is less usable to study the morphologic changes of Merapi edifice due to small changes of distance changes and the possibility of prisms collapsed during Merapi activities.

Achievement of this researches related to research question addressed could be summarized in table 8-1.

## 8.2. Contributions of this Research

From achievements reached in this research some contributions could be revealed as follows:

1. MVO as the main institution for studying and monitoring Merapi volcano should regularly produce an appropriate scale map to develop suitable topographic representation for studying morphologic changes of Merapi edifice with a particular geo-reference system to construct easier monitoring process.
2. The emerging of active remote sensing system as IFSAR, RADAR and Radargrammetry could be utilized to overcome the limitation of ground survey and aerial photogrammetry in delivering the most – up – to date DTMs to monitor rapid morphologic changes of Merapi edifice due to its activity.
3. The utilization of morphologic factors ascertains the direction of Merapi – type eruption: crater breaching and its adjacent ridges would be useful to predict pyroclastic flow hazard generated by dome collapse in the near future.
4. The information of remnants of domes and cracks around Merapi edifice could be employ to enhance preparedness and monitoring system due to the possibility of slide collapse which increases the threat to the community during Merapi activity in the near future.
5. The preliminary predicted affected area could persuade the revision of existing hazard map due to essential contribution of Merapi hazard map to landuse planning and evacuation plans during Merapi activities.

Table 8-1. Relation between research achievements and research questions

| Research Questions | | Reference |
|---|---|---|
| **RO 1: To study changes in summit morphology** | | |
| a | What kind of data needed to study morphology of summit and vicinity area? | Sub Chapter 4.3.2.2; 6.2 |
| b | How to reconstruct changes in summit morphology from 1930 to 2006 eruptions? | Sub Chapter 4.2.2.1.1; 4.2.3.2 |
| c | How to reconstruct the lava dome growth from past 70 years? | Sub Chapter 4.2.2.1.1 number 6 |
| d | How to represent the result of morphologic changes in the summit area? | Sub Chapter 4.2.2.2; 6.2.1.1; 6.3.1.3.1 |
| e | How to assess morphologic changes in recent year after 2006 eruption? | Sub Chapter 4.3.3.1.1; 7.1.1 |
| **RO 2: To forecast the direction dome collapse in the near future** | | |
| a | Which morphologic features need to be observed in summit area to be utilized as factors ascertain direction of Merapi – type eruption? | Sub Chapter 6.2.1.1 |
| b | Which morphologic features need to be observed in vicinity area regarding direction of Merapi – type eruption? | Sub Chapter 6.2.1.2 |
| c | Which morphologic factors ascertain the direction of dome collapse from 1930 to 2006 eruptions? | Sub Chapter 6.3.2 |
| d | Which morphologic factors play the most important roles to determine the direction of dome collapse in the past? | Sub Chapter 6.3.2 |
| e | How accurate do the trend we have in comparison to Merapi historical data? | Sub Chapter 6.5 |
| f | How to predict the direction of dome collapse in the near future by using those factors? | Sub Chapter 7.1.1 |
| **RO 3: To identify areas prone to Merapi – type eruptions in the near future and to improve forbidden zone of Merapi hazard map** | | |
| a | What type of data needed to determine the extent of pyroclastic flows in the near future? | Sub Chapter 4.3.3.1.2 |
| b | How to determine the affected area by considering morphology of river channel and DEMs? | Sub Chapter 4.3.3.1.3 |
| c | How to determine the pyroclastic flow hazard zone of Merapi – type eruption? | Sub Chapter 4.3.3.2 |
| d | How the result of proposed pyroclastic flow hazard zone to improve forbidden zone of Merapi hazard map? | Sub Chapter 7.2.3 |
| **RO 4: To compare the accuracy and efficacy of input data** | | |
| a | How the surface representation of input data establishes DEMs quality for studying morphology of summit and vicinity area and how to compare them? | Sub Chapter 5.1.2 |
| b | How is the usefulness of each type of the data? | Sub Chapter 5.1.2 |
| c | How to compare between DEM of topographic map derived from photogrammetry and active remote sensing | Sub Chapter 4.3.1.2 |
| d | What is minimum accuracy of input data to provide appropriate morphologic quality for this research? | Sub Chapter 5.1.2 |

## 8.3. Recommendation for Future Studies

The emerging of geomorphometry analysis in various applications of geosciences has lead to the utilization of morphologic analysis in determining the volcanic hazard as the result of massive development of active remote sensing and GIS technologies. However, numerous limitations of this research should be resolved by further studies leading to some recommendation regarding better achievement for volcanic hazard assessment as follows:

1. This research only considered pyroclastic flow hazard generated by dome collapse and did not consider other type of hazard produced by Merapi activity. Hence, further studies should consider other types of hazards to produce comprehensive hazard zonation.

2. Broader extent of DEM quality assessment using high quality DTM of active remote sensing techniques should be carried out to have precise elevation error which leads to the complete utilization of active remote sensing to replace conventional ground surface and aerial photogrammetry techniques.
3. The use of simulation models e.g. energy cone, FLOW 2D, FLOW 3D and Titan 2D for Merapi – type eruption based on high quality DTM should be carried out to precisely predict the affected area.
4. Volume calculation of remnant of domes using simulation of volcanic cone could be carried out to precisely predict the volume of dome remnants that have possibility to collapse and produce greater hazard than that of produce from lava dome growth alone.
5. More detail number of inhabitants in predicted affected area should be conducted in order to have more specific number of people threaten by pyroclastic flow hazard and to increase the effectiveness of mitigation program during Merapi activities.

# References


Abdurachman, E. K., J. L. Bourdier, and B. Voight, 2000, Nuées ardentes of 22 November 1994 at Merapi volcano, Java, Indonesia, *Journal of Volcanology and Geothermal Research* 100, 345-361.

Anonymous, Coordinate Systems and Transformations (The Belgian Institute for Space Aeronomy, cited 31 December 2009, available from http://www.spenvis.oma.be/spenvis/help/background/coortran/coortran.html.

Bacharudin, R., 1990, Geomorphological approach to volcanic hazard zonation : using remote sensing images : two case studies from Indonesia : Mount Gede, West java and Mount Agung, Bali, (ITC, Enschede).

Beauducel, F., F. H. Cornet, F. Suhanto, E. Duquesnoy, and K. M, 2000, Constraints on magma flux from displacements data at Merapi volcano, Java, Indonesia, *Journal of Geophysical research* 105, 8193 - 8204.

Bi, H., X. Li, M. Guo, and X. L. a. J. Li, 2006, Digital Terrain Analysis Based on DEM, *Frontiers of Forestry in China* 1, 5.

Bignone, F., and H. Umakawa, 2008, Assessment Of ALOS Prism Digital Elevation Model Extraction Over Japan *The International Archives of the Photogrammetry, Remote Sensing and Spatial Information Sciences* XXXVII, 4.

Brinker, R. C., and P. R. Wolf, 1984, *Elementary Surveying* (Harper & Row Inc, New York).

Camus, G., A. Gourgaud, P. C. Mossand-Berthommier, and P. M. Vincent, 2000, Merapi (Central Java, Indonesia): An outline of the structural and magmatological evolution, with a special emphasis to the major pyroclastic events, *Journal of Volcanology and Geothermal Research* 100, 139-163.

Chaplot, V., F. Darboux, H. Bourennane, S. Leguédois, N. Silvera, and K. Phachomphon, 2006, Article in Press: Accuracy of interpolation techniques for the derivation of digital elevation models in relation to landform types and data density, *Journal of Geomorphology*, 16.

Charbonnier, S. J., and R. Gertisser, 2008, Field observations and surface characteristics of pristine block-and-ash flow deposits from the 2006 eruption of Merapi Volcano, Java, Indonesia, *Journal of Volcanology and Geothermal Research* 177, 971-982.

Charbonnier, S. J., and R. Gertisser, 2009, Numerical simulations of block-and-ash flows using the Titan2D flow model: examples from the 2006 eruption of Merapi Volcano, Java, Indonesia, *Bulletin of Volcanology* Volume 71, Number 8 / October, 2009, 953-959.

Corazzato, C., and A. Tibaldi, 2006, Fracture control on type, morphology and distribution of parasitic volcanic cones: An example from Mt. Etna, Italy, *Journal of Volcanology and Geothermal Research* 158, 177-194.

CVGHM, 2006, Prekursor Erupsi Gunung Merapi (Precursors of Merapi Eruption), in A. Ratdomopurbo, Subandriyo, Y. Sulistiyo and Suharna eds (Merapi Volcano Observatory Yogyakarta) 87.

Davidson, J., and S. D. Silva, 1999, Composite Volcano, in H. Sigursson., B. F. Houghton., S. R. McNutt., H. Rymer. and J. Stix. eds, *Encyclopedia of Volcanoes* (Academic Press, San Diego) 19.

Davis, R. E., F. S. Foote, J. M. Anderson, and E. M. Mikhail, 1981, *Surveying, Teory and Practice* (McGraw - Hill Inc, New York).

Dove, M. R., 2008, Perception of volcanic eruption as agent of change on Merapi volcano, Central Java, *Journal of Volcanology and Geothermal Research* 172, 329-337.

Felix, M., and W. McCaffrey, 2005, Particle-Driven Subaqueous Gravity Processes, in R. C. Selley, L. R. M. Cocks and I. R. Plimer eds, *Encyclopedia Of Geology* (Elsevier, London) 807.

Fink, J. H., and S. W. Anderson, 1999, Lava Domes and Coulees, in H. Sigursson ed, *Encyclopedia of Volcanoes* (Academic Press, New York) 307.

Gallant, J. C., and J. P. Wilson, 2000, Primary Topographic Attribute, in J. P. e. Wilson and J. e. Gallant eds, *Terrain Analysis: Principles and Applications* (Wiley & Sons, New York) 51-85.

Geodata and Geoscience Australia, 2002, Data User Guide: A Digital Elevation Model of Australia with a Grid Spacing of Nine Seconds in Longitude and Latitude (Centre for Resource and Environmental Studies (CERS), Canbera) 46.

Gonçalves, J. A., 2008, Orientation and Dem Extraction from ALOS-PRISM Images Using the SRTM-DEM as Ground Control, *The International Archives of the Photogrammetry, Remote Sensing and Spatial Information Sciences* XXXVII Part B1, 6.

Goudie, A., M. Anderson, T. Burt, J. Lewin, K. Richards, B. Whalley, and P. Worsley, 1990, *Geomorphological Techniques* (Routledge - Taylor and Francis Group, New York).

Goudie, A. S., 2004, *Encyclopedia of Geomorphology* (Routledge, New York).

Hamblin, W. K., 1989, *Earth's Dynamic Systems: a Textbook in Physical Geology* (MacMillan ; Collier MacMillan, New York ; London).

Huggett, R. J., 2007, *Fundamental of Geomorphology* (Routledge, New York).

Hutchinson, M. F., and J. C. Gallant, 2000, Digital Elevation Models and Representation of Terrain Shape, in J. P. e. Wilson and J. e. Gallant eds, *Terrain Analysis: Principles and Applications* (Wiley & Sons, New York) 29 - 49.

Intermap, T., 2009, Product Handbook & Quick Start Guide version 4.3, *Understanding Accuracy* (Intermap Technologies Inc., Denver, USA) 10.

JAXA, 2008, ALOS Data Users Handbook (Earth Observation Research and Application Center, Japan) 158.

Klimanek, I. M., 2007, Geoinformation Support of Derived Mapping Based on Digital Terrain Model (Mendel University of Agriculture and Forestry Brno, Czech Republic, Brno) 8.

Klimasauskas, E., Mount St. Helens Precursory Activity cited 9 December 2009, available from http://vulcan.wr.usgs.gov/Volcanoes/MSH/May18/MSHThisWeek/412425/412425.htm.

Konecny, G., 2003, *Geoinformation: Remote sensing, photogrammetry and geographic information systems* (Taylor & Francis Inc, New York).

Lavigne, F., B. De Coster, N. Juvin, F. Flohic, J.-C. Gaillard, P. Texier, J. Morin, and J. Sartohadi, 2008, People's behaviour in the face of volcanic hazards: Perspectives from Javanese communities, Indonesia, *Journal of Volcanology and Geothermal Research* 172, 273-287.

Lavigne, F., and J. C. Thouret, 2003, Sediment transportation and deposition by rain-triggered lahars at Merapi Volcano, Central Java, Indonesia, *Geomorphology* 49, 45-69.

Lavigne, F., J. C. Thouret, B. Voight, H. Suwa, and A. Sumaryono, 2000, Lahars at Merapi volcano, Central Java: an overview, *Journal of Volcanology and Geothermal Research* 100, 423-456.

Legros, F., and K. Kelfoun, 2000, On the ability of pyroclastic flows to scale topographic obstacles, *Journal of Volcanology and Geothermal Research* 98, 235-241.

Li, Z., Q. Zhu, and C. Gold, 2005, *Digital Terrain Modeling: Principles and Methodology* (CRC PRESS, Florida).

MacDonald, G. A., 1972, *Volcanoes* (Prentice-Hall, Englewood Cliffs).

Marti, J., and G. G. J. Ernst, 2005, *Volcanoes and the Environment* (Cambridge University Press, New York).

Miliaresis, G. C., 2008, Quantification of Terrain Processes, in B. L. Qiming Zhou, Guo-an Tang ed, *Advances in Digital Terrain Analysis* (Springler - Verlag, Berlin Heidelberg).

MVO, 2000, Evolusi 100 Tahun Morfologi Gunung Merapi, Abad XX (100 years Morphologic Evolution of Merapi Volcano, XX Century), in A. a. A. S. D. Ratdomopurbo ed (Merapi Volcano Observatory, Yogyakarta) 57.

Nakada, S., 1999, Hazards From Pyroclastic Flows and Surges, in H. Sigurdsson, B. Houghton, S. R. McNutt, H. Rymer and J. Stix eds, *Encyclopedia of Volcanoes* (Academic Press, San Diego) 10.

Pazera, J., Rozeta 2.0 - English version cited 9 November 2009, available from http://www.pazera-software.com/products/rozeta/.

Peltier, A., B. Scott, and T. Hurst, 2009, Ground deformation patterns at White Island volcano (New Zealand) between 1967 and 2008 deduced from levelling data, *Journal of Volcanology and Geothermal Research* 181, 207-218.

Pike, R. J., I. S. Evans, and T. Hengl, 2009, Geomorphometry: A Brief Guide, in A. E. Hartemink and A. B. McBratney eds, *Development in Soil Science Volume 33* (Elsevier, Amsterdam) 28.

Ping, X., 2003, Digital elevation model extraction from ASTER in support of the coal fire and environmental research project, China, (ITC, Enschede).

Podobnikar, T., 2008, Methods for Visual Quality Assessment of a Digital Terrain Model, *S . A . P . I . E N . S* 1, 10.

Rahman, A. A.-., and M. Pilouk, 2008, *Spatial Data Modeling for 3D GIS* (Springler - Verlag, New York).

Rahman, M. Z. B. A., 2006, Digital Surface Model (DSM) Construction and Flood Hazard Simulation for Development Plans in Naga City, Philippines, (ITC, Enschede).

Ratdomopurbo, A., and S. D. Andreastuti, 2000, *Karakteristik Gunung Merapi (Characteristic of Merapi Volcano)* (Volcanological Survey of Indonesia, Yogyakarta).

Remondo, J., and T. Oguchi, 2009, GIS and SDA Applications in Geomorphology, *Geomorphology* 111, 1-3.

Reuter, H. I., T. Hengl, P. Gessler, and P. Soille, 2009, Preparation of DEMs for Geomorphometric Analysis, in A. E. Hartemink and A. B. McBratney eds, *Development in Soil Science Volume 33* (Elsevier, Amsterdam) 35.

Rifai, R., 2008, Spatial Modelling and Risk Assessment of Sidoarjo Mud Volcanic Flow, (Gajah Mada university (UGM) - ITC, Yogyakarta - Enschede).

Rodriguez-Gonzalez, A., J. L. Fernandez-Turiel, F. J. Perez-Torrado, and D. G. a. M. Aulinas, 2009, Geomorphological Reconstruction and Morphometric Modelling Applied to Past Volcanism, *International Journal of Earth Sciences*, 16.

Rolandi, G., 2009, Volcanic hazard at Vesuvius: An analysis for the revision of the current emergency plan, *Journal of Volcanology and Geothermal Research* 189, 347-362.

Sagala, S. A. H., 2007, Risk Communication for Disaster Preparedness of Earthquake and Volcanic Eruption, Case study: Yogyakarta, Indonesia, *PhD Summer Academy, UNU – EHS* (Disaster Prevention Research Institute (DPRI), Kyoto University, Japan, Kyoto) 15.

Santoso, A. B., S. Sumarti, Sunarta, M.Djilal, and K. Rinekso, 2009, Aktifitas G. Merapi Januari - April 2009 (Merapi Activity January - April 2009), *Merapi* (MVO, Yogyakarta) 5.

Scarth, A., 1994, *Volcanoes : An Introduction* (UCL Press, London).

Spatial Planning Directorate, 2008, Rencana Tata Ruang Kawasan Merapi (Local Spatial Planning of Merapi) (Department of Public Works, Jakarta).

Stevens, N. F., V. Manville, and D. W. Heron, 2003, The sensitivity of a volcanic flow model to digital elevation model accuracy: experiments with digitised map contours and interferometric SAR at Ruapehu and Taranaki volcanoes, New Zealand, *Journal of Volcanology and Geothermal Research* 119, 89-105.

Stinton, A. J., and M. F. Sheridan, 2008, Implications of Long-Term Changes in Valley Geomorphology on the Behavior of Small-Volume Pyroclastic Flows, *Journal of Volcanology and Geothermal Research* 176, 7.

Subandriyo, D. S. Sayudi, and M. Muzani, 2009, Ancaman Bahaya Gunung Merapi Ke Arah Selatan Setelah Erupsi 2006 (Threat of Merapi Hazard toward South Direction after 2006 Eruption), *Merapi* (MVO, Yogyakarta).

Subandriyo, D. S. Sayudi, I. Nurnusanto, M. Muzani, K. Rinekso, and Suharno, 2006, Gejala Awal Erupsi Gunung Merapi 2006; Lahirnya Kubah Lava Baru (Prekursor of Merapi Eruption 2006; New Lava Dome Growth), *Merapi* (MVO, Yogyakarta) 11.

Sutikno, L. W. Santosa, Widiyanto, A. Kurniawan, and T. H. Purwanto, 2007, *Kerajaan Merapi (Merapi Kingdom)* (Badan Penerbit Fak. Geografi, Universitas Gadjah Mada, Yogyakarta).

Székely, B., and D. Karátson, 2004, DEM-based morphometry as a tool for reconstructing primary volcanic landforms: examples from the Börzsöny Mountains, Hungary, *Geomorphology* 63, 25-37.

ThinkQuest, Pelean Eruptions and Nuees Ardentes cited June 2 2009, available from http://library.thinkquest.org.

Thompson, G. R., and J. Turk, 1997, Introduction to Physical Geology (Brooks Cole USA).

Thornbury, W. D., 1958, *Princples of Geomorphology* (John Wiley & Sons, New York).

Thouret, J. C., 1999, Volcanic geomorphology - An Overview, *Elsevier Science B.V.* 47, 95 - 131.

Thouret, J. C., F. Lavigne, K. Kelfoun, and S. Bronto, 2000, Toward a revised hazard assessment at Merapi volcano, Central Java, *Journal of Volcanology and Geothermal Research* 100, 479-502.

Tiede, C., J. Fernandez, C. Gerstenecker, and K. F. Tiampo, 2007, A Hybrid Model for the Summit Region of Merapi Volcano, Java, Indonesia, Derived from Gravity Changes and Deformation Measured Between 2000 - 2002, *Pure and Applied Geophysics* 164, 837-850.

Trisakti, B., and F. A. Pradana, 2007, DEM Generation from PRISM-ALOS and ASTER, Paper presented at the Bridging Interdisciplinary Toward Sustainability, Indonesia.

Verstappen, H. T., 2000, *Outline of the Geomorphology of Indonesia* (ITC Enschede, The Netherlands).

Voight, B., E. K. Constantine, S. Siswowidjoyo, and R. Torley, 2000, Historical eruptions of Merapi Volcano, Central Java, Indonesia, 1768-1998, *Journal of Volcanology and Geothermal Research* 100, 69-138.

Wilson, C. J. N., and B. F. Houghton, 1999, Pyroclast Transport and Deposition, in H. Sigurdsson, B. Houghton, S. R. McNutt, H. Rymer and J. Stix eds, *Encyclopedia of Volcanoes* (Academic Press, San Diego) 10.

Wilson, J. P., and J. C. Gallant, 2008, Digital Terrain Analysis, in J. P. Wilson and J. C. Gallant eds, *Terrain Analysis: Principles and Applications* (Wiley & Sons, New York) 1-10.

Wilson, T., G. Kaye, C. Stewart, and J. Cole, 2007, Impacts of the 2006 Eruption of Merapi Volcano, Indonesia, on Agriculture and Infrastructure (Institute of Geological and Nuclear Sciences Limited, New Zealand) 69.

Yang, Q., T. G. V. Niel, T. R. McVicar, M. F. Hutchinson, and L. Li, 2005, Developing a Digital Elevation Model using ANUDEM for the Coarse Sandy Hilly Catchments of the Loess Plateau, China (CSIRO Land and Water Canberra, Australia) 82.

Young, K. D., B. Voight, Subandriyo, Sajiman, Miswanto, and T. J. Casadevall, 2000, Ground Deformation at Merapi Volcano, Java, Indonesia: distance changes, June 1988 - October 1995, *Journal of Volcanology and Geothermal Research* 100, 233 - 259.

Zuidam, R. A. V., 1983, *Guide to Geomorphologic Aerial Photographic Interpretation and Mapping* (ITC Enschede, The Netherlands).

# Appendixes

## Appendix A. Data inventory from institution and MOPs

**1. Data Inventory From Institutions**
**Purpose: obtaining spatial data for topographic representation of Merapi**

| Date | Institutions | Contact Persons | Results |
|---|---|---|---|
| 07/07/09<br>22/07/09 | MVO | Sri Sumarti<br>Head of Merapi Sub Division | 1. No data could be achieved except they could participate in the research, as supervisor.<br>2. Accessible library and some publications |
| 08/07/09 | PUSPICS | Badrun | AMS Topographic Map scale 1: 50.000, production date: 1964 |
| 09/07/09 | NASA LP DAAC | - | ASTER GDEM data of Merapi (30 m) |
| 14/07/09 | BAPPEDA Sleman | Agus<br>Technology and Interrelation Sub Division | 1. No satellite data could DEM<br>2. Statistic data of year 2007<br>3. Landuse planning for Merapi |
| 14/07/09 | BPPD | Bambang Pamungkas | Merapi summit of IKONOS Imageries (2003) covered by cloud |
| 14/07/09 | BPN | Bayu<br>Head of Survey and Mapping Sub Division | 1. The GCPs available in 2D coordinate (X,Y)<br>2. No GCP located nearby Merapi volcanic cone |
| 16/07/09 | Dinas P3BA | Singgih/Asih<br>Head of Disaster Management Division/Sub division | 1. Report of mitigation and response for Merapi eruption in 2006<br>2. 8 EWS for lahars<br>3. Mitigation plan based on MVO recommendation |
| 16/07/09 | SNVT SABO | Bambang Cosmas Sukatja | Digital contour map scale 1: 5.000, acquisition date: 2006 |
| 17/07/09 | PSBA | Joko<br>Merapi Disaster Division | No digital data for Merapi area |
| 23/07/09 | TNGM | Silviana, Dhani S.<br>Technical Sub Division | 1. No digital data for Merapi area<br>2. Some pictures of Merapi crater and surrounding area |
| 11/08/09 | BAKOSURTANAL | - | Topographic map of Merapi, production date: 2000 |
| 10/08/09 | Previous researcher | Ruli Andaru | VSI contour map overlying orthophoto, acquisition date: 1982 |
| 11/08/09 | Geodesy GMU | Wagiyo | Topographic map of Merapi, production date 1944 |
| 08/09/09 | Geological Survey Indonesia | - | Topographic maps of Merapi, production date 1964 and 1944 |
| 22/08/09 | Museum Ketep Pass | - | Pictures of Merapi summit |
| 13/10/09 | ExsaMap Asia | Daniel Adi Nugroho | Request for Merapi DEM |
| 12/11/09 | Intermap Tech. Inc Canada | Stephen Griffiths<br>Daniel Adi Nugroho | Data delivered from Denver, USA through ExsaMap Asia, Jakarta |
| 16/12/09 | Infoterra – global Germany | Christian Thiergan<br>Ralf Duering | No further information about data request |

**2. Data Inventory From MOPs**
**Purposes:**
**a. Collection of EDM data**
**b. Picture of Merapi sides, Sketches and Remnant of Domes Recognition**
**c. Interview of PIC in MOPs**

| Date | MOPs | Contact Persons | Results |
|---|---|---|---|
| 01/08/09<br>14/08/09<br>22/08/09 | Babadan, Magelang | Yulianto, Triyono | 1. EDM data 2006 – 2009<br>2. Remnant of domes recognition and delineation<br>3. Publications of Merapi<br>4. Map of Merapi scale 1: 25.000, production date 1939 |
| 22/08/09<br>09/09/09 | Selo, Boyolali | Ismail, Singat | 1. EDM data 2006 – 2009<br>2. Sketches of Merapi |
| 09/09/09 | Jrakah, Boyolali | Trimujiyanto | 1. EDM data 2006 – 2009<br>2. Sketches of Merapi |
| 11/09/09 | Kaliurang, Sleman | Panut, Suramto | 1. EDM data 2006, 2007, 2009<br>2. Some pictures from eruption 2006 |
| 11/09/09 | Ngepos, Magelang | Retiyo | Some pictures of Merapi edifice |

## Appendix B. Field work form

**Double Degree M Sc. Program**
**Geoinformation for Spatial Planning and Risk Management (ITC-GMU)**

**MOP FIELD WORK FORM**

Researcher : Komang Sri Hartini
Contact : hartini20739@itc.nl
Title : Morphologic Analysis of Merapi Edifice in Studying Merapi – Type Eruption, To Improve Volcanic Hazard Map

A. General Information

1. Date :
2. MOP :
3. PIC
   a. Name :
   b. Contact :
4. Equipment :

B. Electronic distance meter

1. Benchmark coordinate E :
   S :
2. EDM equipment type :
3. EDM Data available :
4. Fixed Prism

| Numbers | Positions on Merapi edifice or flank |
|---|---|
| 1. | 1. |
| 2. | 2. |
| 3. | 3. |
| 4. | 4. |
| 5. | 5. |
| 6. | 6. |

C. Supporting equipment

| | | |
|---|---|---|
| 1. Seismograph | □ Yes | □ No |
| 2. EDM | □ Yes | □ No |
| 3. Camera | □ Yes | □ No |
| 4. Computer | □ Yes | □ No |
| 5. Siren | □ Yes | □ No |

D. Interview

| Questions | Answers |
|---|---|
| 1. EDM measurement | |
| a. Time of EDM measurement | |
| b. Measurement series | |
| c. Obstacle of EDM measurement | |
| d. Distance changes during precursor | |
| e. Daily distance changes | |
| f. Transferring data to MVO | |
| 2. Remnant of domes | |
| a. Number of remnant observed | |
| b. Dome remnants identification | |

**Double Degree M Sc. Program**
**Geoinformation for Spatial Planning and Risk Management (ITC-GMU)**

**PICTURE OF MERAPI SIDES FIELD WORK FORM**

Date :
Equipment :
Coordinate E :
S :
Descriptions :

**Appendix C. Example of EDM data, sketches, pictures of dome remnants and equipment**

**Appendix D. DEM generation using ANUDEM with different output resolution**